Internal Report
DESY M 98-11
October 1998

Reports at the XIX International Linear Accelerator Conference LINAC 98

August 23 –28, 1998
Chicago, USA

Deutsches Elektronen-Synchrotron DESY, Hamburg, Germany

"Die Verantwortung für den Inhalt dieses
Internen Berichtes liegt ausschließlich beim Verfasser"

CONTENTS

Invited Talks

Talks

C.-M. Kleffner, N. Holtkamp, M. Nagl, H. Poggensee, J. Peters, A. Schempp	Operation of the Upgraded H^- - Injection System of the Linac III at DESY
M. Liepe, S.N. Simrock	Adaptive Feed Forward for the Digital RF Control System at the TESLA Test Facility
W.-D. Möller, for the TESLA Collaboration	The Performance of the 1.3 GHz Superconducting RF Cavities in the First Module of the TESLA Test Facility Linac

REVIEW OF NEGATIVE HYDROGEN ION SOURCES HIGH BRIGHTNESS/ HIGH CURRENT

J.Peters
Deutsches Elektronen-Synchrotron DESY, Notkestraße 85, 22607 Hamburg, Germany

Abstract

Due to the development of reliable H^- ion sources, charge-exchange injection into circular accelerators has become routine. This paper reviews recent developments in negative hydrogen ion sources. The underlying physics, operating parameters and beam characteristics of selected sources will be described and compared.

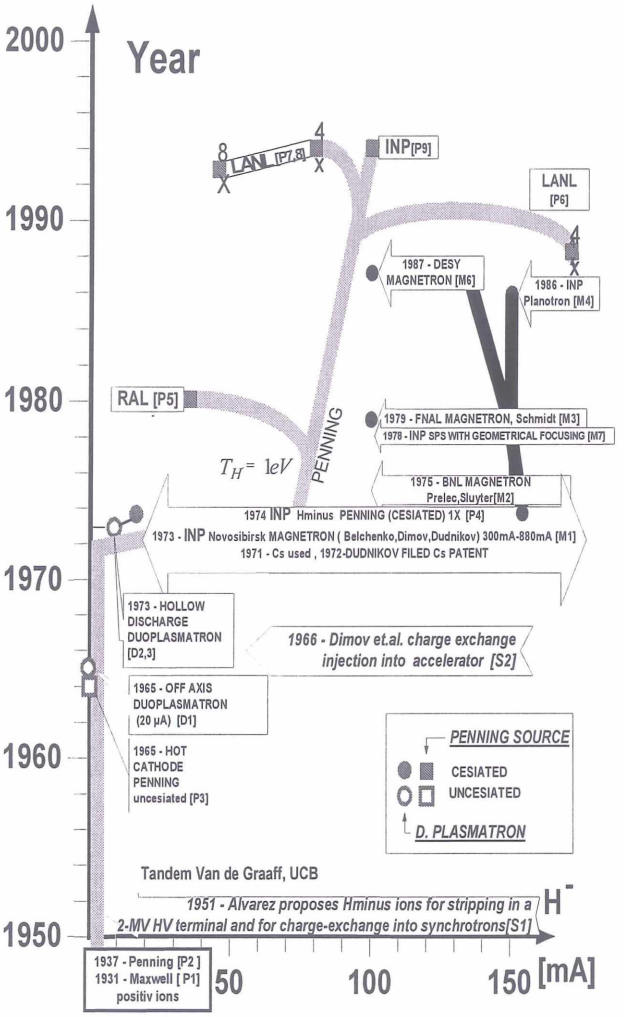

Figure 1: History of duoplasmatron and surface source development.

1 INTRODUCTION

This paper will deal primarily with H^- sources used as injectors for high energy accelerators. Usual (high) H^- currents are 10 to 100 mA dependent on the duty factor. It has taken two decades to reach these currents since Alvarez proposed H^- ions for stripping in a high voltage terminal and for charge-exchange injection into synchrotrons (Fig.1 S1) [1].
Duoplasmatrons (D1,2,3) with their low currents are excluded as well as multi aperture sources which have high currents but low brightness .

1.1 Definition of brightness and emittance

Several definitions of brightness are in use. The following relation is adopted here :

$$B = \frac{I}{\varepsilon^N_{x,90\%}\ \varepsilon^N_{y,90\%}} \quad ,$$

where $\varepsilon^N_{x,90\%}$ is the energy normalized emittance in the (x ,x') plane for the contour containing 90% of the brightest beam and

$$\varepsilon^N = \varepsilon\ \beta\ \gamma \quad ,$$

with : $\beta = v_{BEAM}/c$ and $\gamma = 1/(1-\beta^2)^{1/2}$.
In the ideal case the contour is an ellipse and ε is the product of the semimajor and semiminor axes times π. Emittances quoted in conventions other than 90% area values can be converted using the following equations :
$\varepsilon_{90\%} = 4.6\ \varepsilon_{rms}$ and $\varepsilon_{90\%} = 1.125\ \varepsilon_{4rms}$
assuming a Gaussian distribution.

1.2 Emittance scanners and emittance errors

Emittance values found in the literature may differ very much even for the same source type and current. For this paper the labs were asked for emittances and the related current, type of emittance scanner, distance from scanner to extractor and other relevant source data. Most labs now use slit-multiwire scanners [DESY, BNL, RAL] or electrostatic sweep scanners (Allison) [LANL, LBL]. These devices are able to measure rms and area emittances. The pepperpot is also still in use. It measures only area emittances. In recently published emittance collections [2] area definitions have been used.

2 SURFACE SOURCES (SPS)

After the discovery of cesiation of surfaces at INP in 1971, the attainable H^- currents increased dramatically. The magnetron was invented (see Fig.1 M1)[3] and the penning source developed to its present standard (P4) [4] in Novosibirsk at INP .

2.1 Magnetron

Magnetron technology was transferred from INP to BNL (M2) [5] and from there to FNAL (M3) [6]. There was a mutual exchange between these two labs. In 1987 magnetron plans were brought from FNAL to DESY.

Figure 2 shows the structure of a magnetron in front and side views. It consists of a central cylindrical cathode surrounded by an anode. The discharge voltage, U_D , is typically ≈150 V and the current 40 A. A magnetic field (≈0.17 T) is parallel to the cathode axis. Hydrogen gas is introduced from the top by a pulsed gas valve.

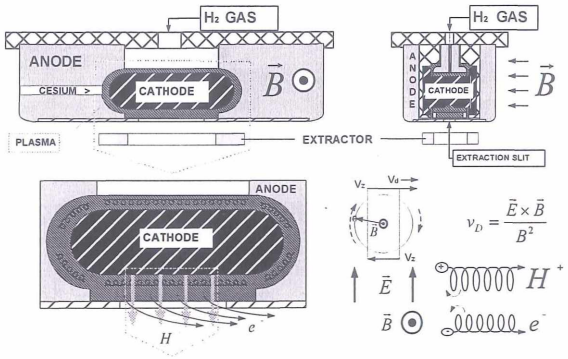

Figure 2: Magnetron source and E×B drift.

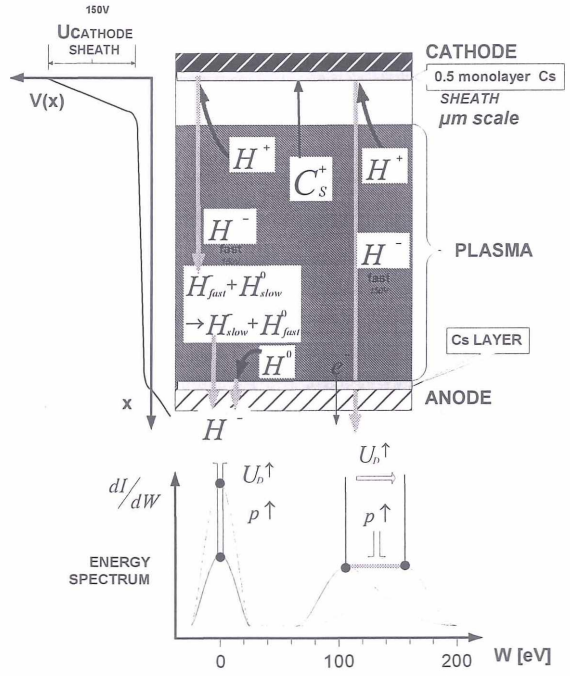

Figure 3: Production of H^- at cathode and anode of the source and their energy spectrum.

Cesium is obtained by heating metallic cesium or a mixture of cesium chromate and titanium.The mixture is available as pellets or powder.

H^- ions are extracted at 18 kV (FNAL, DESY) or 35 kV (BNL) together with electrons. Modern magnetrons have geometric focussing, developed at INP in 1978, with a groove in the cathode and slit extraction followed by a bending magnet [7]. Another possibility is to dimple the cathode and to use a hole as aperture toward the extractor electrode [8].

The electric field between anode and cathode leads to an E×B drift around the cathode, which is shown on a magnified scale Fig.2 (lower part). Positive and negative ions move in the same direction. There is no movement parallel to E as particles gain as much energy as they lose. But parallel to E×B there is a resulting difference v_d (see Fig.2). Charges are not separated due to this effect. A dense plasma is produced.

If one looks with a bigger magnification at the space between anode and cathode (Fig. 3) one notices a transition zone, the so-called sheath, between the plasma and the cathode. Here the potential drops to cathode level. There is only a small potential difference across the plasma. H^+ ions generated in the plasma are accelerated through the sheath. They produce H^- ions at the cathode surface, which is covered in the ideal case with approximately half a mono layer of Cs in order to minimize the surface work function. These H^- particles are then accelerated to U_D passing through the sheath. Some move through the plasma and are extracted. They form a maximum in the energy spectrum (Fig.3 lower part). Others hit slow H^0 particles and exchange speed and charge; this is resonant charge exchange. In this way slow H^- ions are produced. Slow H^- can also be produced by H^0 hitting the cesiated anode surface.

Due to these mechanisms a low and a high energy peak appear in the energy spectrum. To increase the fraction of low temperature ions one can increase the source pressure and discharge voltage U_D, as indicated in the plot. In addition, the position of the high energy peak can be changed by varying U_D and the amplitude lowered by increasing the pressure.

2.2 Semiplanotron

The semiplanotron is an optimized magnetron, with geometric focussing and without a discharge at the back of the cathode. These modifications make it more efficient. Operational experience is, however, limited. Source lifetime may be limited by the accumulation of

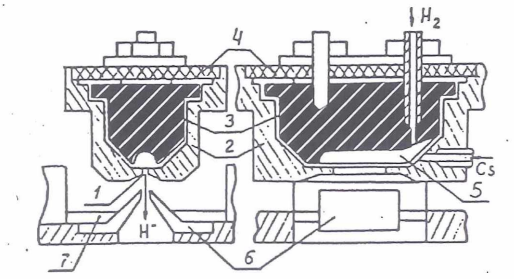

Figure 3: The semiplanotron source. 1. emission slit, 2. anode, 3. cathode, 4. insulator, 5. groove, 6. extractor, 7. steel inserts

sputtered particles from the cathode as a result of their drift path being blocked. This might result in a short circuit, consistent with DESY experience.

2.3 Penning

In order to avoid the high energy peak of the magnetron spectrum the cathode surface should not face the ion extraction aperture. This is how the penning source is constructed (see Fig. 4).

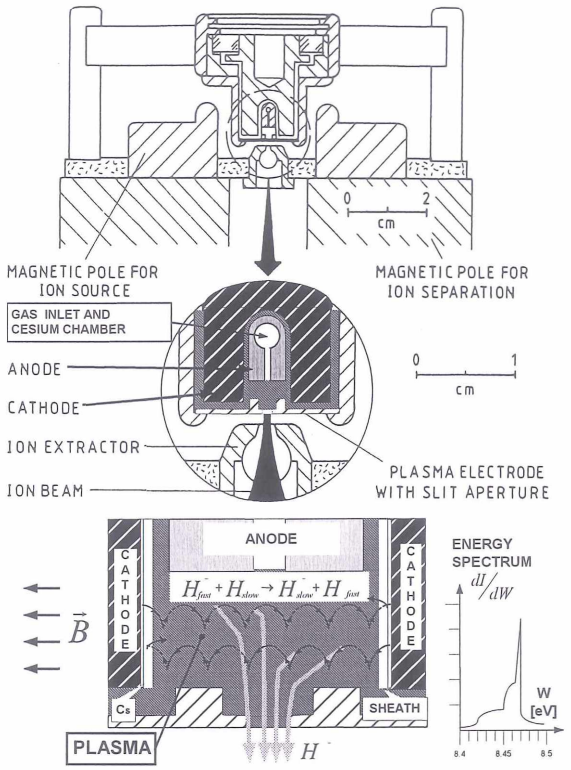

Figure 4 : Penning source schematic and its energy spectrum

A strong magnetic field parallel to the electric field of the sheath guides electrons and ions on cyclotron spirals from cathode to cathode. Fast H^- ions are generated at the cathodes as in the magnetron. They are slowed down due to the charge exchange reaction as they migrate to the plasma aperture. There is only one low energy peak and the H^- temperature has been measured to be less than 1eV [9].

2.4 Multicusp Surface-plasma (converter) source

Fig. 5 shows a multicusp surface-plasma source. A discharge is produced with filaments. The plasma is confined by a multicusp field. A converter biased at ≈-300 V is located in the middle of the source. Secondary emission of negative ions takes place.

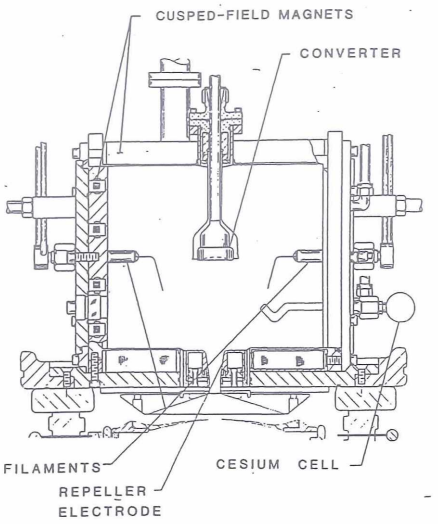

Figure 5: LANL surface production multicusp

The H^- ions are produced by H^+, H_2^+ and H_3^+ bombarding the converter. Cesium is injected into the source to increase the H^- yield. Self extraction of H^- takes place with focussing provided by the curvature of the converter. A magnetic filter is used to repel electrons.

3 VOLUME SOURCES

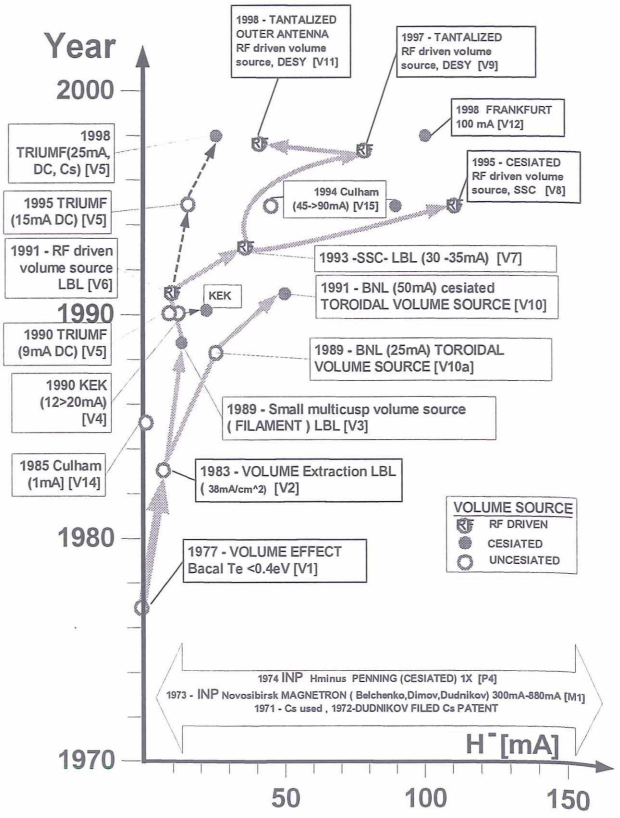

Figure 6 : History of volume source development

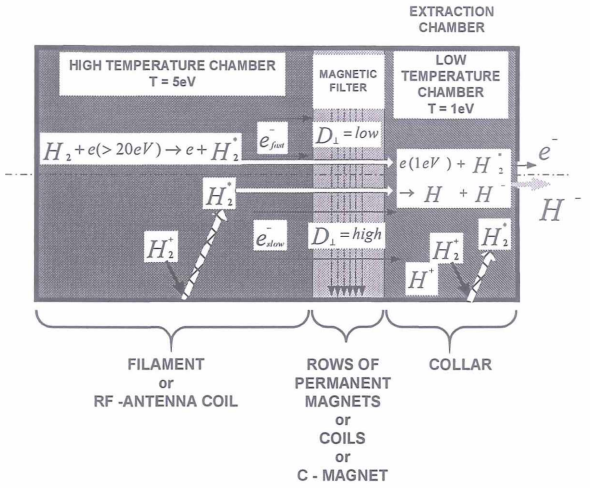

Figure 7 : Tandem source for volume production

In 1977 M. Bacal [10] discovered volume production for H^- generation. This started the development of a new type of sources (Fig. 6). The volume source consists of two chambers, which are connected by a magnetic filter (Fig. 7). In the high temperature chamber energetic electrons hit H_2 , which become vibrationally excited. Excited molecule are also produced at the chamber walls out of H_2^+ and H^+ . Electrons from the high temperature chamber move by diffusion through a perpendicular magnetic field into a second chamber. Whereas high energy electrons are effectively blocked, slow electrons collect in the second chamber. In this low energy chamber, low temperature 1eV electrons attach to the H_2^* producing H^- ions.

Multi cusp magnets are used to confine the plasma.

3.1 Filament Volume Source

The first volume sources were uncesiated and had filaments. Currents of up to 20 mA DC [11] were reached with small sources and 45 mA [12] (Fig. 6 V15) with larger ones. Cesiated currents of 25 mA DC [13] and 90-100 mA at 6% duty factor [12,14] V12 have been achieved. The lifetime of these sources is limited by that of the filament.

3.2 RF Volume Source

The filament was first replaced by an rf antenna coil in 1991 [15]. Fig. 8 shows the DESY RF volume source; it is similar to the sources of LBL and SSC. The antenna heats the high temperature chamber and the filter is constructed with two rows of permanent magnets. The low temperature chamber is located inside a collar.

The antennas are coated to reduce plasma modulation by the rf voltage and sputtering. With uncesiated rf volume sources 35 mA were reached. At DESY the collar was biased and tantalum coated, and currents of 80 mA were achieved uncesiated.

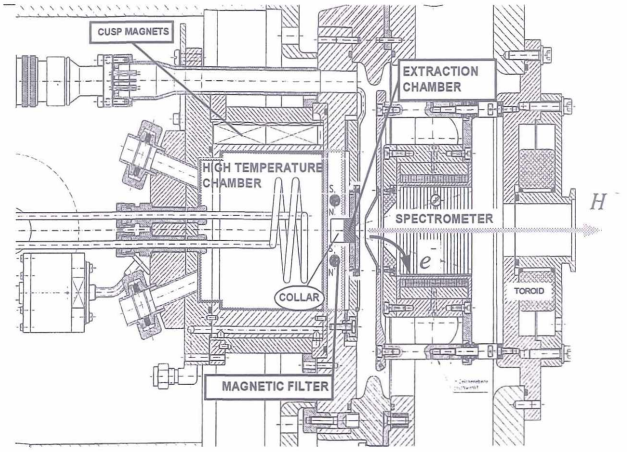

Figure 8 : RF driven volume source

The antennas used by LBL, SSC and DESY were all coated by the same manufacturer. An analysis of the coating found a high percentage of K and Na (Table 1). Different contents of potassium might have contributed to reported differences in source performance.

ELEMENT	PERCENTAGE
Si	46.9 %
Ti	29.6 %
K	15.2 %
Al	5.7 %
Na	2.6 %

Table 1 : Results of analyses of the antenna coating

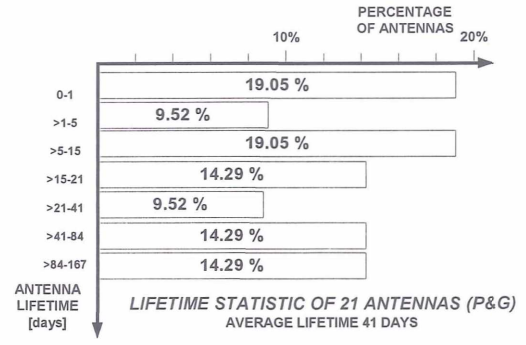

Figure 9 : Lifetime statistic of the coated antennae

DESY has the longest experience in running this type of volume source with the P&G antenna. The performance of the antennae is first limited by spots in the coating. If it survives this period then cracks due to sputtering of the coating material become the lifetime limitation. The average lifetime of only 41 days is higher than that of a filament. However ≈50% of all antennae fail during the first 15 days. This unpredictability is a serious problem for reliability

In addition it was found that sputtered glass from the coating insulates the chamber walls. After such an event it is necessary to do a careful time consuming cleaning of the whole source. Based on this experience a new rf coupling was developed, which couples through a ceramic of Al_2O_3. This type of ceramic has a sputter rate seven times lower than that of glass and three times lower than Ti.

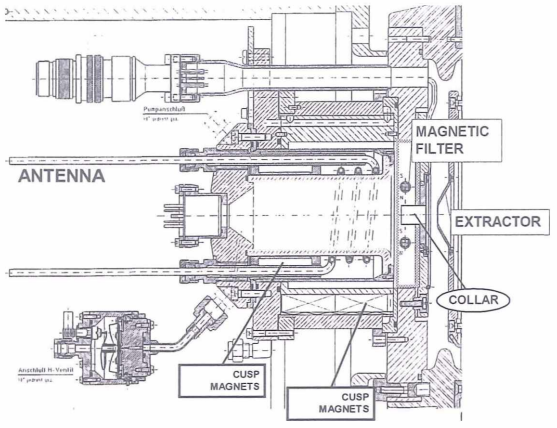

Figure 10 The DESY volume source with an rf coil shielded by Al_2O_3 ceramic.

A source of this type, Fig. 11, was run for 2800 h at 40 mA with a duty factor of 0.05 % and a pulse length of 100 µsec. No degradation in performance was observed.

4 SUMMARY

tested uninterrupted run [h]	SOURCE TYPE	DUTY FACTOR [%]	$\varepsilon_{n,90\%}$ [π mm mrad]	REF.	BRIGHTNESS [mA/mm² mrad²]	C_s CONS. [mg/day]	CURRENT I/mA
7224	MAGNETRON	0.05	.98	[16]	6.4	2.8	60 (->120)
4320	16 years a. exp.	0.48	1.2	[17]	4.9		75
	PLANOTRON	0.25	0.14	[19]	500	24	100
960	PENNING	2.5	0.3	[18]			35 (->170 [ref.26])
	15 years. a. exp	2.5	->0.1	[19]	670	24	80
500	VOLUME FILAMENT 9 years a. exp.	100	0.75	[20]	3.6	NO Cs	20
	FILAMENT	100	0.52(0.6)	[21]		5	20 (25)
		6	≈0.23	[22]		29	100
72-984	RF Antenna in Plasma	0.1	0.5	[23]	12	NO Cs but K	30 (->80 [ref.27])
	RF Antenna in Plasma	0.1	0.5	[24]	28	Cs	91 (->120)
2800	RF Antenna out of Plasma	0.05	0.75	[25]	7.2	NO Cs	40

Table 2 : Collection of source data.

For high energy accelerators it is important to have a reliable source. Magnetrons have been used for the longest time in accelerators and have tested runs of 7000 h. They have, however a poor brightness. Penning sources provide the highest brightness but run for only about 900 h.

The best tested volume source is a DC 6 - 20 mA source, which runs (limited by the filament) for 500 h.

A new rf volume source with an rf coil shielded by ceramic exhibited no degradation in performance after a run of 2800 h.

According to recent results [11, 14] the future prospects of filament volume sources as high duty factor accelerator sources are very good.

Since the antenna problem was solved [27] rf sources are expected to replace magnetrons. They have a higher brightness, higher reliability and are easier to maintain.

5 ACKNOWLEDGEMENTS

The author is grateful for the contribution of the following colleagues at DESY :

N.Holtkamp, I.Hansen, H.Sahling and R.Subke. I wish to thank the technical groups at DESY for their support, and M. Lomperski of DESY for helpful suggestions to the wording of the report. The support of the source groups of BINP, BNL, FNAL, LANL, LBL, RAL and TRIUMF is gratefully acknowledged.

6 REFERENCES

[1] L.W.Alvarez,Rev.Sci.Instrum. 22,705(1951)

[2] J. R. Alonso, Rev. Sci. Instrum., Vol. 67, No.3, March 1996

[3] Yu.I.Belchenko, G.I.Dimov, V.G.Dudnikov, NUCLEAR FUSION 14 (1974)

[4] V.G.Dudnikov, Proc. IV All-Union Conf. on Charged Particle Accelerators, Moscow, 1974,Nauka 1975, Vol 1, p. 323

[5] K.A.Prelec,Th.Sluyters,M.Grossman,IEEE Trans.Nuc.Sci. NS-24(1977) 1521

[6] C.W.Schmidt, C.D.Curtis, IEEE Trans. Nuc. Sci. NS-26 (1979) 4120 }

[7] C.W.Schmidt, Proceedings of LINAC90, Albuquerque, New Mexico, September 10-14, 1990, 259-263 (1990).

[8] J.G.Alessi et al., BNL – 42426, ICIS 1989, Lawrence Berkeley Lab, July 10-14, 1989

[9] J.D.Sherman et al., Rev. Sci. Instrum. 62 (10), October 1991

[10] M. Bacal et al., Phys. Rev. Lett. 42 1538, J. Phys. (Paris) 38, 1399 (1977)

[11] T. Kuo et al.,Rev. Sci. Instrum. 67 (3), March 1996 and private communication

[12] A.J.T.Holmes et al, Rev. Sci. Instrum. 65 (4) April 1994

[13] private communication with T. Kuo , TRIUMF

[14] private communication with K. Volk and A. Maser

[15] K.N.Leung, G.J.DeVries, W.F.DiVergilio and R.W.Hamm, Rev.Sci.Instrum.62(1),100(1991)

[16-27] private communication with DESY, BNL, RAL, BINP, TRIUMF, TRIUMF, FRANKFURT UNIVERSITY, LBL, LBL, DESY, LANL, DESY

THE TESLA FREE ELECTRON LASER – CONCEPT AND STATUS

J . Rossbach, for the TESLA FEL Collaboration
Deutsches Elektronen-Synchrotron, DESY, 22603 Hamburg, Germany

Abstract

The aim of the TESLA Free Electron Laser (FEL) is to develop and realize an Angstrom wavelength, high gain FEL in parallel with the TESLA superconducting e+/e- linear collider. As a first step, an FEL for the VUV wavelength regime is now under construction at DESY, making use of the TESLA Test Facility (TTF).

The VUV FEL at the TTF comes in two phases, which are both approved. The paper describes the over-all layout of each phase and the status of components.

1 FREE ELECTRON LASERS FOR SHORT WAVELENGTH

Over the past 30 years, synchrotron radiation has turned into a most powerful research tool that has been applied in many fields of science ranging from physics, chemistry and biology to material sciences, geophysics, and medical diagnostics. This rapid progress was driven by the development of new, increasingly brilliant sources based on electron storage rings. Due to the recent progress in accelerator technology the possibility has been opened up to complement storage ring based sources by ultra-brilliant Free-Electron Lasers operating in the soft X-ray regime.

In a Free Electron Laser (FEL), an electron beam radiates photons at much higher power and better coherence than it does due to spontaneous synchrotron radiation. The key point is that electrons moving in a transverse magnetic field of alternating polarity (undulator) may amplify an existing electromagnetic radiation field (see e.g. [1]). For properly chosen phase and wavelength (see eq. 1) the scalar product of the electron's velocity vector and the electric field vector does not vanish on average, resulting in an average energy transfer between the electron beam and the radiation field. As a consequence of this interaction, depending on the relative phase, some electrons get accelerated and others decelerated. This results in a longitudinal density modulation of the electron beam at the optical wavelength during the passage through the undulator. With the onset of this "microbunching", coherent emission at the resonant wavelength sets in which results in an exponential growth of the power in the radiation field (high gain mode), characterized by the gain length L_{gain} :

$$I(z) = I_0 \cdot \exp(z / L_{gain})$$

Similar to synchrotron radiation sources, there is no fundamental limit in the choice of the photon wavelength.

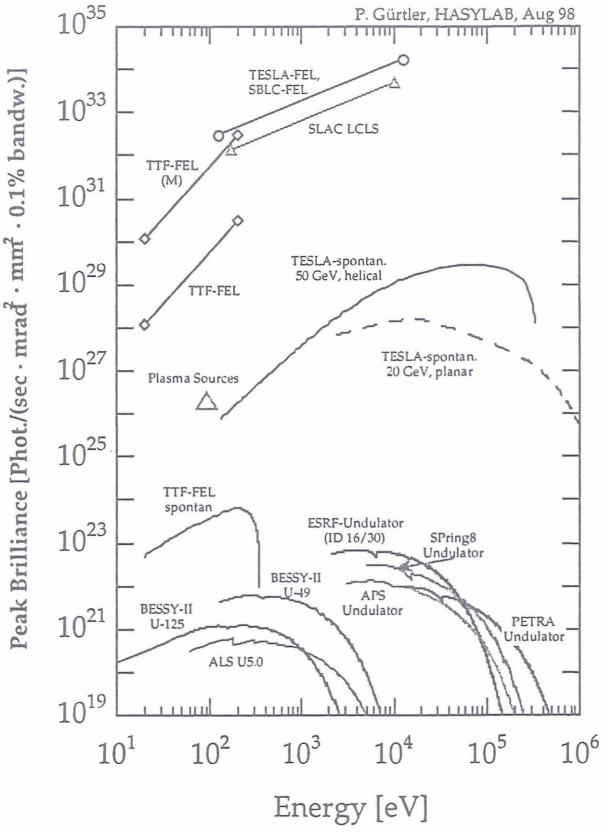

Fig. 1. Spectral peak brilliance of short-wavelength FELs compared with third generation radiation sources and plasma lasers. For comparison, the spontaneous spectrum of an X-ray FEL undulator at 20 GeV is also shown.

The photon wavelength λ_{ph} of the first harmonic is related to the period length of a planar undulator λ_u by

$$\lambda_{ph} = \frac{\lambda_u}{2\gamma^2}\left(1 + \frac{K^2}{2}\right) \quad , \qquad (1)$$

where $\gamma = E/mc^2$ is the relativistic factor of the electrons and $K = eB_u\lambda_u / 2\pi mc$ the 'undulator parameter', e being the elementary charge, m the electron rest mass, c the speed of light, and B_u the peak field in the undulator. It is seen that very short photon wavelength can be achieved if only the electron energy (i.e. γ) is chosen sufficiently high.

For most FELs presently in operation, the electron beam quality and the undulator length result in a gain of only a few percent per undulator passage, so that an optical cavity resonator and a synchronized multi-bunch electron beam have to be used. For the TESLA FEL however, we aim at very short wavelength, for which normal-

incidence mirrors of high reflectivity are not available. Thus we have to provide an electron beam quality (emittance, peak current, energy spread) good enough and an undulator long enough to reach the power saturation level within a single passage. At the saturation length $L_{sat} \approx 4\pi L_{gain}$, the electrons run out of resonance due to their energy loss.

Since the desired wavelength is very short, there is no conventional laser to provide the "initially existing radiation field". Instead, one may consider the spontaneous undulator radiation from the first part of the undulator as an input signal to the downstream part of it. FELs based on this principle of Self-Amplified-Spontaneous-Emission (=SASE) [2,3] are presently considered the most attractive candidates to deliver extremely brilliant, coherent light with wavelength in the Angstrom regime[4-6]. Compared to state-of-the-art synchrotron radiation sources, one expects full transverse coherence, larger average brilliance, and, in particular, up to eight or more orders of magnitude larger peak brilliance (see Fig. 1) at a pulse lengths of about 200 fs FWHM. An important step has been done recently in demonstrating a SASE FEL gain larger than 10^5 at 12 μm wavelength [7].

2 SASE FEL RADIATION

Theoretical description of SASE distinguishes three steps of the process: The start-up-from-noise (or lethargy) regime, the steady-state regime and the saturation regime. The steady-state regime, where a well-defined external electromagnetic input wave is linearly amplified resulting in exponential growth, is accessible for analytical and numerical treatment since many years. The start-up from noise process, however, is much more difficult to analyze, since it is determined by statistical properties and by mutual interaction of more than 10^9 radiating particles. Fully 3-dimensional simulations became available only recently. One of these codes uses Cartesian coordinates and performs direct solution of the paraxial equations for the radiation field and is thus capable of dealing with arbitrary undulator field errors [22]. The other one [23] uses a Greens-function approach for calculation of the radiation field, is much faster and includes far-field mode analysis of the radiation. Results of these codes are in perfect agreement with a SASE proof-of-principle experiment performed recently in Los Alamos at 12 μm wavelength [7, 23]. Finally it is noted, that fluctuation properties of SASE FEL radiation have been analyzed both in the linear and in the saturation regime [24]. Experimental results obtained for the linear regime are again in agreement with theory and simulation, while experimental results on saturation are not yet available.

3 THE TESLA FEL CONCEPT

TESLA aims at a 500 GeV e+/e- collider with integrated X-ray laser Facility [6]. The TESLA linac is indeed exceptionally well suited for a short-wavelength Free Electron Laser: Excellent beam quality is maintained during acceleration and a large variety of pulse train patterns can be provided to users.

The problem with SASE FELs is that, in going to shorter and shorter wavelengths, several technical problems arise such as:

- Some 100m long undulators
- Small (normalized) emittance around 1 π mrad mm for a 1 nC bunch charge
- Bunch compression down to 25 μm bunch length

The ambitious goal of an 1 Å FEL is approached in three steps. Table 1 summarizes main parameters of both electron and photon beams for all these steps.

1. **TTF FEL Phase 1** (approved) [8]: A SASE FEL experiment at wavelength down to 42 nm using the 390 MeV TESLA Test Facility (TTF) linac at DESY[9], see Fig. 2. Besides proving the principle, technical components will be tested: the rf photoinjector, bunch compressors, a 14m long undulator, diagnostics for both electron and photon beams. First operation is scheduled for 1999.

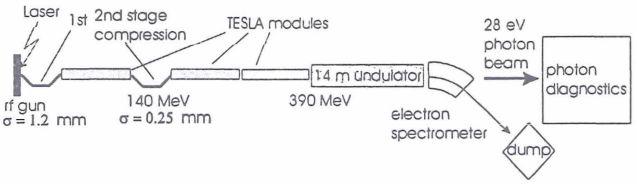

Fig. 2: Schematic layout of phase 1 of the SASE FEL project based on the TESLA Test Facility at DESY.

2. **TTF FEL Phase 2** (approved) [10,11]: By adding 5 more TESLA modules [12], the linac will be upgraded to (at least) 1 GeV, bringing the wave-length down to 6 nm, see Fig. 3. The undulator will be 27m long and the rms bunch length will be reduced to 50 μm by a further compressor stage. Open to users by the year 2003, this facility will give the opportunity to develop experimenting techniques with extraordinary photon beam characteristics like high peak power, short pulse length and fluctuating, spiky substructure typical for SASE FEL photon pulses [13].
3. **TESLA** linear collider with Integrated X-ray Laser (in its technical design phase) [5,6]. For large field gradients, even a superconducting linac has to operate in a pulsed mode. Thus there is room for adding further rf pulses between those driving the high-energy physics beam. By adding a specialized injector providing the electron beam properties needed for the FEL, one can utilize a linear collider installation for driving an X-ray FEL without mutual interference. The plan is to eject the electron bunch train for the FEL at the required beam energy (e.g. at 50 GeV) in the TESLA tunnel, and then transport it to the TESLA interaction region, where a big enough area could accommodate both the high energy physics experimental halls and the X-ray laboratory. A schematic of a switchyard distributing the bunch train over different radiation facilities is shown in Fig. 4.

Concerning the necessary electron beam parameters, all the critical issues are being addressed during phases 1 and 2 (see also Table 1): An rf photoinjector with small emittance and many thousand bunches within each rf pulse [14], bunch length compression by magnetic chicanes including control of coherent radiation effects [15], acceleration without beam degradation [16], and long undulators combined with a periodic FODO lattice [17,18]. In the remainder of this paper we briefly address some key issues of these components.

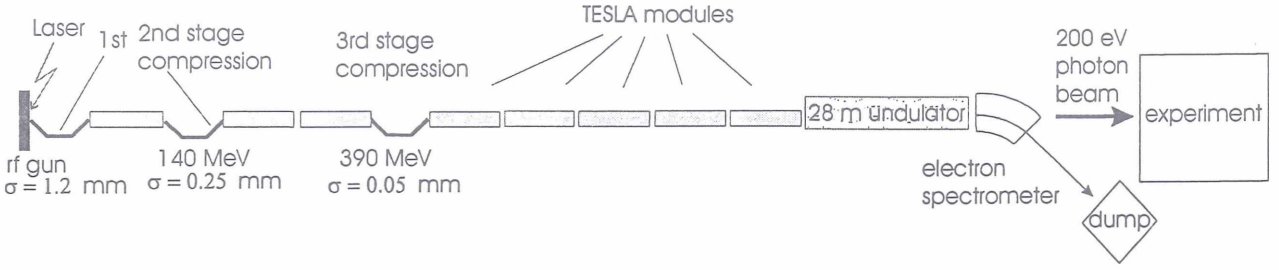

Fig. 3. Schematic layout of phase 2 of the SASE FEL project based on the TESLA Test Facility at DESY. The linac consists of 8 TESLA modules, each 12.2m long. The over-all length of phase 2 is some 300 meters.

Parameter	Units	TTF FEL Phase 1	TTF FEL Phase 2	TESLA X-ray FEL*
beam energy	GeV	0.300	1.000	25.0
λ_{ph} (radiation wavelength)	nm	71	6.4 (193 eV)	0.1
λ_u(undulator period)	mm	27.3	27.3	50
Effective undulator length	m	13.5	27	87
rms beam size	μm	70	50	18
ε^n (normalized emittance) in the undulator	π mrad mm	2.0	2.0	1.0
peak electron current	A	500	2490	5000
No. of electrons per bunch		6.24E+9	6.24E+9	6.24E+9
No. of photons per bunch		1.7E+14	4E+13	7E+12
rms energy spread σ_γ/γ	10^{-3}	1.7	1.00	0.04 at entrance
rms bunch length σ_s	μm	250.	50.	25
L_g (power gain length)	m	0.6	1.00	4.1
P_{sat} (saturated peak power)	GW	0.3	2.6	65
Average brilliance [photons/s/mm^2/mr/0.1%]		up to 2E+21	up to 6E+22	8E+25
bunch train length	μsec	800	800	1052
Number of bunches per train		Up to 7200	up to 7200	Up to 11315
Repetition rate	Hz	10	10	5

Table 1: Main parameters of the TESLA Test Facility FEL (TTF FEL), phases 1 and 2 [10] and of the TESLA X-ray FEL[6]. The insertion devices are planar hybrid undulators. These values should be used as a guideline only since experimental experience has still to be gained in this wavelength regime.
*) For the TESLA X-ray FEL there will be a beam switchyard serving a number of FELs operating at different wavelengths down to 1 Angstrom, and using different beam energies. The parameters given are typical for the 1 Angstrom case.

4 THE PHOTOINJECTOR

The electron source consists of a 1½ cell , 1.3 GHz normal conducting resonator and a photocathode located at the mid-plane of the first (1/2) cell, where the accelerating field is maximum (approx. 45 MV/m). The klystron must provide 4.5 MW power at up to 800 μs pulse length for the long bunch train that can be accelerated in the s.c. linac,. Thus, since the gun cavity is normal conducting, thermal load is a critical issue. The mechanical design provides direct water cooling of the irises and avoids any brazing between water channels and vacuum. For achieving minimum emittance in all 3 dimensions, the design criteria are

- High accelerating gradient to reduce transverse space charge effects.
- Coaxial rf input coupling to reduce rf asymmetries in the cavity.
- Optimum position of the solenoid focussing field to achieve, in the subsequent drift space, "space charge compensation" [19].
- Short laser pulses.

5 THE BUNCH COMPRESSOR

In phase 1, two stages of longitudinal bunch compression are foreseen to reach the high peak current (500A) that is needed to achieve high FEL gain. This compression is done at beam energies high enough so that space charge forces are tolerable. The key compression step is at 140 MeV from 1 mm to 0.25 mm rms bunch length and consists of a 4 dipole magnet chicane. While magnet chicane compression, using path length differences of particles with different momenta, is the only possible way for ultra-relativistic particles, this method unavoidably involves radiation effects when electrons pass the dipole magnets. It has been shown [17,20] that space charge forces and coherent radiation need to be treated simultaneously in order to describe properly beam dynamics. Radiation effects are the dominant contribution to emittance growth in our chicane, see Fig. 5.

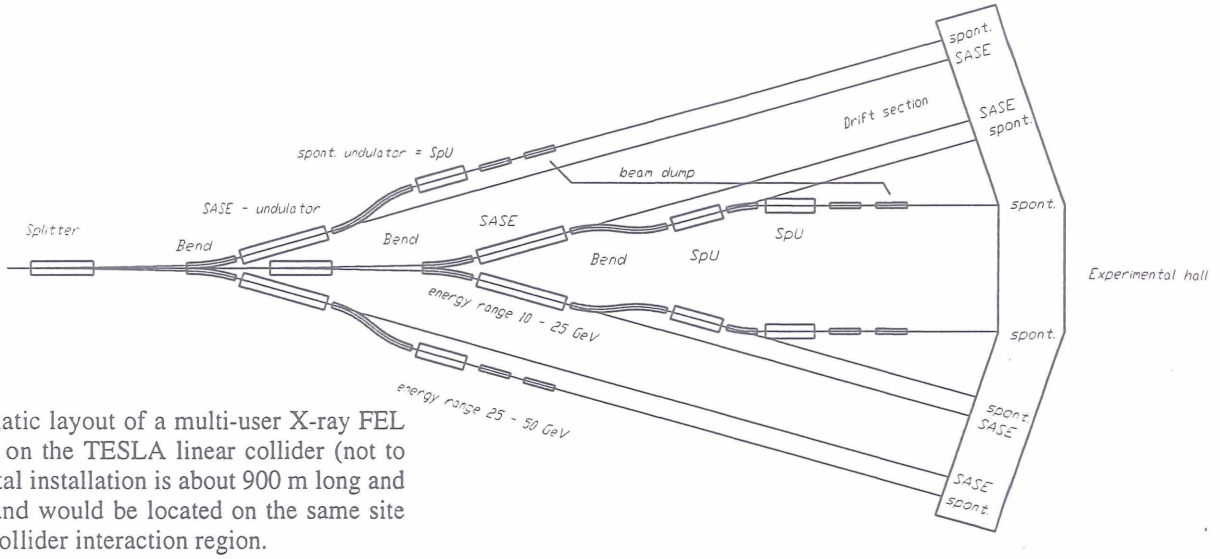

Fig. 4. Schematic layout of a multi-user X-ray FEL facility based on the TESLA linear collider (not to scale). The total installation is about 900 m long and 200 m wide and would be located on the same site as the linear collider interaction region.

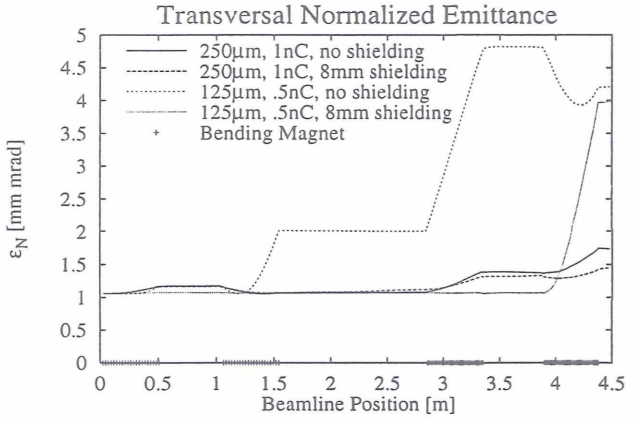

Fig. 5: Evolution of the uncorrelated emittance at the longitudinal center of the electron bunch passing bunch compressor 2. Coherent radiation and space charge are taken into account in this simulation [17]. Two different parameter set are considered, corresponding both to 500 A peak current in the bunch. It is seen that the 125 μm case is more heavily affected.

Significant suppression of coherent radiation by the metallic vacuum chamber is expected at a vacuum chamber height below 8 mm. For experimental verification of this theoretical prediction, the chamber height of bunch compressor 2 will be varied during phase 1 operation. Another issue of test operation will be the stability of rf phase vs. laser phase, since this determines stability of the bunch length, particularly in view of compressor 3. Phase stability below 1 ps has been demonstrated for both the laser and the klystron, which should be sufficient to reach 50 μm rms bunch length in phase 2.

Although compression takes place at high beam energies, space charge turns out to be critical for the whole TTF FEL beam line, from the gun to the undulator, and needs to be taken into account even in the linear optics calculation.

6 BEAM DYNAMICS IN THE ACCELERATOR

Besides space charge and coherent radiation, also wakefields may degrade beam quality. In spite of the low rf frequency of TESLA, longitudinal wake fields are still a concern due to the extremely small bunch length (or to be more precise, due to the large time derivative of the bunch current). It has been shown in [16] that the wake potential of a short bunch is considerably modified while the bunch is passing a longer and longer accelerator structure. For the TTF, the asymptotic case of an infinitely long, periodic structure is reached well before the end of the linac. The bunch still generates extremely high frequency components >680 GHz for which Niobium is known to loose superconductivity. Absorption of these frequency components in the Niobium walls does not seem to be a problem regarding superconductivity, nevertheless, but it may increase the dynamical cryogenic load on the 2K Helium level [21]. Experimental studies on this issue is a subject of TTF FEL, as well as the optimum technical realization

of higher order mode absorbers and additional wake fields due to surface roughness of the vacuum pipe.

7 LONG UNDULATORS

The main technological challenge of the FEL undulator is that the electron beam trajectory must be straight within a tolerance of 10 μm over several meters. This is particularly difficult to achieve since strong quadrupole focussing is superimposed to the undulator field in order to realize the small β function of about 1 m which is optimum for maximum FEL gain. The undulator for TTF FEL phases 1 and 2 is made in permanent magnet, hybrid technology with modules 4.5 m long each [17], see Fig. 6. Since it is impossible to guarantee this straightness from undulator field measurement alone, a beam based alignment strategy has been worked out using a large number of high-resolution beam position monitors [18].

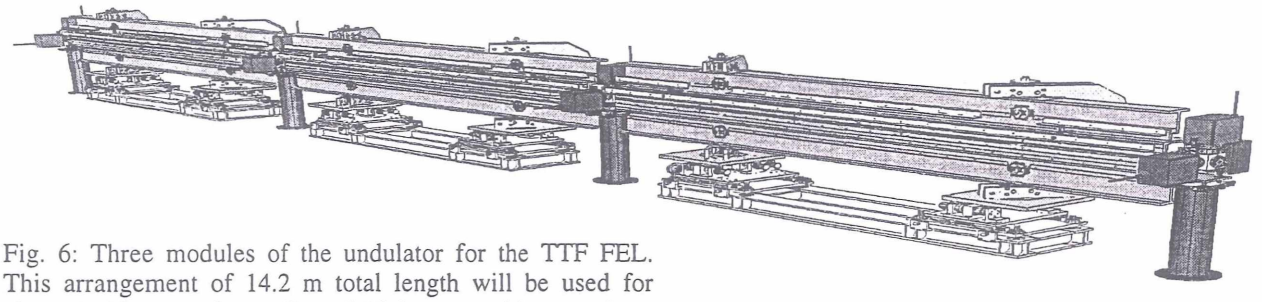

Fig. 6: Three modules of the undulator for the TTF FEL. This arrangement of 14.2 m total length will be used for phase 1. 10 correction coils and 10 beam position monitors per module are squeezed into the 12 mm magnet gap.

8 REFERENCES

[1] J.M. Madey 1971 *J. Appl. Phys.* **42** 1906

[2] A.M. Kondratenko, E.L. Saldin 1980 *Part. Accelerators* **10**, 207

[3] R. Bonifacio, C. Pellegrini, L.M. Narducci 1984 *Opt. Commun.* **50** 373

[4] H. Winick, et al. 1993 *Proc. PAC Washington* and SLAC-PUB-6185

[5] R. Brinkmann et al. 1997 *Nucl. Instr. and Meth. in Phys. Res.* **A 393** 86-92

[6] R. Brinkmann, G. Materlik, J. Rossbach, A. Wagner (eds.) 1997 DESY 1997-048 and ECFA 1997-182

[7] D.C. Nguyen, et al. 1998, Proc. 1998 FEL Conf., to be published in *Nucl. Instr. and Meth. A*

[8] W. Brefeld, et al. 1997 *Nucl. Instr. and Meth. in Phys. Res.* **A 393** 119-124

[9] D. Trines, Status of the TESLA Design, this conference

[10] T. Åberg, et al. 1995, A VUV FEL at the TESLA Test Facility at DESY, Conceptual Design Report, DESY Print TESLA-FEL 95-03

[11] J. Rossbach 1996 *Nucl. Instr. Meth. in Phys. Res.* **A 375** 269

[12] H. Weise, High Gradient Superconducting RF Structures, this conference

[13] Proceedings of workshops on these issues are available at DESY-Hasylab

[14] S. Schreiber et al., The RF-gun based Injector for the TESLA Test Facility Linac, Proc. 1998 EPAC

[15] M. Dohlus, A. Kabel, T. Limberg, Uncorrelated emittance growth in the TTF-FEL Bunch Compression Sections due to Coherent Synchrotron Radiation and Space Charge Effects, Proc. 1998 EPAC

[16] A.N. Novokhatski, A. Mosnier 1996 DAPNIA/SEA-96-08

[17] J. Pflüger et al., *Proc 1996 FEL Conf. Rome* II-107 and *Nucl. Instr. Meth. in Phys. Res.* **A 393** 380

[18] P. Castro: Orbit Correction by Dispersion Minimization in an Undulator with Superimposed FODO Lattice, , Proc. 1998 EPAC, Stockholm

[19] B. Carlsten 1989 *Nucl. Instr. Meth.* **A 285** 313

[20] E.L. Saldin, E.A. Schneidmiller, M.V. Yurkov, 1997 *Nucl. Instr. Meth.* **A 398** 373

[21] P. Schmüser, private communication

[22] S. Reiche, Proc. 1998 FEL Conf., to be published in *Nucl. Instr. and Meth. A*

[23] E.L. Saldin, E.A. Schneidmiller, M.V. Yurkov,, Proc. 1998 FEL Conf., to be published in *Nucl. Instr. and Meth. A*

[24] E.L. Saldin, E.A. Schneidmiller, M.V. Yurkov,, Proc. 1997 FEL Conf., to be published in *Nucl. Instr. and Meth. A*

STATUS OF THE TESLA DESIGN

D. Trines for the TESLA Collaboration *
Deutsches Elektronen-Synchrotron DESY, 22603 Hamburg, Germany

Abstract

The status of the layout of the linear collider project, TESLA, which employs superconducting accelerating structures, will be presented. Latest results from the R&D program on 1.3 GHz superconducting cavities, the accelerating gradients and quality factors which were achieved will be shown as well as the performance of the TESLA Test Facility linear accelerator.

1 INTRODUCTION

Since the first proposal for a superconducting linear e^+e^- collider by M. Tigner [1] in 1965, accelerator builders [2,3,4] have been fascinated by the potential of superconductivity for high energy linear e^+e^- colliders. The low resistive losses in the walls of superconducting cavities yield a high conversion efficiency from mains to beam power. As energy can be stored very efficiently in the cavities, a large number of bunches can be accelerated spaced far apart in a long RF pulse. This allows for a fast bunch to bunch orbit feedback which guarantees that bunches from the opposing beams hit head on at the IP despite ground motion effects.

The shunt impedance per unit length for superconducting cavities depends on RF frequency ω as

$$r_s \sim \frac{\omega}{A\omega^2 + R_{res}} \qquad (1)$$

favouring RF frequencies in the range of 0.5 to 3 GHz. A is a function of temperature and material and R_{res} is the residual surface resistance. Because low frequencies are preferred for s.c. cavities, this make them ideally suited to accelerate low emittance beams, as the emittance dilution by wakefields is small ($W_\perp \sim \omega^3$). In addition tolerances on the fabrication and alignment of cavities are very relaxed.

The luminosity of a linear collider is given by [5,6]

$$L \approx const. \frac{\sqrt{\delta_B}}{E_{CM}} \cdot \frac{\eta}{\sqrt{\varepsilon_{yN}}} \cdot P_{AC} \cdot H_D \qquad (2)$$

where δ_B is the relative energy loss caused by beamstrahlung, E_{CM} is the centre of mass energy of the e^+e^- collision, η is the conversion efficiency from mains power P_{AC} to beam power, ε_{yN} is the normalised vertical emittance at the IP and H_D is the disruption factor. Thus, the figure of merit [7] for the luminosity performance of a linear collider is given by $\eta/\sqrt{\varepsilon_{yN}}$. Therefore the combination of high conversion efficiency and small emittance dilution makes a superconducting linear collider the ideal choice with respect to the achievable luminosity.

2 A SHORT HISTORY OF TESLA

The major challenges to be mastered so that a superconducting linear collider becomes feasible were to increase the accelerating gradients from about 5 MV/m to 25 MV/m and to reduce the cost per length from existing systems by about a factor of four to obtain ~ 2000 $/MV. Encouraged by results from R&D work at CEBAF, CERN, Cornell, DESY, KEK, Saclay and Wuppertal [12,13,14], several institutions - the nucleus of the TESLA Collaboration formally established in 1994 - decided in 1991 to set up the necessary infrastructure at DESY [8] to process and test 40 industrially produced 9 cell 1.3 GHz solid Niobium cavities. The aim was to achieve gradients of 15 MV/m at a Q value of $3 \cdot 10^9$ in a first step and finally reach 25 MV/m at a Q value of $5 \cdot 10^9$ suitable for the linear collider. The infrastructure of the TESLA Test Facility TTF consists of cleanrooms, chemical treatment installations, a 1400° C purification furnace, a high pressure water rinsing system, a cryogenic plant to operate vertical and horizontal cavity test stands at 1.8 K and a 1.3 GHz RF source. A detailed description of the infrastructure, which was completed by the end of 1995, will be given in [9].

In addition the collaboration decided to build a 500 MeV linac as an integrated system test to demonstrate that a linear collider based on s.c. cavities can be constructed and operated with confidence.

Considerable attention has been given to the subject of cost reduction [10,11]. For example:

- The number of cells per accelerating structure was increased to 9 compared to the customary 4-5. This

* TESLA Collaboration: **Armenia:** Yerevan Physics Institute, **P.R. China:** IHEP Academia Sinica, Tsinghua Univ., **Finland:** Inst. of Physics Helsinki, **France:** CEA/DSM Saclay, IN2P3 Orsay, **Germany:** Max-Born-Inst. Berlin, DESY Hamburg and Zeuthen, GH Wuppertal, Univ. Hamburg, IAP Univ. Frankfurt, GKSS Geesthacht, FZ Karlsruhe, IfH TU Darmstadt, ITE TU Berlin, IKK TU Dresden, RWTH Aachen, Univ. Rostock, **Italy:** INFN Frascati, Legnaro, Milano, Univ. Roma II, **Poland:** Polish Acad. of Sciences, Univ. Warsaw, INP Krakow, Univ. of Mining & Metallurgy, Polish Atomic Energy Agency, Soltan Inst. for Nuclear Studies, **Russia:** JINR Dubna, IHEP Protvino, INP Novosibirsk, **USA:** Argonne National Lab., Cornell Univ., Fermilab, UCLA

reduces the number of RF input and HOM couplers, tuning systems and cryostat penetrations, it also simplifies the RF distribution system and increases the filling factor.

- Costly cryostat ends and warm to cold transitions were avoided by combining eight 9 cell cavities and optical elements, which were all chosen to be superconducting, into one long, simple cryostat. Also the complete helium distribution system has been incorporated into the cryostat using the cold low pressure gas return tube as support structure for cavities and optical elements.

From the work starting in 1990 [13] a concept for a 500 GeV cm energy superconducting linear collider emerged, operating at 1.3 GHz with a gradient of 25 MV/m at $Q=5\cdot10^9$ and a luminosity of some $5\cdot10^{33}$ cm^{-2} sec^{-1}. A conceptual design report (CDR) was published in May 1997 [15] giving a complete description of the machine including all subsystems. The report includes a joint study with ECFA on the particle physics and the detector layout.

Since 1990 interest has grown [16,17] in linac driven X-ray FEL radiation, based on the Self-Amplified Spontaneous Emission (SASE) principle [18,19]. As the requirements on the emittance of the beam for a short wave length FEL are very demanding, again a superconducting low RF frequency linac lends itself as the best choice for such an application. The CDR includes the layout of an X-ray FEL facility integrated into the linear collider as well as various scientific applications of the FEL radiation. A detailed report on the status of the X-ray facility will be given at this conference [20].

3 R&D RESULTS AND ACTIVITIES

Up to now 25 9-cell Niobium cavities have been tested at the TTF. The majority of the cavities exceeded the initial TTF design goal of 15 MV/m at $Q=3\cdot10^9$. Fig. 1 shows the measurements in the vertical test stand [26] of all cavities excluding only those with a well identified fabrication error. On average a gradient of 22 MV/m at $Q=10^{10}$ is obtained. In the most recent measurement in the horizontal test [25] a gradient of 33 MV/m at $Q=4\cdot10^9$ has been achieved.

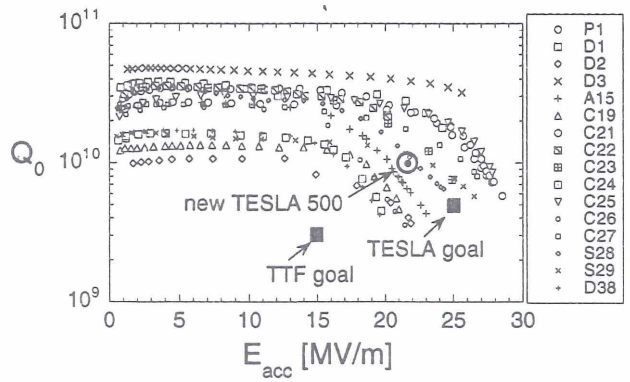

Figure 1: Quality factor Q versus acc. gradient for all 9-cell cavities without fabrication error (vertical test).

The performance limitations seen in six cavities were due to an improper welding procedure and could be eliminated in the subsequent cavity production. The remaining cavities not performing to expectations showed inclusions of Tantalum grains in the Niobium. Such defects will be avoided by scanning all Nb sheets for impurities with an eddy-current method. For a detailed information on cavity treatment procedures and results see [9,21].

All components for beam acceleration through the first cryomodule were installed in May 97. As the 14 MeV injector was already in operation at design values [22], stable beam acceleration in the first module could be established within a few days. Although the module contained 5 out of 8 cavities with fabrication errors, acceleration gradients of 16.7 MeV/m were obtained in a RF pulse of 100 μsec. For more details see [21,27].

The measurement of cryogenic properties of the module such as cryogenic loads, behaviour of cavity positions during thermal cycles and vibrations stayed well within the expected limits [23]. Detailed reports on the low level RF control, achieving a very impressive stability of phase and amplitude of the accelerating fields, will be given at this conference [24].

Several alternatives to the welding of dumb-bells for the production of 9-cell Niobium cavities - like hydroforming [28,32], spinning [29], or plasma spraying of copper on thin walled Nb cavities [30] - are being pursued within the collaboration. If successful, these methods may eventually lead to a further cost reduction in the cavity fabrication.

A very important new development was initiated by the proposal of a cavity "superstructure" [31]. In this scheme the spacing between adjacent cavities is reduced from 1.5 to 0.5 RF wavelengths and a group of 4 or more of these closely spaced cavities is supplied with RF power by only one input coupler. In this way the filling factor - the ratio of active to total length - increases from 66 % to 76 % or more, thus reducing the required gradient for 500 GeV cm operation from 25 to 21.7 MV/m for fixed linac length. The cost reductions due to the smaller number of RF input couplers and cryostat penetrations, and the simplification of the RF distribution system are obvious.

4 TESLA PARAMETERS

In the Conceptual Design Report the machine parameters were chosen such that luminosity and beamstrahlung energy loss were comparable to other linear collider designs [33]. The potential of the superconducting linac to accelerate a very small emittance beam with small emittance dilution was not exploited intentionally, keeping requirements on the alignment and stability of the linac and final focus components quite relaxed. Since the completion of the CDR, however, this strength of the TESLA concept has been investigated to some extent [34] leading to a new parameter set [35] suited for high luminosity operation at 500 GeV cm energy (see Table 1). The bene-

fits of the new "superstructure" concept have been incorporated into the design.

Table 1: Updated parameters at E_{cm}=500GeV in comparison with the original reference parameters.

	TESLA (ref.)	TESLA (new)
site length [km]	32.6	32.6
active length [km]	20	23
acc. Gradient [MV/m]	25	21.7
quality factor Q_0 [10^{10}]	0.5	1
t_{pulse} [μs]	800	950
# bunches n_b/pulse	1130	2820
bunch spacing Δt_b [ns]	708	337
rep. rate f_{rep} [Hz]	5	5
N_e/bunch [10^{10}]	3.6	2
ε_x / ε_y (@ IP) [10^{-6}m]	14 / 0.25	10 / 0.03
beta at IP $\beta_{x/y}^*$ [mm]	25 / 0.7	15 / 0.4
spot size σ_x^*/σ_y^* [nm]	845 / 19	553 / 5
bunch length σ_z [mm]	0.7	0.4
beamstrahlung δ_B [%]	2.5	2.8
Disruption D_y	17	33
P_{AC} (2 linacs) [MW]	95	95
efficiency $\eta_{AC \to b}$ [%]	17	23
luminosity [10^{34} $cm^{-2}s^{-1}$]	0.68	3

The reduction of the required gradient (25→21.7 MV/m) leads to an increase of the quality factor from $5 \cdot 10^9$ to 10^{10}. Both effects lower the required power for the cryogenics. This power savings has been invested in the beam power. The resulting lower loaded Q-value corresponds to a shorter filling time of the cavities, which in turn results in an increased conversion efficiency from mains to beam power (17→23 %).

Although the vertical emittance has gone down by almost an order of magnitude as compared to the CDR, tracking simulations [36] show that the emittance only grows by 23 % and 17 % due to single bunch and multi bunch effects respectively. However, most of the growth due to multibunch effects is not an incoherent spot size dilution but a systematic variation of the beam center along the bunch train at the IP. In combination with the larger disruption parameter - as compared to the CDR - these offsets may drive the opposing beams apart and critically reduce the luminosity. Fortunately, being mostly systematic, the offsets can be strongly reduced by the fast bunch to bunch orbit feedback. Further investigations of this topic will be needed, however.

As is to be expected the smaller spot sizes of the colliding beams put stronger requirements on the accuracy of the fast orbit feedback at the IP [37]. To keep the luminosity loss below 7 % the relative offset of the opposing beams at the IP has to be kept below 0.1 σ_y [38]. This requires a bpm resolution at the final focussing quadrupoles of 2 μm, which should be feasible.

As, for a given beam energy and beam power, the disruption parameter D_y is proportional to the product of luminosity and bunch length [35], the increase of D_y at a higher luminosity can be compensated by shortening the bunchlength. This handle has been applied only moderately up to now in the new design due to problems in the damping rings.

The TESLA damping rings are quite unconventional machines. At a beam energy of only 3.2 GeV they have a circumference of 17 km, of which 95 % are straight sections, located inside the TESLA tunnel (see Figure 2). Only two short return bends on either side with extra tunnels are needed ("dogbone"), thus saving substantially on civil engineering costs. However, the large circumference C and the low energy lead to an unfavourable enhancement factor of the incoherent space charge tune shift:

$$\Delta Q \sim \frac{C}{E^2} \cdot \frac{N_e}{\sigma_z \sqrt{\varepsilon_x \varepsilon_y}} \qquad (3)$$

Already for the CDR parameters the vertical tune shift amounted to -0.18. Further reductions of bunchlength and emittances therefore would lead to uncomfortably large tune shifts. The proposed cure for this problem [39] is to increase the beam size in the long straight sections by coupling the longitudinal or horizontal emittance to the vertical plane. First calculations [40] show that the space charge tune shift can be very effectively reduced in this way without trading in problems due to intra-beam scattering.

5 LAYOUT OF THE COLLIDER FACILITY

There has been consensus within the collaboration that the linear collider facility must be built at an existing high energy physics laboratory to make use of the existing infrastructure and staff. In the CDR two possible sites have been envisaged, one being DESY, the other Fermilab. Both sites allow for a future option to collide 500 GeV e^-/e^+ with high energy protons circulating in HERA or the Tevatron.

This option fixes the possible direction of the linear collider. At DESY the tunnel is foreseen with the main linac axis being tangential to the West straight section of HERA, extending about 32 km into the state of Schleswig-Holstein. The countryside is flat at about 10 m above sea level with maximum height variations of some 10 m. The tunnel axis is foreseen at 8 m below sea level, giving more than sufficient soil coverage for radiation protection. The soil, consisting mainly of sand, allows for easy tunneling by the hydroshield method, which was also used at HERA. The tunnel follows the earth's curvature

over most of its length, except for a section of about 5 km length to direct the tunnel axis tangentially to HERA.

A view into the planned tunnel (diameter 5.2 m) is shown in Fig. 2 at a section which contains the straight sections of the "dogbone" damping ring (upper left side) and several beam lines (right below the cyromodule) to the FEL facility. At the top of the tunnel there is a monorail for the transportation of equipment and personnel.

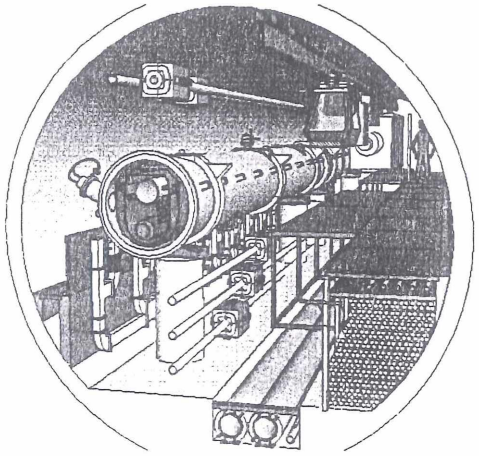

Figure 2: View into the TESLA Tunnel.

Klystrons and their pulse transformers are installed horizontally below the floor in the middle of the tunnel above the cooling water tubes. There is a total of about 625 10 MW klystrons including about 2.5 % spare. Each klystron feeds 32 9-cell cavities corresponding to a length of about 48 m. With a lifetime of 40,000 hours about 10 klystrons will have to be replaced in a one day interruption once per month.

The experience of the SLC [41] on the failure rate of modulators does not permit an installation into the tunnel, inaccessible during machine operation. Therefore in the present layout the modulators are housed in service halls above ground connected to the pulse transformers in the tunnel by long cables (Fig. 2, lower right). However, the design of modulators reliable enough to be installed into the tunnel is being investigated.

Service halls, spaced along the collider at a distance of about 5 km are needed for the cryogenic plants [42] in any case. The length of superconducting linac that can be cooled by a cryoplant is about 2.5 km. This distance is mainly determined by the pressure drop in the large return tube (300 mm diameter) for low pressure Helium gas at about 2 K. The pressure in tube determines the vapour pressure of the superfluid helium surrounding the cavities and thus the operating temperature of the cavities.

Each service hall houses two cryoplants each supplying a 2.5 km section of the linac. In case of a failure of one plant, the other one can supply two sectors operating the collider at a reduced repetition rate. The big cryogenic boxes are planned to be installed in the 14 m diameter shaft connecting the service hall with the tunnel (see Fig. 3).

Due to the large spacing between consecutive bunches, there is no crossing angle required at the IP and consequently no angle between the tunnel axis of the two linacs. The beams are deflected by electrostatic separators, having passed the interaction region and the large aperture, superconducting quadrupole doublet. A tunnel length of about 1.2 km between the IP and the ends of either superconducting linac is needed for the beam delivery system [15] containing beam collimation systems, beam diagnostics and orbit correction elements, and the final focus system, demagnifying the beam size and correcting chromatic effects. These tunnel sections also house the beam dumps and the positron source.

As the amount of positrons needed for a beam pulse exceeds the potential of conventional positron sources, the electron beam having passed the interaction region is used to produce the required number of positrons. In this scheme, proposed in the original VLEPP design [43], the spent electron beam is collimated and passed through a wiggler producing large quantities of γ-rays, which convert in a thin rotating target into e^+e^- pairs. The fraction of positrons which can be captured by the source optics, accelerated to 3 GeV and stored in the dogbone damping ring yields a sufficient number of particles for the operation of the linear collider. With the new design parameters the fraction of the spent electron beam usable for positron production actually increases from 86 % to 93 % due to the smaller beam emittance, thus substantially reducing the power load on the collimators [44]. Although a detailed technical layout of the positron source is still missing, first investigations indicate that the whole system can well be accommodated into the tunnel.

6 ENERGY UPGRADE POTENTIAL

With the new "superstructure" concept the gradient needed for 800 GeV cm energy is 34 MV/m. From the results on cavity R&D (section 3) the optimism, that average gradients well above 30 MV/m at Q values of $5 \cdot 10^9$ can be reached within the near future, is well justified. The theoretical maximum gradient for our structures limited by the critical magnetic field is at about 55 MV/m.

All subsystems of the collider have been laid out for 800 GeV operation. The number of klystrons and modulators will be doubled. With the present layout of the cryogenics the repetition rate of the collider will have to be reduced from 5 to 3 Hz to maintain the level of available cooling capacity. By further reducing the normalised vertical emittance by a factor 3 to 10^{-8} m , a luminosity of $5 \cdot 10^{34}$ cm^{-2} sec^{-1} can be obtained [35], the beamstrahlung energy loss staying below 5 %. The mains power requirement will go up to 130 MW. An upgrade of the cryogenic cooling capacity will allow luminosities close to 10^{35} cm^{-2} sec^{-1} to be reached by running the collider at a repetition rate of 5 Hz.

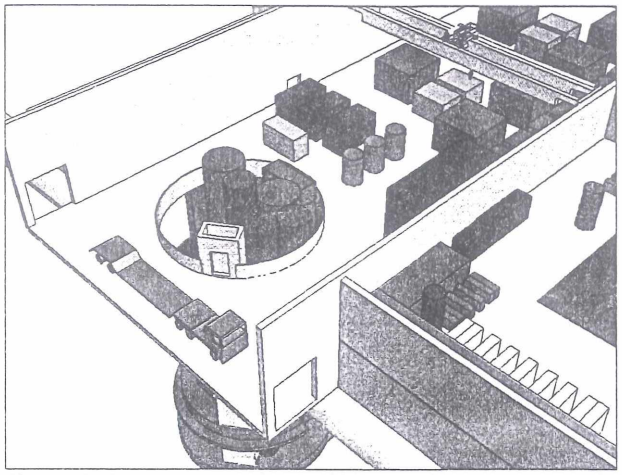

Figure 3: Service hall with shaft connection to the tunnel.

7 OUTLOOK

On the basis of the existing knowhow, orders to industry are being issued to evaluate the requirements of large scale industrial cavity production. Together with a detailed layout of all subsystems of the collider the information from the industrial studies will allow for a proposal containing technical design of the facility, and a reliable schedule and cost evaluation, to be submitted in two to three years from now. To obtain public acceptance the states, the communities, and the residents involved have been informed about the planning. An administrative procedure to eventually ensure the necessary legal conditions for the construction of the facility - if approved - is underway.

8 ACKNOWLEDGMENTS

I would like to express my respect to the many people in and outside the collaboration who have been working on the cavity R&D over the years. This work has been certainly cumbersome at times but finally lead to the beautiful cavity results, which we have today. Many people have contributed to the present status of the TESLA design, whom I cannot give proper credit to. But I would like to give special credit to the late G. Horlitz for designing the complete cryogenics system of TESLA.

9 REFERENCES

[1] M. Tigner, Nuovo Cimento, 37 (1965) 1228.
[2] U. Amaldi, Phys. Lett., B61 (1976) 313.
[3] J. Kirchgessner et al., HEACC, Geneva 1980.
[4] H. Gerke and K. Steffen, DESY PET-79/04 (1979).
[5] R. Palmer, New Developments in Particle Acceleration Techniques, Orsay 1987, CERN 87-11, ECFA 87/110.
[6] R. Brinkmann, DESY M-95-10 (1995).
[7] J.P. Delahaye, G. Guignard, T. Raubenheimer and I. Wilson, LC97, Zvenigorod, Russia, Vol. I, p. 428.
[8] TTF-Proposal, DESY-TESLA-93-01.
[9] H. Weise, Contribution to this conference.
[10] H. Padamsee, EPAC92, Berlin.
[11] D. Trines et al. HEACC92, Hamburg, Vol. II.
[12] 4th Workshop on RF Superconductivity, Tsukuba 1989, KEK Report 89-21, Ed. Y. Kojima.
[13] 1st International TESLA Workshop, Cornell 1990, CLNS 90-1029.
[14] 5th Workshop on RF Superconductivity, Hamburg 1991, DESY M-92-01.
[15] Conceptual Design of a 500 GeV e^+e^- Linear Collider with Integrated x-ray Laser Facility, Ed. R. Brinkmann, G. Materlik, J. Rossbach, A. Wagner, DESY 1997-048, ECFA 1997-182.
[16] L. Serafini, M. Ferrario, C. Pagani, A. Ghio, P. Michelato, A. Peretti, LNF-90/035 (R).
[17] C. Pellegrini, Workshop on Fourth Generation Light Sources, SSRL Report 92/02, p. 364.
[18] R. Bonifacio, C. Pellegrini, L. N. Narducci, Opt. Communi Vol. 50, No. 6 (1984).
[19] Ya. S. Derbenev, A. M. Kodratenko and E. L. Saldin NIM, A193, 415 (1982).
[20] J. Rossbach, Contribution to this conference.
[21] M. Pekeler, EPAC98, Stockholm.
[22] T. Garvey et al., PAC97, Vancouver.
[23] J. G. Weisend II et al., ICEC98, Bournemouth, UK.
[24] S. Simrock, Contribution to this conference.
[25] P. Clay et al., ICEC95, Columbus, Ohio.
[26] T. H. Nicol et al., IEEE Proceedings PAC93, Vol. 2.
[27] W.-D. Möller, Contribution to this conference.
[28] I. Gonin et al., TESLA 98-09
[29] V. Palmieri, Contribution to this conference.
[30] M. Fouaidy et al., EPAC98, Stockholm.
[31] J. Sekutowicz, M. Ferrario and C. Tang, EPAC98, Stockholm and TESLA 98-08.
[32] C. Z. Antoine et al., 8th Workshop on RF Superconductivity, Abano Terme 1997, DAPNIA/SEA-98-10.
[33] G. Loew (ed), Int. Linear Collider Technical Review Commmittee Report, SLAC-R-95-471.
[34] R. Brinkmann, TESLA 97-13.
[35] R. Brinkmann, EPAC98, Stockholm.
[36] A. Mosnier, unpublished contribution.
[37] I. Reyzl, PhD Thesis, TU Berlin, 1998, to be published.
[38] O. Napoly, D. Schulte, unpublished contribution.
[39] N. Walker, unpublished contribution.
[40] K. Balewski, unpublished contribution.
[41] A. R. Donaldson, J. R. Ashton, 20th Int. Power Mod. Symp., Myrtle Beach, South Carolina, 1992.
[42] S. Wolff et al., ICEC98, Bournemouth, UK.
[43] V. E. Balakin, A. A. Mikhailichenko, Preprint INP 79-85.
[44] R. Glantz, unpublished contribution.

HIGH GRADIENT SUPERCONDUCTING RF STRUCTURES

H.Weise for the TESLA Collaboration
Deutsches Elektronen-Synchrotron DESY, 22607 Hamburg, Germany

Abstract

Superconducting (s.c.) RF structures for the acceleration of electrons have been known for over 30 years (HEPL, Stanford). More than 10 years after their successful start a new generation (i.e. standing wave, π-mode cavities), made from niobium and operated at frequencies between 352 MHz and 3 GHz, was established at accelerators being operated for high energy physics (CERN, DESY, KEK) as well as nuclear physics (CEBAF, Darmstadt) experiments. Although the HEPL s.c. cavities were limited to a 10% duty cycle and the 2nd generation now allows continuous wave operation, the increase of the accelerating gradient was remarkably small with respect to the > 50 MV/m limit given by the physics of RF superconductivity.

Thirty years ago HEPL cavities reached about 2 MV/m; 15 years later DESY cavities achieved 4 MV/m. And the large 338-cavity CEBAF installation is based on a 5 MV/m gradient, the commissioning of the accelerator being less than 10 years ago. Since 1992 the TESLA (TeV Energy Superconducting Linear Accelerator) collaboration has studied the fundamental problems in cavity fabrication as well as operation. Last year an 8 mA electron beam was successfully accelerated in a 15 MV/m module containing 8 s.c. 9-cell cavities. Two more modules (20 to 25 MV/m) will be installed. From recent cavity tests a gradient of 25 MV/m can be taken as state of the art. Cavity production, preparation, and installation was remarkably improved, a prototype linac (TESLA Test Facility Linac) for a large linear collider shows good performance.

1 RF SUPERCONDUCTIVITY AND LINEAR ACCELERATORS

In 1961 Banford and Stafford [1] at Harwell proposed the feasibility of a superconducting proton linac, and have carried out experimental measurements on lead and niobium at 400 MHz using quarter-wavelength hairpin resonators. Similar measurements were started by Susini [2] and others at CERN and the University of Lausanne on lead and niobium surfaces at 300 MHz using a capacitively-loaded coaxial resonator. Here the interest was in building a s.c. separator. Also in 1961, a program was started at Stanford University to measure the properties of superconductors in a microwave cavity at 2856 MHz [3]. This program started the pioneering work for the application of superconducting RF structures for the acceleration of electrons.

The Stanford cavity was about 14 cm in diameter by 14 cm in length and was resonant at 2865 MHz in the TE011 mode. In this mode there is no current flux across the joints between the cavity side wall and the two end plates, so that the quality factor Q is independent of these joints. Several types of tin and lead surfaces were measured. Electroplated surfaces gave the highest Q's. A residual resistivity was always observed as T approached zero. Today we know from the theory of RF superconductivity that this is not due to improper cavity fabrication but can be explained by the BCS theory of superconductors. Nevertheless, material properties are limiting the achievable accelerating gradient. We characterize the state of the art material by the so-called RRR (residual resistivity ratio) which is a direct measure of the thermal conductivity.

At the 1963 International Conference on High Energy Accelerators in Dubna the Stanford group published a very preliminary design of a 20 GeV - 10% duty cycle superconducting accelerator. This at a time at which no real cavity has ever been built. The remarkable numbers were an assumed length of 3000 m corresponding to about 10 MV/m (active/total length ratio of 66%), and a power dissipated in the walls of the structure of 200 kW average, i.e. 100 W/m; the forward power was claimed to be 2 MW average, so that the total beam power of 1.8 MW average corresponded to almost 100 μA average electron beam current. Ref. [4] can be used to compare this design with the actual TESLA design [5] for a 500 GeV c.m. linear collider.

Based on the TE011 measurements the Stanford group designed and built the first two accelerating cavities, one TM010 and one 2 π/3 mode cavity. In 1965 an accelerating gradient of 3.7 MV/m was reached at an unloaded Q_0 of $2.5 \cdot 10^8$ [6]. The cavity was electroplated with lead and operated close to 2856 MHz. Radiation exceeding 100 mR/h provoked the optimistic statement *The radiation provides indirect evidence of strong accelerating fields*. The explanation for the field emission limit was a possible local enhancement of the electric field by a factor 200 caused by sharp projections on typical surfaces [7]. Today we use enhancement factors of

100 to 1000 to explain the level of field emission using Fowler-Nordheim theory.

During the discussion of a LINAC 64 conference paper [8] the author felt that *the present state of knowledge of RF superconductivity was sufficiently discouraging to abandon further work on a superconducting proton linac.* Suelzle from Stanford wrote almost 10 years later *lower-than-expected accelerating gradients have necessitated the re-evalution of the energy objectives* [9]. The hope for getting roughly 14 MV/m in a 6-meter long, 1300MHz accelerating structure was not fulfilled. By the end of 1972 the 1300 MHz structures were limited to 3 MV/m. But the first superconducting electron linac was commissioned. It produced an 8 MeV, 250 μA beam with 12 keV · deg (FWHM) and a transverse emittance of less then 1 π mm mrad. Today the HEPL accelerator is used to drive different undulators and produce Free Electron Laser radiation in the infrared.

2 S.C. CAVITIES FOR STORAGE RINGS

The somewhat disappointing results from Stanford certainly have de-emphasized the search for high gradients. But in the late 70's the use of s.c. cavities in storage rings was considered. Here gradients of a few MV/m were sufficient. Important were instability thresholds - an adequate damping of higher order modes (HOMs) for multiturn operation was needed. Tests in existing storage rings led to promising results as reported [10-11]. Today we can find 352-MHz cavities in LEP as well as 500-MHz cavities in HERA. The first Workshop on RF Superconductivity, organized in 1980 by the Kernforschungszentrum Karlsruhe (KfK), summarized all activities aiming for the use of RF superconductivity for acceleration of ions as well as electrons.

While all first β=1 cavities were of cylindrical symmetry, i.e. a pill box with slightly smoothed out edges, one can find the first spherical resonators around 1980. According to [12] the Genoa / Italy 3-cell C-band structure was built in spherical geometry because of easier manufacturing. The result was amazing, the comparison of the maximum accelerating field shows the remarkable gradient of 8 MV/m. Somewhat later the spherical geometry was found to be the best in order to avoid multipacting. The high radiation levels in the HEPL tests were not only caused by simple field emission but by resonant electron emission, i.e. multipacting.

Within a short time the five laboratories being the driving forces towards high gradient β=1 structures, CERN, Cornell, DESY, KEK, and Wuppertal, concentrated on the spherical geometry. The E_{peak}/E_{acc} ratio was optimized to be about 2 for any geometry. Some cavities had a wall section being exactly perpendicular to the cavity axis (remains of the old pill box). Later the elliptical geometry was found to be best because of easier chemistry and water cleaning. The resonator frequencies and the number of cells varied from 352 MHz / 4-cell (CERN) to 3 GHz /5 & 20-cell (Cornell; Wuppertal - for the S-DALINAC / Darmstadt).

A significant frequency dependence of the maximum obtainable accelerating field could not be found. The choice of frequency was determined by the need to combine the cavity operation with other normal conducting structures or by the existence of klystrons. For most of the listed cavities the maximum number of cells was chosen from HOM calculations. The need to damp HOMs and to have sufficient coupling between the input coupler and the cavity led to slightly different designs.

3 HIGHER GRADIENTS, LOCALIZED DEFECTS, AND HIGHER RRR

For many years the design goal for superconducting structures was about 5 MV/m. This was based on experience with multicell cavities. Nevertheless, the goal of high gradients was never forgotten since the BCS theory predicted maximum gradients of almost 50 MV/m at 2 K. Considerable effort has been devoted to the understanding of surface defects. Larger defects could be localized and sometimes even eliminated by grinding. In 1979 the technique of temperature mapping was developed at CERN and it was demonstrated that well localized defects were one of the prime causes of quenching [13]. Over the years these temperature mapping devices have been improved, and more diagnostics like X-ray diodes and RRR measuring devices using eddy current induced by small coils have been introduced.

Cornell pointed out that the threshold for thermal instabilities could be increased if the thermal conductivity, i.e. the RRR of the cavity wall is improved. In a close collaboration with industry the RRR value for the used Nb material was raised from typically 40 (corresponding to a heat conductivity λ = 10 W/(m·K) at 4.2K) to values between 150 and 200. To increase the RRR even further yttrification at about 1250°C was used at Cornell. Later the use of 1400°C UHV baking in the presence of titanium vapor was established.

The combination of eliminating defects and using higher RRR has guaranteed a more reliable way towards accelerating fields of 5 to 10 MV/m in multicell cavities. As examples one can quote results from CEBAF prototype cavities which reached 6-8 MV/m, a single cell KEK 500 MHz cavity (RRR 80) with 7.6 MV/m, the first CERN LEP prototype cavity (4-cell, 352 MHz) with 7.5 MV/m, and last but not least one 20-cell 3GHz cavity for the S-DALINAC which reached 7.8 MV/m after the preparation at Wuppertal. Cornell was able to reach really high gradients in 1.5 GHz single cell cavities: 22.5 MV/m. Wuppertal followed with 23.1 MV/m for a 3 GHz single cell structure.

A few years later the standard material for s.c. cavities was RRR 280. The first multicell cavities reached again higher gradients but shortly after the installation of the first 20-cell cavity in the S-DALINAC the enthusiasm was damped by a new phenomenon. After keeping the cavity at temperatures just above nitrogen temperature (70 - 100K), which can happen in a linac installation, the quality factor dropped, the cryogenic losses were increased by a factor of 10. Darmstadt and DESY found the Q-degradation (sometimes also called Q-disease) at about the same week. Months later it was clearly identified as a clustering of hydrogen and therefore creation of normal conducting niobium hydride areas [14]. For increasing the RRR of the Nb material the oxygen was removed with the disadvantage that the hydrogen is not chemically bound anymore. A cooling of the acid during chemical polishing is necessary to avoid high hydrogen concentration in the niobium. Otherwise Niobium hydride areas start to grow. Baking at temperatures above 750°C can cure the problem.

4 THE STATUS BEFORE TESLA

At the LINAC 92 Conference R. Sundelin presented a good overview about the state of the art in s.c. cavity production [15]. Assembly in clean rooms was standard, the Cornell group had improved gradients using high peak power processing, and CERN used high pressure water rinsing to suppress field emission in the LEP cavities which are made from copper but sputter coated with Nb. The number of superconducting cavity operating hours in larger installations increased substantially.

Table 1:
S.c. cavities in operation as known at the time of the LINAC 92 Conference, i.e. before the start of the TESLA program. The CEBAF installation was ongoing at a rate of 16 cavities per month.

	Nbr.of Cav.		MHz	m	MV/m
MACSE	5	5-Cell	1500	2.5	6.5
S-DALINAC	10	20-Cell	3000	10.0	5.9
HERA	16	4-Cell	500	19.2	3.6
HEPL				30.8	3.0
TRISTAN	32	5-Cell	508	47.2	6.6
CEBAF	106	5-Cell	1497	53.0	7.6
LEP	12	4-Cell	352	20.4	3.7

The achieved accelerating gradients of the different machines are listed above. The CEBAF installation was ongoing at a rate of 16 cavities per month.

5 CEBAF AND LEP INSTALLATION

The CEBAF recirculating superconducting electron linac at Jefferson Lab went in full operation and is now using 330 s.c. cavities operating at 2.0 K. The operation frequency is 1497 MHz. Four pairs of the 0.5-m-long cavities are contained in one cryomodule but each cavity is separately powered by one 5 kW klystron. According to [16] the distribution in the accelerating gradients has its maximum at about 7.5 MV/m with a spread of 5 MV/m FWHM. The principal limitation of the installed cavities is electron field emission and associated phenomena, such as X-ray production, charging and arcing at the cold ceramic RF window, and anomalous 2 K heat load. This affects about 80% of the cavities. Only 12% of the cavities are limited by quench. The average quench limit is at 13 MV/m.

The cavity operation in CEBAF has been quite stable and reliable. In 1997 the maximum energy delivered to the nuclear physics experiments was 4.4 GeV at a beam current of 115 μA. The RF could have supported 5.6 GeV with a five pass beam delivery. In-situ RF-helium processing of the cavities was tested and yielded an additional 41 MeV/pass. Jefferson Lab intends to upgrade the machine to the 6-8 GeV region by this method. Further steps towards higher electron beam energy are described elsewhere [17]. The Jefferson Lab Free-Electron Laser installation can operate above 10 MV/m.

In 1997 CERN operated 240 s.c. cavities in LEP. Out of the 240 cavities 16 were made from solid niobium and 224 were sputtered Nb/Cu cavities. The operation frequency is 352 MHz, the nominal operating field 6 MV/m. Eight cavities are grouped each and driven by one klystron. Two klystrons are connected to one HV power converter. According to [18] the overall performance of the s.c. RF system was good during the 1997 operation period. The average operational gradient of the 224 Nb/Cu cavities was 5.9 MV/m even though some cavities were limited at lower gradients. The four solid Nb modules were running at about 3.6 MV/m (nominal gradient 5 MV/m).

6 THE TESLA R&D EFFORT

Since 1991 the international TESLA collaboration [19] is following an approach to a 500 GeV linear collider using superconducting accelerating cavities. Altogether 35 institutes from nine countries are developing linac components as there are s.c. accelerating structures, couplers, cryostats, RF sources, beam diagnostics etc. The TESLA Collaboration tries in a joint effort to increase the usable accelerating gradient to more than 25 MV/m. A test facility, located at DESY with major components flowing in from members of the collaboration, is going to establish a well-developed collider design. The status of this design work is described elsewhere [5].

The TESLA Test Facility (TTF) includes cavity preparation and testing as well as the final test of cavities in a linac installation [20]. About 25 standard 9-cell 1.3 GHz structures operating in the pi-mode have been prepared and tested. Out of the first production series eight cavities were taken for the assembly of one TESLA cryogenic unit, the TTF module #1.

The goal for the accelerating gradient was set to 15 MV/m average (to be compared with the 1992 state of the art given in table 1) at an unloaded quality factor Q_o=3·10^9. This goal was reached with module #1. Although some cavities are limited below 15 MV/m the maximum achieved electron energy was 125 MeV in short macropulses and 105 MeV in 800 µs long macropulses. The overall performance is limited by the weakest cavities since all eight cavities are driven by one common klystron and the RF forward power is equally split. Details about the operation can be found in [21].

7 THE FIRST TTF CAVITY PRODUCTION

About 25 cavities from 4 different manufacturers were tested in a vertical test cryostat. The average gradient was 19.2 MV/m at $Q_o > 3\cdot10^9$. 14 cavities showed $E_{acc} > 20$ MV/m, 3 cavities showed $E_{acc} > 28$ MV/m. The last 9 cavities delivered and tested had a clearly increased gradient of 24.3 MV/m at $Q_o > 3\cdot10^9$. Figure 1 shows the test results as a function of time. Maximum gradients are plotted as well as the usable gradient defined by the onset of increased cryogenic losses. Some of the very first cavities had maximum acceleration voltage being almost high enough for TESLA 500 but the strong field emission limited the usable gradient.

During 1996 the first group of cavities was tested. High pressure rinsing with ultraclean water reduced the field emission but most of the tested cavities were limited around 13 MV/m. The reason was found to be an insufficient cleaning after the preparation for electron beam welding of the equator. Since summer 1997 another 11 cavities were tested. The average maximum gradient is almost 25 MV/m. Field emission is still an issue and limits the usable gradient to roughly 22 MV/m. Nevertheless, all four manufacturers were able to produce cavities with gradients above or close to 25 MV/m. The gradient of the best TESLA 9-cell cavity is above 30 MV/m. Figure 2 shows the horizontal test result. This cavity is going to be used in the second cryogenic module.

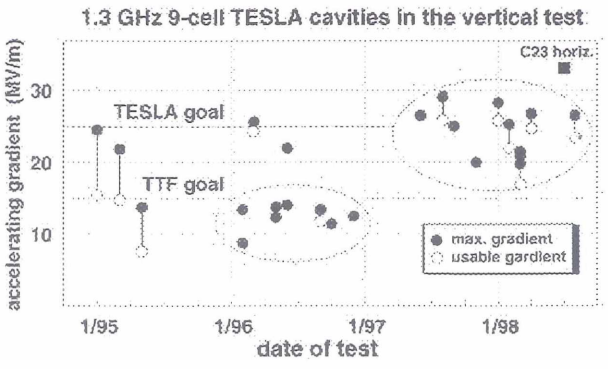

Fig. 1: Vertical test of 1.3 GHz 9-cell cavities.

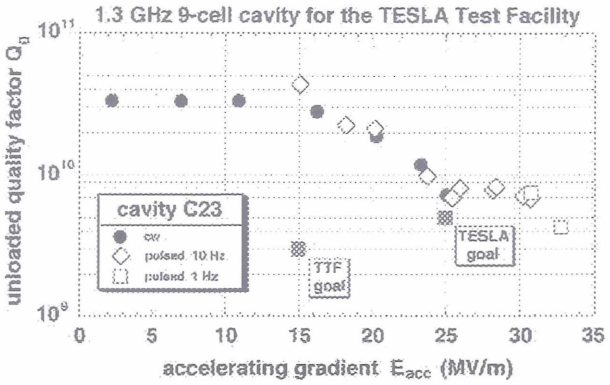

Fig. 2: The best TESLA 9-cell cavity measured in a horizontal test cryostat. For this test the cavity is equipped with the main RF input coupler and the HOM couplers.

8 OUTLOOK

The goal for the second TTF Linac module being just in the assembly phase is 20 MV/m. The third module is expected to reach 25 MV/m. All three modules will be used for a Free Electron Laser experiment in the UV [22]. Further modules will be built to finalize the design of accelerating units of the large TESLA machine [23]. Being installed in the TTF Linac they will finally drive a VUV free-electron laser. Therefore a new cavity production was started. A total number of 26 cavities is expected to be at DESY by end of 1998. The material for all cavities was scanned for inclusions of other metals. A special eddy current scanning apparatus was developed.

Single cell cavities have reached 40 MV/m accelerating field [24]. The members of the TESLA collaboration and also Jefferson Lab as well as KEK are still improving the gradients of resonators made from solid niobium. Electropolishing is studied again in order to smoothen the inner surface. High pressure water rinsing is the most successful method to decrease field emission. Nevertheless, the installation procedure of all RF couplers seems to be a main issue.

With the aim to decrease the cavity production costs two new fabrication methods are studied. Spinning of cavities is described elsewhere [25]. Hydroforming of multicell cavities is also under investigation. Both methods allowed the production of L-band single-cell cavities with accelerating gradients above 20 MV/m. A slightly decreasing Q vs. E_{acc} is not understood. Multicell-cavities are underway and will be measured next.

10 REFERENCES

[1] A. P. Banford and G. H. Stafford, Plasma Physics, J. Nucl. Energy, Part C, 3, 287 (1961).

[2] A. Susini, "Initial Experimental Results Concerning Superconductive Cavities at 300 MHz," CERN Internal Report 63-2, (Febr. 1963).

[3] P. B. Wilson, Nucl. Instr. And Methods, 20, 336 (1963).
[4] P.B. Wilson, H. A. Schwettman, W. M. Fairbank, "Status of Research at Stanford University on Superconducting Eletron Linacs", IV Int. Conf. on High Energy Acc., Dubna 1963, p. 694 (1963).
[5] D. Trines, "Status of the TESLA Design," this conference.
[6] H. A. Schwettman, P. B. Wilson, G. Y.Churilov, "Measurements at High Electric Field Strengths on Superconducting Accelerator Cavities", V Int. Conf. on High Energy Acc., Frascati 1935, p.690 (1965).
[7] H.A. Schwettman, J. P. Tourneaure, R. Waites,"Evidence for Surface-state-enhanced Field Emission in RF Superconducting Cavities", Journ. of Applied Physics, Vol.45, No.2 (1974).
[8] J. M. Dickson, "RF Superconductivity Measurements", LINAC 64 Conference, p. 540 (1964).
[9] L. R. Suelzle, "Progress on RF Electron Superconducting Accelerators", 1973 Part. Acc. Conf., San Francisco, p. 44 (1973).
[10] R. Sundelin, IEEE NS-32 (1985) 3570.
[11] H. Piel, IEEE NS-32 (1985) 3565 and LINAC 84 Conf., p. 260 (1984).
[12] C. Pagani, private communication.
[13] Ph. Bernard et al., XI Int. Conf. on High Energy Acc., Geneva 1980, p .878 (1980).
[14] W. Bonin and R. W. Roeth, "5th RF Supercond. Workshop, Hamburg 1991, DESY M-92-01.
[15] R. M. Sundelin, "Review of Progress in Superconducting High-Beta Structures", LINAC 92 Conf., p. 840 (1992).
[16] C.E. Reece, "Operating Experience with Superconducting Cavities at Jefferson Lab.," 8th RF Supercond.Worksh., Padova 1997, to be publ.
[17] J. R. Delayen, "Development of an Upgrade of the CEBAF Acceleration System", this conference.
[18] O. Brunner, "RF System Reliability and Performance in 1997", 8th LEP Performance Workshop, CERN Internal Reports, CERN-SL-98-006 DI.
[19] The TESLA (TeV Energy Superconducting Linear Accelerator) R&D effort is carried out by a number of institutions which includes: Armenia: Yerevan Physics Institute; China: IHEP, Academia Sinica, Beijing; Tsinghua-University, Beijing; Finland: Institute of Physics, Helsinki; France: CEA/DMS (DAPNIA, CE Saclay); IN2P3 (INP Orsay + LAL Orsay); Germany: RWTH Aachen; Max-Born-Institute, Berlin-Adlershof; TU Berlin; TU Darmstadt; TU Dresden; University of Frankfurt; GKSS, Geesthacht; DESY, Hamburg + Zeuthen; University of Hamburg; FZ Karlsruhe; University of Rostock; University of Wuppertal; Italy: INFN Frascati; INFN Legnaro; INFN Milano; INFN and University Roma II; Poland: Polish Academy of Science; University of Warsaw; Institute of Nuclear Physics, Cracow; Univ. of Mining & Metallurgy, Cracow; Pol. Atomic Energy Agency, Warsaw; Soltan Institute for Nuclear Studies; Otwock-Swierk; Russia: JINR, Dubna; IHEP Protvino; INP Novosibirsk; USA: ANL, Argonne IL; Cornell University, Ithaca NY; FNAL, Batavia IL, UCLA, Los Angeles CA.
[20] D. A. Edwards (ed.), TESLA Test Facility Linac - Design report, DESY-TESLA-95-01 (1995).
[21] W. D. Moeller, "The Performance of the 1.3 GHz Superconducting RF Cavities in the First Module of the TESLA Test Facility Linac", this conference.
[22] J. Rossbach, "The TESLA Free Electron Laser - Concept and Status", this conference.
[23] R. Brinkmann, G. Materlik, J. Rossbach, A. Wagner (eds.), "Conceptual Design of a 500 GeV e^+e^- Linear Collider with Integrated X-ray Laser Facility, DESY 1997-048 and ECFA 1997-182.
[24] M. Ono et al., "Achievement of 40 MV/m Accelerating Field in L-Band SCC at KEK", 8th RF Superconducting Workshop, Padova 1997, to be published.
[25] V. Palmieri, "Review of Fabrication of SC Cavity Structures", this conference.

PERFORMANCE OF AN S-BAND KLYSTRON AT AN OUTPUT POWER OF 200MW

S. Choroba, J. Hameister, S. Jarylkapov*
DESY, 22603 Hamburg, Germany, * on leave from INR, 117312 Moscow, Russia

Abstract

In order to provide RF power to the accelerating sections of a future S-Band linear collider, klystrons producing 150MW of output power at a frequency of 2.998GHz are required. Two S-Band klystrons with a nominal output power of 150MW at a pulse duration of 3μs and a repetition rate of 50Hz were developed in a collaboration between SLAC, Philips, TH Darmstadt and DESY [1]. They were built and successfully tested at SLAC in 1994 and 1995 and then shipped to DESY to feed the accelerating sections of the S-Band test facility linac. In order to explore their power potential one of the klystrons was operated at an even higher output power of more than 200MW at the test facility. HV pulses up to 610kV at a current of 780A were applied to the klystron cathode. This paper reports the results of the measurements of the various parameters of the klystron at this power level (e.g. output power, efficiency, perveance). It describes the performance and the limitations of the klystron in this power range.

1 INTRODUCTION

A possible future S-Band linear collider would require more than 5000 klystrons, capable of an output power of 150MW at a pulse duration of 2.8μs and repetition rate of 50Hz. Until 1992 klystrons meeting these demands were not available. The well known SLAC 5045 klystron achieved 65MW at a pulse duration of 3.5μs [2]. A klystron with an output power of 150MW at 1μs pulse width was developed at SLAC in 1985 [3]. In 1992 a collaboration between SLAC, TH Darmstadt, Philips and DESY was settled to develop a klystron meeting the demands of an S-Band linear collider. Two klystrons were built and successfully tested at SLAC. The results are reported in [1]. Table 1 shows the design and the parameters of the two klystrons, which were measured during the tests at SLAC.

Later C. Bearzatto and G. Faillon of Thomson in France reported, that they had developed and tested an S-Band high power klystron with an output power of 150MW at a pulse width of 1μs [4].

Both klystrons, built at SLAC, are now in operation at the S-Band test facility at DESY. The second tube was used to investigate whether an even higher peak output power than 150MW is possible. The output waveguides of the klystron were connected to RF water loads. The klystron cathode voltage was carefully raised from 550kV to a higher voltage. In the following we describe the klystron operation at the higher power level. The results of the measurements are presented.

Table 1: Parameters of the klystrons for the S-Band test facility (design and measured during tests at SLAC)

	Design	Tube#1	Tube#2
Power Out	150 MW	153 MW	150 MW
Pulse Duration	3 μs	3 μs	3 μs
Repetition Rate	60Hz	60Hz	60Hz
Beam Voltage	535 kV	527 kV	508 kV
Beam Current	700 A	680 A	652 A
Microperveance	1.79	1.78	1.80
Efficiency	40 %	43 %	45 %
Gain	> 50 dB	56 dB	57 dB

2 THE KLYSTRON

Figure 1 shows klystron #1. The total height is 2.6m, the diameter of the anode housing is 40cm and the weight is about 300kg. The cathode has a diameter of 13.3cm and a cathode loading of 6.12A/cm^2. The beam area convergence is 40:1. The maximum electric fields on the focus electrode and anode are 180kV/cm and 210kV/cm, respectively. Seven cavities including the input and output cavities are in the 3.2cm wide drift tube.

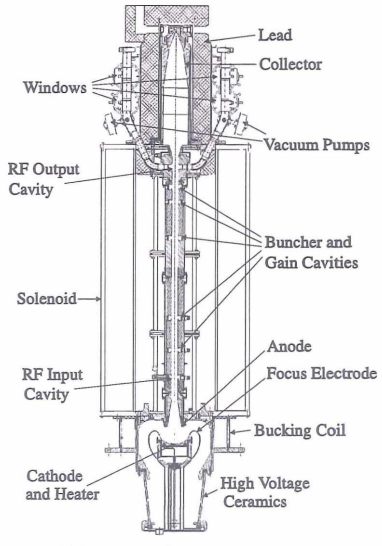

Figure 1: Layout of klystron #1

The klystron has two output waveguides, which are splitted and recombined again, so that there are two RF windows in each output waveguide. The waveguide

assembly on each side is the well proven design of the SLAC 5045 klystron.

The klystron requires a solenoid with a magnetic field of 1800G and a power consumption of 14kW. A bucking coil is needed to achieve zero magnetic field on the cathode surface.

Although the two tested tubes are very similar in general, there are three major differences between tube #1 and #2. Already at the design state it was decided to use different output cavities for the two tubes. Tube #1 has one single cavity, whereas tube #2 has two coupled cavities at the output. The expectation was, that the second tube would have a slightly better efficiency than the first tube. During the tests of tube #1 an oscillation at 8.1GHz was observed depending on the beam voltage and solenoid field settings. Therefore it was decided to fabricate tube #2 with a stainless steel drift tube between the cavities 3 and 4, and 4 and 5 instead of using only copper for the drift tube as for klystron #1. This added additional losses to the disturbing oscillation. No oscillations were observed during testing of tube #2. The cathode of tube #2 was changed to a scandate cathode for tube #2, whereas tube #1 uses an osmium coated M-type cathode. More details can be found in [1].

3 OPERATION OF KLYSTRON #2

Since klystron #2 did not show disturbing oscillations up to an output power of 150MW and in addition has a slightly better efficiency than klyston #1, it was chosen to investigate the power potential of this type of klystron. Whereas klystron #1 has to provide RF power to the accelerating sections of the test facility, two sets of high power water loads, made by Nihon Koshuha, Yokohama, Japan, were installed at the two output waveguides of klystron #2. Each of the loads consists of a splitting T which devides the output power of each output waveguides. At the end of each waveguides the power is absorbed by water flowing behind a thin ceramic window. The VSWR of the loads is less than 1.10 at 2.998GHz.

Two 75dB hole coupler were installed at each output waveguide to measure the forward and reflected output power. A 2.998GHz band pass filter (30MHz bandwidth) was used to eliminate other frequency components in the measurements. In addition the output power could be determined by calorimetric measurements by measuring the water flow rate through the loads and by taking the loads water in and outlet temperatures. By taking into account these numbers, the repetition rate and the output pulse shape it was possible to calculate the klystrons peak output power. Since we were also able to measure the temperatures and flow rates in the klystron coolant circuits, e.g. the collector and body cooling circuit, we were also able to determine the power absorbed in the klystron itself. The difference between the power absorbed in the klystron at operation with and without RF power generation gives the klystron output power, too.

The high voltage pulse duration could be changed by adding or removing capacitors of the line type modulators pulse forming network. A detailed description of the modulator can be found in [5].

4 MEASUREMENTS

The measurements were performed at a high voltage flat top pulse duration of 1μs and a repetition rate of 12.5Hz, because both, klystron and modulator, were operated beyond their peak power specification during the tests. The cathode voltage was slowly raised from 550kV up to the maximum possible voltage of 610KV at a current of 780A. At a voltage level of 600kV it was necessary to increase the magnetic field in the solenoid by about 6%. Otherwise the RF output power would break down at the end of the 1μs long RF pulse. Later it turned out, that by adjusting the independent coils of the solenoid, operation at a beam voltage up to 610kV could be achieved even with a lower setting of the solenoid currents. Figure 2 shows the waveforms at a voltage of 610kV and total output power of 213MW.

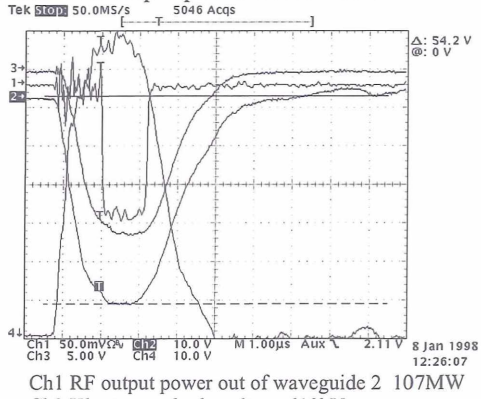

Ch1 RF output power out of waveguide 2 107MW
Ch2 Klystron cathode voltage 610kV
Ch3 Klystron collector current 781A
Ch4 Klystron gun current 778A
Time 1μs/div

Figure 2: Waveforms at a voltage of 610kV

The measurement of the perveance of klystron #2 gives numbers lower than in the SLAC measurements. Although klystron #1 is operated at a different modulator with different devices for voltage and current measurement as klystron #2, we measure also a lower perveance than in the SLAC tests. The reason for the difference is not clear up to now. Figure 3 shows perveance and efficieny as a function of the beam voltage. The klystron efficiency increases with increasing beam voltage and reaches 47%. Figure 4 shows the output power as function of the beam voltage. At a voltage of 610kV a power of 213MW in a 1μs long pulse can be extracted from the klystron. Figure 5 shows the dependence of the output power from the drive power for different beam voltages. Four data points are included, which were taken at four different beam voltages but at fixed drive power.

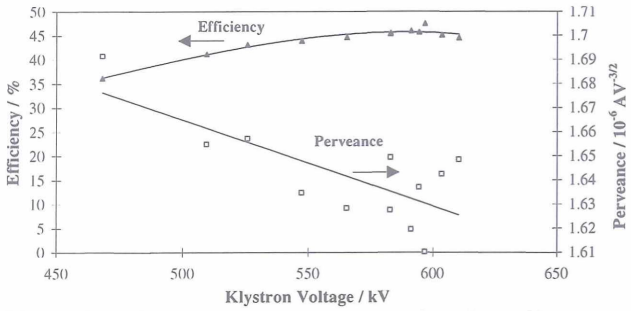

Figure 3: Efficiency and perveance as function of beam voltage

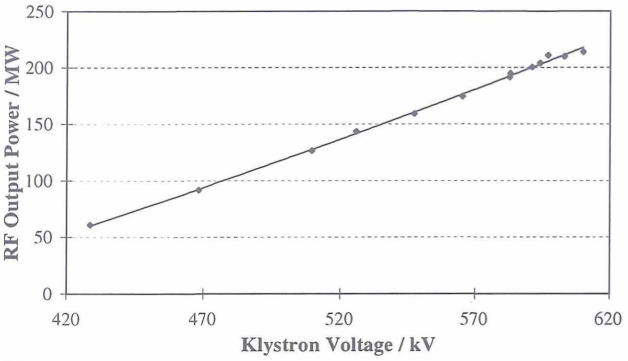

Figure 4: Output power versus beam voltage

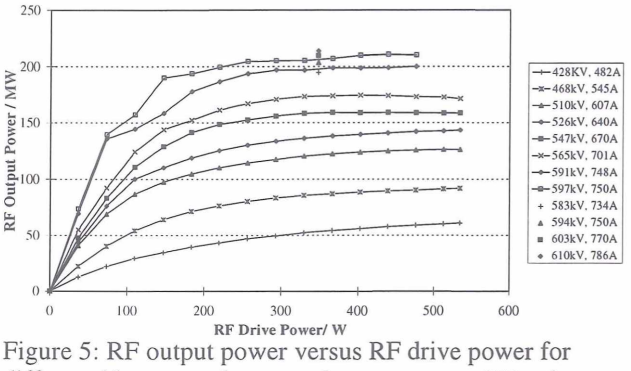

Figure 5: RF output power versus RF drive power for different klystron voltages and currents at an RF pulse duration of 1μs

At a drive power of 300W the output power is saturated. The saturated gain at this point is 58dB for an output power of more than 200MW. For beam voltages above 550kV the curves start to show a strange behavior on the rising part of the curve, where bumps appear. This can be seen more easily in figure 6, which shows the gain at a beam voltage of 583kV. The gain, which usually decreases with increasing drive power, shows a bump at 95W of forward drive power. Since the reflected drive power increases almost linearly as function of the forward drive power and shows no distinct bump, the drive power absorbed by the klystron should show a similar behavior. The vacuum pressure in the tube was not conspicuous in any way. A variation of the solenoid field affected the bumps. The bumps could be shifted to other points or could be made more or less distinct. It is even possible to find curves which show two or three of these bumps on the gain curve. The reason for this behavior is not clear up to now. It might be, that it indicates multipacting in the tube.

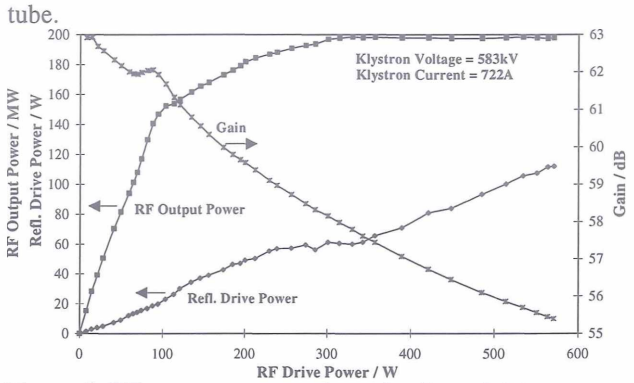

Figure 6: RF output power, gain and reflected drive power at 583kV and 722A

5 CONCLUSION

It is possible to operate an S-Band klystron at a pulse duration of 1μs at more than 200MW of output power. Even longer RF pulses at this power level might be achievable. Since we wanted to use the klystron to provide RF power for the test facility, we refrained from trying to reach more than 200MW at longer pulse duration. Both, the klystron and the modulator, were operated beyond their original specification. The e-beam needs careful focussing when the beam voltage is in the 600kV range. The reason for the bumps on the gain curves is not clear. Since these can be affected by varying the magnetic field, this might indicate multipacting in the tube.

6 REFERENCES

[1] D. Sprehn, G. Caryotakis, R.M. Phillips, "150-MW S-Band Klystron Program at the Stanford Linear Accelerator Center", Proceedings of the RF96, Kanagawa, Japan, April 8-12, 1996, P 91-99

[2] T.G. Lee, J.V. Lebacqs, G.T. Konrad, "A Fifty Megawatt Klystron for the Stanford Linear Collider", SLAC-Pub-3214, September 1983

[3] T.G. Lee, G.T. Konrad, Y. Okazaki, M. Watanabe, H.Yonezawa, "The Design and Performance of a 150MW Klystron at S-Band", SLAC-Pub-3619, April 1985

[4] C. Bearzatto, G. Faillon, "Short Presentation of High Peak Power TH 2153 Klystrons", Proceedings of the RF96, Kanagawa, Japan, April 8-12, 1996, P 116-122

[5] S. Choroba, M. Bieler, J. Hameister, Y. Chi, "A 375MW Modulator for a 150MW Klystron at the S-Band Linear Collider Test Facility at DESY", Proceedings of the XVIII International Linear Accelerator Conference, Linac 96, Geneva, Switzerland, 26 -30 August, 1996, P 785-787

PERFORMANCE OF THE KLYSTRON MODULATORS AT THE S-BAND TEST FACILITY AT DESY

S. Choroba, J. Hameister, M. Kuhn
Deutsches Elektronen-Synchrotron, DESY, 22603 Hamburg, Germany

Abstract

The klystrons at the S-band test facility at DESY require high voltage pulses of 550kV at a flat top pulse duration of 3µs, at a current of 700A and a repetition frequency of 50Hz. Two HV pulse modulators with a nominal power of 375MW were built. The design and results of the commissioning of the first system were described in [1]. The second system came into operation and was operated at an output power up to 475MW (610kV, 780A). In addition it was modified to investigate capacitor charging power supplies, which might be used in a linear collider tunnel. This type of power supply promises a better efficiency than the conventional resonant charging method and also saves space in the linear collider tunnel. This paper describes the operation experience with the HV modulators at the test facility especially with the second system. It reports the modifications, which were required to operate the modulator with the new type of HV power supply and presents results of the operation.

1 INTRODUCTION

The S-band test facility at DESY is a 400MeV electron linac, which serves for the development and evaluation of components which might be used for an S-band linear collider. Two pulse klystrons operating at 2.998GHz with a nominal output power of 150MW are installed at the test facility. The pulse duration is 3µs and the repetition rate 50Hz. In order to generate the microwave power of 150MW a klystron cathode voltage up to 550kV and a current up to 700A are required. The high voltage pulses of 3µs flat top pulse duration are produced by line type modulators. Although the resonance charging method, used in both modulators, is a well established and reliable technique to charge the capacitors of pulse forming networks, a new type of capacitor charging power supply, which is now available from different manufacturers, was installed at the second modulator. It can be used alternately with the existing resonance charging system. Constant current capacitor charging power supplies have a high efficiency and a compact size. Both are properties, which are especially desirable for modulators, which need to be installed in a linear collider tunnel, but of course are also of interest for other linear accelerators. The first modulator is in operation since three years and the second since one year. In the following we present a short overview of the modulator system and report on our operation experience so far. After that we describe the modifications required to install the new charging power supply and present results of the measurements performed on the system.

2 LINE TYPE MODULATOR LAYOUT

Table 1 shows the parameters of the modulator and figure 1 shows the basic circuit diagram.

Table 1: Modulator parameters

Pulse Voltage	550 kV
Pulse Current	700 A
Flat Top Pulse Duration	3 µs
Repetition Rate	50 Hz
Equivalent Square Wave Duration	4.8 µs
Rise Time 10 - 90 %	700 ns
PFN	four lines parallel, each line ten sections
PFN Impedance	1.34 Ω
Total Capacitance	1.8 µF
Capacitor Capacitance	45 nF
Coil Inductance	1.3 µH
Charging Voltage	50 kV max.
Peak Current (primary side)	16 kA
Pulse Transformer Ratio	1 : 23

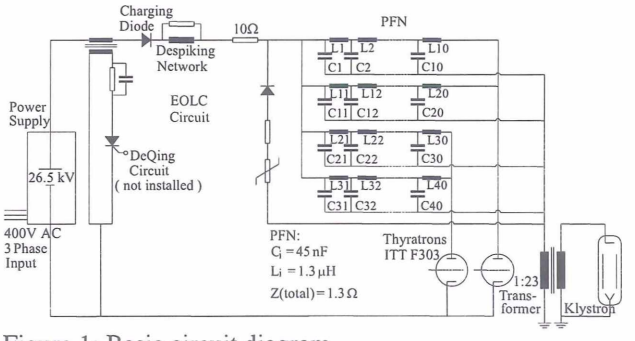

Figure 1: Basic circuit diagram

The pulse forming network is formed by four parallel lines of ten sections. They are discharged by two thyratrons, ITT F303, via the pulse transformer into the klystron. There is a slight positive mismatch between the pulse forming network and the klystron. The capacitors of the lines are charged by a resonant charging system consisting of a DC power supply (26.5kV, 5A), a charging choke of 16H and a charging diode capable to withstand

80kV. The PFN can be charged up to 50kV by a sinus half wave current of 17ms duration. This allows to operate the modulator at a repetition rate up to 50Hz. The DeQing system shown in the figure 1 was not installed, because the DC power supply has good regulation properties, which already allow a pulse to pulse variation smaller than 0.5%. Figure 2 shows typical waveforms at more than 500kV.

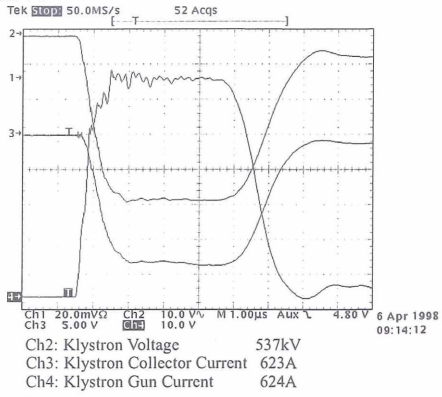

Figure 2: Typical waveforms

More detailed information can be found in [1].

3 OPERATION EXPERIENCE

At the beginning of operation electromagnetic noise generated by the modulators was a major concern. It entered the interlock system or other components and could lead to interruptions of the modulator operation. In the worst case it could even muddle up the thyratron driver trigger logic and damage components in the driver, especially the drivers thyristor switches. Since the source of noise could not be eliminated, we installed RC filters in the drivers and also in other components, which were affected by the noise. This solved our problem and allowed to operate without interruptions.

It is necessary to control the thyratrons reservoir voltage carefully. Otherwise the situation can occur, that instead of firing both thyratrons simultaneously, the thyratrons fire at different times or in the worst case one thyratron fails to fire. This does not harm the klystron, but leads to large thyratron grid spikes and can damage the thyristor switches in the driver circuits.

Besides these we had no major problems.

The klystron output power of 150MW could be reached with a cathode voltage of 550kV. With a PFN charging voltage of 50kV even 610kV could be achieved at the klystron. At this voltage an output power of 213MW could be extracted from the klystron. Since the klystron was developed for an RF power of 150MW at 3µs pulse duration and a repetition rate of 50Hz, we reduced the RF and HV pulse duration to 1µs and the repetition rate to 12.5Hz. The reduction in pulse width was accomplished by removing five capacitors per PFN line. At a flat top pulse duration of 1µs a maximum voltage of 610kV at 780A, which corresponds to a power of 475MW, was achieved and could be handled without problems. Longer pulses might be even possible but have the risk of damaging the klystron or the modulator. Since we need the klystron to operate the test facility linac, we refrained from running at longer pulse width at this power level.

4 MODIFICATION

The second modulator was modified in order to investigate the properties of a constant current capacitor charging power supply. This type of power supply might be able to replace the resonant charging method. It charges a pulse forming line with a constant current to the desired voltage without the use of a charging choke. Maxwell (San Diego, USA) offers power supply modules up to a voltage of 50kV and a power rating of 10kJ/s. Modules can be connected in parallel to build one power supply with more output power. In a first stage we installed three modules, which are sufficient to operate the modulator at maximum peak power, but at a reduced repetition rate of 12.5Hz instead of 50Hz. In a later stage the new power supply could be upgraded to full average power by installing up to twelve modules in parallel. In the meantime the existing resonance charging system must be used, if operation at 50Hz repetition rate is required. Therefore all modifications of the existing modulator needed to be done in a way, which allows to switch easily between the two charging methods.

A freewheeling diode and two series resistors must be installed between the pulse forming network and the constant current charging power supply output. This is necessary, because the charging power supply must be protected from negative voltage at its output. In this case a current could flow through the power supply rectifier diodes, which might exceed their capabilities. Negative voltage at the power supply output arise during fault conditions like klystron arcing or PFN breakdown and even also during normal operation conditions. The EOLC diode is not sufficient to protect the power supply, because it does not connect the power supply output and ground. We therefore installed a another diode at the thyratron side of the PFN. Figure 3 shows the diagram of the modified circuit.

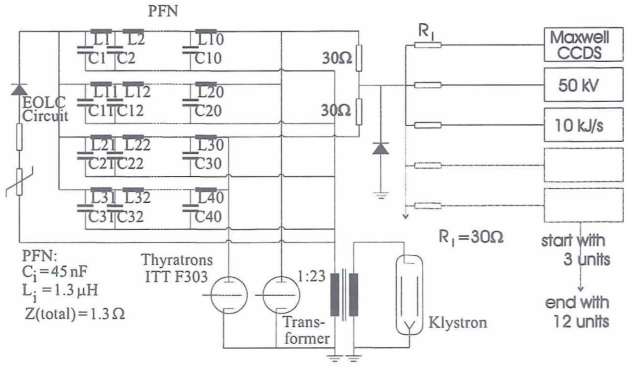

Figure 3: Diagram of the modified circuit

The protecting diode is made of 25 high voltage diodes in series (4kV each), each with a varistor in parallel. Two 30Ω series charging resistors serve for the decoupling of the two thyratrons. This allows switching of both thyratrons at the same time. Each of the power supply modules has a separate output cable, which is terminated by a another series resistors. We did not combine the output of modules directly after the output and did not use just one cable and resistor instead of many, because this would have made it more difficult to install or remove modules for test purposes. For a set up, which does not require this flexibility, a connection with just one cable could of course be made. The protecting diode and the resistors were installed in the PFN cabinet.

The compact size of this new type of power supply makes it attractive if space availability is an important aspect, e.g. in the case of a linear collider tunnel. The size of each of the modules in use is 220mm high, 508mm long and 19 inch wide. All modules, which would be sufficient for a modulator operation at full average power, would fit in two 19 inch racks. This reduces the space required by the existing DC power supply and the charging unit by about a factor of ten.

Another motivation to test the new type of power supply results from the efficiency demands of a linear collider. The existing resonance charging method has an efficiency of 88% for the charging path from the mains to the PFN, partly caused by the DC power supply efficiency and partly caused by ohmic and eddy current losses due to the charging choke. We measured the efficiency of the power supply at various output voltage settings. At the maximum voltage of 50kV it reaches 93%. Even if one includes the losses in the series charging resistors, the efficiency for the charging path from the mains to the PFN is still 91.5%.

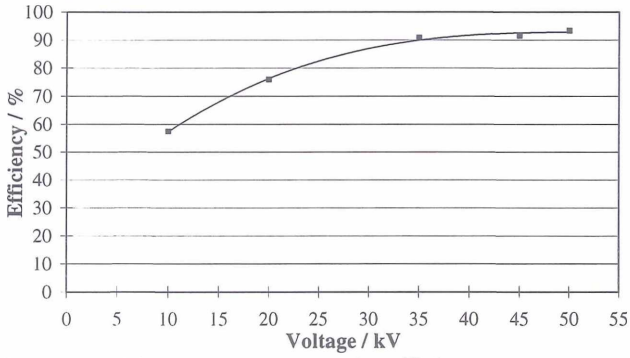

Figure 4: Charging power supply efficiency versus PFN voltage

The pulse to pulse variation was measured in the same way as for the resonance charging method by superposing 1500 klystron voltage pulses. The variation did not change significantly. and is still smaller than 0.5%.

An important aspect for a linear collider is the impact of the modulator power supplies on the line. Therefore we measured the voltage and the current of each of the input phases and calculated the input power of each phase. Figure 5 shows the linear ramp of the PFN voltage and the power extracted from the three phases of the mains. It is basically a picture one would expect from a three phase double way rectifier, which has do provide a linear increasing output power. This process is repeated with the modulators repetition rate. The power consumption from the mains is not constant and in case of a large number of modulators would probably disturb the mains. Further development to limit this effect is required.

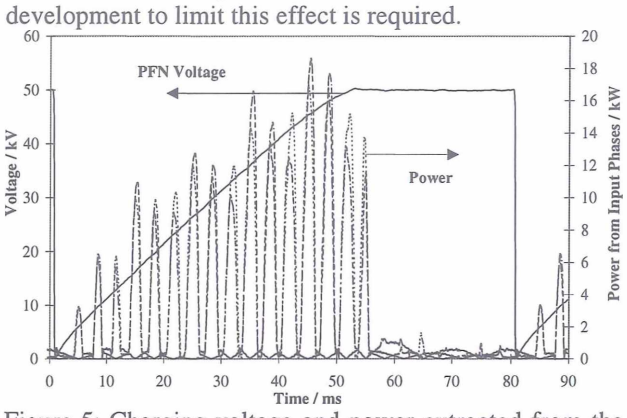

Figure 5: Charging voltage and power extracted from the three phases of the mains during one charging cycle

More detailed information about the modification of the second modulator can be found in [2].

5 CONCLUSION

The high voltage pulse modulators at the S-band test facility are in operation at nominal conditions of 550kV at 3μs pulse duration and a repetition rate of 50Hz. The second system can be even operated at a higher power level up to 475MW (610kV, 780A) at 1μs pulse duration and 12.5Hz repetition rate. The operation of the modulators is reliable, but the thyratron reservoir voltage setting needs careful control and adjustment. A new type of charging power supply was installed at the second system. It has a high efficiency and is of compact size, which makes it attractive for linear collider applications. Its reaction to the mains was investigated, but further work is necessary to limit disturbing effects to the mains.

6 REFERENCES

[1] S. Choroba, M. Bieler, J. Hameister, Y. Chi, A 375MW Modulator for a 150MW Klystron at the S-Band Linear Collider Test Facility at DESY, Proceedings of the XVIII International Linear Accelerator Conference, Linac96, Geneva, Switzerland, 26 -30 August, 1996, P 785-787

[2] S. Choroba, J. Hameister, M. Kuhn, "Operation of a HV Pulse Modulator at the S-Band Test Facility at DESY with a Constant Current Capacitor Charging Power Supply", to be published in the Proceedings of the 1998 Third Modulator-Klystron Workshop, SLAC, Stanford, June 29 - July 2, 1998

DESIGN OF A HOM BROADBAND ABSORBER FOR TESLA

M. Dohlus, A. Jöstingmeier, N. Holtkamp and H. Hartwig, DESY, D-22607 Hamburg, Germany

Abstract

For the TESLA FEL operation very short intense bunches of electrons have to be accelerated. These bunches excite a broad spectrum of HOM (Higher Order Modes) up to frequencies of some THz. Two HOM couplers per cavity are foreseen in the present design proposal in order to extract some of the low frequency HOM from the superconducting accelerating structure. In this contribution an additional HOM broadband absorber is suggested which is to be installed between two cryogenic modules at a temperature of 70 K. Its task is to prevent that the really high frequency HOM are absorbed in the accelerator structure at the 2 K level. The absorption characteristics and the short range wake of four structures which make use of SiC as absorbing material are investigated using the MAFIA computer code. The proposed structures are easier to manufacture and better suited for the operation under vacuum conditions than the recently suggested waveguide array absorber.

1 INTRODUCTION

It is planned to operate TESLA in the FEL mode with very short bunches ($\sigma = 25\,\mu$m) [1] which excite wakefields with spectral components up to some THz. If we do not extract these fields from the accelerating structure by a special absorber we expect a considerable reduction of the quality factor of the superconducting cavities because the photon energy gets larger than the binding energy of the Cooper pairs for frequencies larger than 700 GHz.

This phenomenon would consequently lead to an excessive energy deposition in the 2 K cooling circuit which has to be prevented for the following reason: The time averaged power deposition due to the wakefields is about 25 W per module [1]; and a typical refrigerator requires about 800 W of wall plug power per Watt dissipated at 2 K [2]. Thus we would have to supply 20 kW of cooling power per module which is not tolerable.

A HOM absorber which is sketched in Fig. 1 has already been proposed in [2]. This absorber consists of an array of outward directed rectangular waveguides surrounding the beampipe. The extraction of the high frequency wakefields from the beampipe by such an array has been investigated in detail in [3]. The outward propagating waveguide fields are attenuated by the ohmic losses of the stainless steel waveguides which are considerably high for frequencies above the cutoff frequency of the fundamental waveguide mode which is 100 GHz. Note that low frequency spectral components cannot penetrate much into the absorber.

A cutoff frequency of 100 GHz corresponds to a width of the waveguides of 1.5 mm. The waveguide height is only

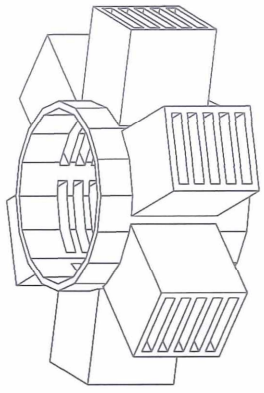

Figure 1: Schematic drawing of the waveguide array absorber.

0.3 mm in order to have a high attenuation of the waveguide modes. Furthermore it is obvious that the waveguide walls should be as thin as possible for a good efficiency of the absorber. A wall thickness of 0.1 mm has been proposed which seems to be the lower limit from the mechanical point of view. The TESLA beampipe has a radius of 35 mm; and approximately 100 mm of space are available for the absorber in the axial direction. Therefore the actual absorber consists of an array of about 140×250 waveguides in the azimuthal and the axial direction, respectively.

The manufacturing of such a structure is very difficult even if etching techniques are applied [2]. Moreover the problem of cleaning the waveguide array before it is installed in the TESLA vacuum system has yet not been solved. Thus four new absorber structures are proposed which do not have these disadvantages. The MAFIA computer code [4] is used in order to study their absorption characteristics as well as their contribution to the short range wake.

2 PROPOSED ABSORBERS

The absorbers which are investigated in this contribution are shown in Figs. 2-5. In each of these configurations the actual absorbing structure is accomodated in a shielding which is similar to a single cell of the TESLA accelerating structure. For the simulations we have assumed $r_{iris} = 30$ mm, $r_{cell} = 100$ mm and $l_{cell} = 100$ mm.

We have chosen SiC as absorbing material because it is suitable to be used in a vacuum system; and it has a large loss-tangent which is about 0.3. This number has been confirmed by measurements at room temperature up to a frequency of 20 GHz. For our simulations we assume that it is still valid in the THz region and that it does not change significantly if the absorber temperature is 70 K.

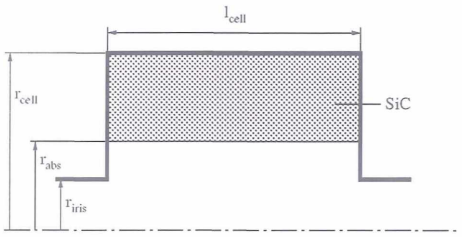

Figure 2: Solid SiC absorber.

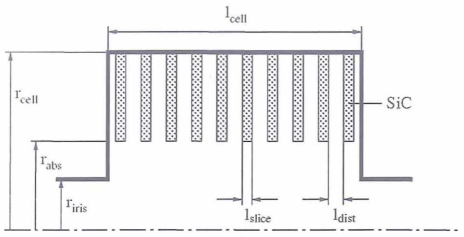

Figure 3: Laminated SiC absorber.

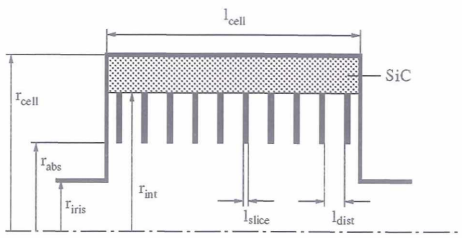

Figure 4: Combined absorber.

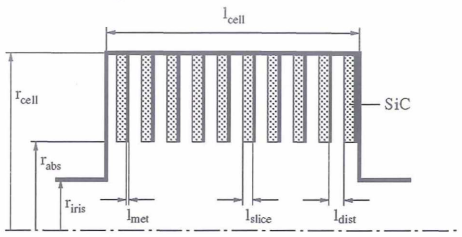

Figure 5: Metallized laminated SiC absorber.

For each proposed HOM absorber we are going to consider two versions. In the original version we have $r_{abs} = r_{iris}$. This seems to be favourable for a good coupling between the absorber and the HOM. On the other hand, the absorber itself also contributes to the beam impedance. This contribution can be decreased if we hide the absorbing structure behind the iris of the shielding cell. A bunch does not see the actual absorbing structure if the relation $r_{abs} - r_{iris} \geq \sqrt{5 l_{cell} \sigma}$ is fulfilled. In this case the short range wake of the HOM absorber is equal to that of a single accelerating cell. Bearing in mind that a module contains 72 such cells, the additionally introduced beam impedance due to the HOM absorber seems to be tolerable.

Note that in the above relation $r_{abs} - r_{iris}$ is proportional to $\sqrt{\sigma}$ which means that the absorbing structure may be arranged close to the beampipe for short bunches. Nevertheless it must also be possible to operate TESLA with 1 mm long bunches for which the condition for $r_{abs} - r_{iris}$ cannot be satisfied if we are interested in a good coupling between the HOM and the absorber. Thus we have to find a trade-off between the efficiency of the absorber and its contribution to the beam impedance. For our simulations we choose $r_{abs} - r_{iris} = 5$ mm.

The first proposed absorber is a solid SiC tube accomodated in the shielding cell. This configuration is shown in Fig. 2. Since the permittivity of SiC is large ($\varepsilon_r \approx 30$) we expect considerable reflections at the SiC-vacuum interface. Therefore the second structure which is presented in Fig. 3 consists of a stack of 50 SiC washers with $l_{slice} = l_{dist} = 1$ mm in order to reduce the effective permittivity of the absorbing structure.

The idea of the combined and the metallized laminated absorber which are shown in Figs. 4 and 5 is basically different than that of the first two structures in which all spectral components of the HOM are damped by the absorbing material in the shielding cavity. The combined and the metallized laminated absorber additionally contain a stack of stainless steel parallel-plate waveguides which attenuate the really high frequency HOM by ohmic wall losses similar to the previously discussed waveguide array absorber. In these structures SiC is used to suppress the long range wake. For this purpose it is sufficient that it has good damping properties up to a frequency of some 10 GHz. Hence the required bandwidth of the absorbing material is much less for these structures than that for the solid and the laminated absorber.

The difference between the combined and the metallized laminated absorber is that in the latter one the low frequency fields are continuously damped by the absorbing material while they are propagating outwards whereas they are absorbed at the ends of the waveguides in the combined absorber. The parameters of both structures read: $l_{slice} = l_{dist} = 1$ mm and $r_{int} = 80$ mm. Note that the actual thickness of the metallization l_{met} which is very thin can be neglected for the field analysis. In the MAFIA simulations we have assumed that l_{met} is equal to the thickness of one mesh layer.

3 SIMULATION RESULTS

The absorption characteristics of the proposed absorbers are given in Fig. 6. Here it is assumed that $r_{iris} = r_{abs}$.

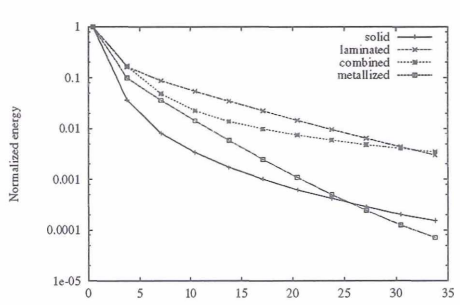

Figure 6: Absorption characteristics of the investigated structures.

The curves represent the total energy normalized to its value at the time $t = 0$. At this time the exciting bunch

has just left the absorber cell. The transient behaviour is then computed for the next 33 ns. An ultra-relativistic particle just travels 10 m during this time interval.

Two classes of absorbers can be well-distinguished with respect to their absorption efficiency. In the solid and the metallized laminated absorber the energy drops to about 10^{-4} of its initial value after 33 ns. On the other hand, the absorption of the laminated and the combined absorber is approximately two orders of magnitude less.

The transient absorption behaviour of the combined and the metallized laminated absorber and the corresponding hidden structures are compared in Fig. 7. It is expected that

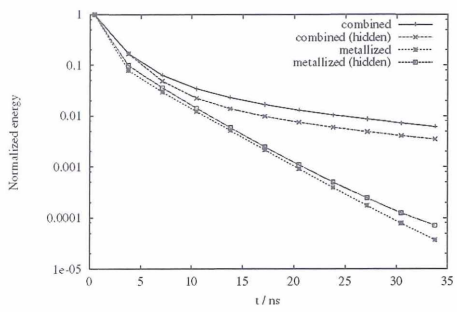

Figure 7: Comparison between the original and the hidden structure.

the hidden structures are less efficient than the corresponding absorbers with $r_{iris} = r_{abs}$. It is found that this is in fact true for the metallized laminated absorber. Nevertheless the efficiency of the hidden version of this absorber is only slightly less than that of the original structure. For the combined absorber it even turns out that the absorption can be improved a little bit if we hide the absorbing structure.

In order to illustrate the different absorption mechanisms of the metallized laminated and the solid absorber the relation between the total energy and that which is stored in the beampipe is shown in Fig. 8. Both energies are approx-

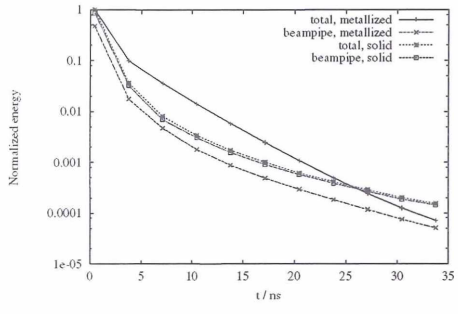

Figure 8: Total energy and energy which is stored in the beampipe.

imately the same for the solid absorber. This means that the electromagnetic field cannot penetrate significantly into the absorbing material because it is absorbed in the immediate vicinity of the dielectric-vacuum interface.

On the other hand the total energy is much larger than the beampipe energy in the metallized laminated absorber because the electromagnetic field propagates a considerably large distance into the parallel-plate waveguides before it is finally absorbed.

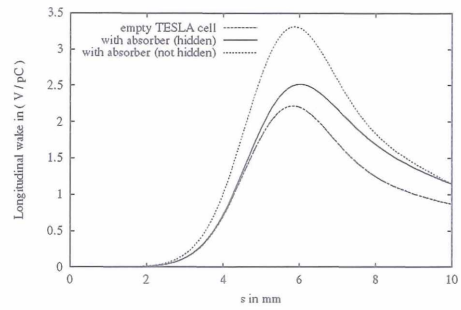

Figure 9: Short range wake of various structures for $\sigma = 1$ mm.

Fig. 9 shows the longitudinal short range wake of the empty TESLA cell, the laminated absorber with $r_{iris} = r_{abs}$ and the hidden version of this structure. The wake of the empty cell, which has a maximum value of 2.2 V/pC, is smaller than that of the two other structures as it is expected. The wake function corresponding to the non-hidden absorber is about 50% higher than this value. On the other hand, the short range wake is only 15% increased for the hidden version of the absorber which is acceptable.

4 CONCLUSIONS

Four types of HOM absorbers for TESLA which are easier to manufacture and more appropriate to be used in a vacuum system than the previously suggested waveguide array absorber have been investigated in this contribution. It has turned out that two of the absorbers, namely, the solid and the metallized laminated absorber have good absorption properties; and that the efficiency of the absorbers is not significantly decreased if we hide the absorbing structure behind the iris of the shielding. The short range wake of such a hidden structure is equal to that of a single TESLA accelerating cell for short bunches; and it is still tolerable for an intermediate bunch length. The solid absorber is less complicated concerning manufacturing and installation than the metallized laminated one. Nevertheless the simulation results for the solid absorber are based on the assumption that SiC has the same favourable attentuation properties in the THz region at a temperature of 70 K as in the frequency range up to 20 GHz at room temperature.

5 REFERENCES

[1] *R. Brinkmann et al. (ed.), Conceptual design of a 500 GeV e^+e^- linear collider with integrated X-ray laser facility, DESY 1997-048, 1997.*

[2] *M. Dohlus, N. Holtkamp, A. Jöstingmeier, H. Hartwig and D. Trines, "Design of a HOM broadband absorber for TESLA", Meeting note: 31 Linear collider project meeting at DESY, 1998.*

[3] *A. Jöstingmeier, M. Dohlus, N. Holtkamp and M. Shahabadi, "Application of the mode matching technique for the computation of the beam parameters of an infinite periodic structure", will be published as TESLA report, 1998.*

[4] *The MAFIA collaboration, User's Guide MAFIA Version 3.2, CST GmbH, Lauteschlägerstr. 38, D64289 Darmstadt.*

SYSTEMATIC DESIGN OF AN S-BAND PILLBOX-TYPE RF WINDOW

A. Jöstingmeier, M. Dohlus and N. Holtkamp, DESY, D-22607 Hamburg, Germany

Abstract

The scattering matrix technique and the MAFIA computer code are employed for the systematic design of an 75 MW S-band pillbox-type window. It is shown that with the standard pillbox-type design the window cannot be matched using ceramic disks with a thickness in the range from 4 mm to 8 mm. Nevertheless such disks are mechanically more robust and easier to manufacture than the usual 3 mm disks. Therefore a new design of the pillbox-type window with an additional inductive iris is presented so that ceramic disks of arbitrary thickness may be used. Furthermore it is demonstrated how the bandwidth of the window can be optimized by fine tuning the thickness of the ceramic disk. The final design of the pillbox-type window with smoothed edges is validated by the application of the MAFIA time domain module.

1 INTRODUCTION

The S-band linear collider at DESY requires approximately 2600 klystrons operating at an output power of 150 MW, a pulse duration of 3 μs and a repetition rate of 50 Hz. Until 1995 two klystrons have already been built and successfully tested [1]. The klystron has two output waveguides which are split and recombined so that each of the four rf windows has to withstand a peak transmission-power of about 37.5 MW. The production costs of the klystrons can significantly be reduced if each tube contains only two rf windows. In this paper we will report on the systematic design of such a window.

Fig. 1 presents the schematic drawing of a pillbox-type rf window. The practical use of rf-windows in the high-power regime is still a challenging task although strong efforts have been made during the past to improve their reliability [2]. The mechanismen which is responsible for an rf window failure has not yet been understood in detail. Nevertheless it seems to be clear that multipactor electron bombardment of the ceramic disk [3] is mainly responsible for a breakdown.

Computer simulations have demonstrated that the component of the electric field normal to the disk is mainly responsible for this phenomenon. Hence a long pillbox-type rf window has been suggested in [2] which has a length of more than 150 mm instead of 30 mm for the standard window. The axial electric field is effectively suppressed by this new geometry because only the TE_{11} mode is propagating in the empty circular waveguide sections of the pillbox cavity.

The higher order modes which are excited at the transition from the rectangular to the circular waveguide do not

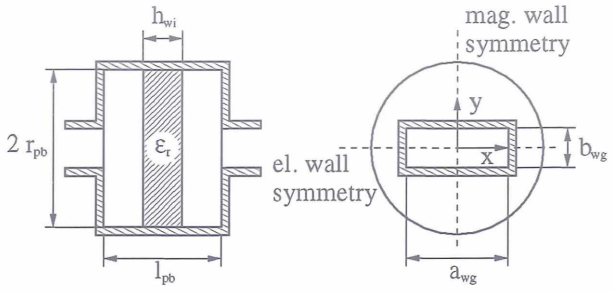

Figure 1: Schematic drawing of the pillbox-type rf window.

interact with the ceramic disk in a long window. Thus we can apply the scattering matrix technique taking only one propagating mode into account. From this analysis we get analytic expressions which are very useful for the window design. Only the scattering matrix corresponding to the waveguide transition will be calculated numerically using MAFIA [4]. Hence the scattering matrix technique leads to a numerically efficient formulation so that a large variety of parameter sets can be studied.

Pillbox-type rf windows usually contain ceramic disks with a thickness of about 3 mm. Especially if high purity alumina is to be used it is desirable to increase the thickness of this disks from the mechanical point of view. The analytic design formulas show that such windows cannot be matched if the thickness of the disk is in the range from 4 mm to 8 mm because the input reflection of the transition from the rectangular to the circular waveguide is too small. Therefore a new type of rf window is presented which contains additional inductive irises in order to increase the reflectivity of the waveguide transition.

Both features of the new window, which are an increased thickness of the ceramic disk and a long pillbox cavity, lead to a significant reduction of the bandwidth. Especially if the SLED-option [5] is taken into account the VSWR must be less than 1.1 over a band of about 90 MHz centered at 3 GHz. It is shown how a maximum bandwidth is obtained by properly adjusting the thickness of the ceramic disk.

In order to prevent the structure from arcing we have to round off the sharp edges at the waveguide transition which are characterized by $y =$ constant. Although the inductive irises do not give rise to a singularity of the electric field they are also assumed to be rounded off in the final design which is validated by the time domain module of the MAFIA code.

2 WINDOW DESIGN

Let us assume that the dimensions of the rectangular waveguide and the permittivity of the ceramic disk are

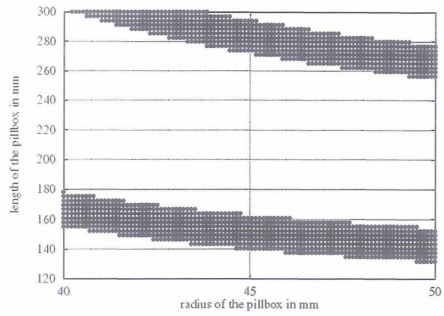

Figure 2: Distribution of possible solutions in the r_{pb} - l_{pb} plane. Parameter: $h_{wi} = 5$ mm.

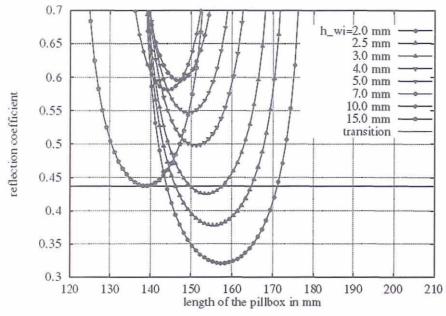

Figure 3: Required reflection coefficient of the waveguide transition as a function of l_{pb} and h_{wi}. Parameter: $r_{pb} = 46$ mm.

$a_{wg} = 72.14$ mm, $b_{wg} = 34.04$ mm and $\varepsilon_r = 10$.

From the application of the scattering matrix technique it turns out that the rf window can only be matched if the window parameters obey certain relations. Fig. 2 shows all possible solutions for which the window can be matched in the r_{pb} - l_{pb} plane assuming $h_{wi} = 5$ mm. In the considered parameter range two sets of solutions are found which are separated just by one wavelength of the TE_{11} mode in the empty circular waveguide.

For the variation of the radius of the pillbox cavity some transitions from the rectangular to the circular waveguide have been analyzed using MAFIA. Actually the radius of the pillbox cavity has been varied in steps of 2 mm. The scattering parameters at intermediate points are then found by the application of an interpolation scheme.

Fig. 3 presents the required input reflection of the waveguide transition as a function of the length of the pillbox cavity for a cavity radius of 46 mm whereas the thickness of the ceramic disk serves as a parameter. The input reflection of the waveguide transition is also given as a straight line.

Starting from $h_{wi} = 2$ mm, the required input reflection of the waveguide transition increases. For $h_{wi} = 2$ mm, 2.5 mm and 3 mm, Fig. 2 predicts two solutions for each thickness corresponding to different lengths of the pillbox cavity. But for thicker disks, the parabolas do not intersect with the straight line so that no solution exists. Only if we consider very thick disks, $h_{wi} > 10$ mm, the required input reflection decreases again. Consequently, the window can only be matched for disks in the range from 4 mm to

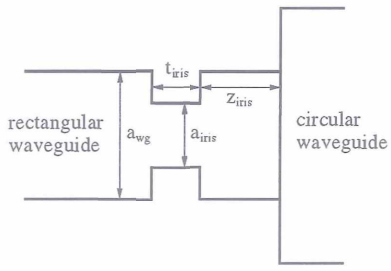

Figure 4: Schematic drawing of the waveguide transition with an inductive iris.

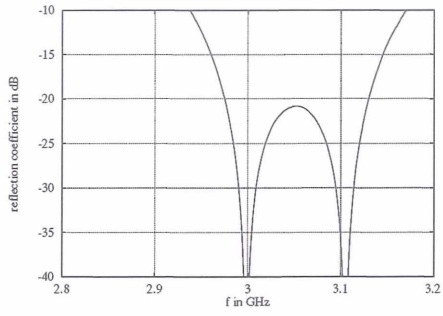

Figure 5: Reflection coefficient of the window as a function of frequency. Parameter: $r_{pb} = 46$ mm, $l_{pb} = 144.9$ mm, $h_{wi} = 5$ mm, $z_{iris} = 40$ mm and $a_{iris} = 57$ mm.

8 mm if we choose a waveguide transition with a higher input reflection.

In order to increase this quantity we introduce an inductive iris in front of the waveguide transition according to Fig. 4. t_{iris} is assumed to be 5 mm. For a given iris one gets a maximum increase of the reflectivity for $z_{iris} = 40$ mm. For the adjustment of a specific value of the input reflection, which is necessary for the proper design of a window, the width of the iris a_{iris} is used.

We have now all the data together which we need for a systematic design of the window. Let us start assuming the following parameters: $r_{pb} = 46$ mm, $h_{wi} = 5$ mm and $z_{iris} = 40$ mm. According to Fig. 3, the input reflection of the waveguide transition has to be greater than 0.55 in this case. We choose an input reflection of 0.57 which corresponds to an iris width of about 57 mm in order to show that really two solutions exist if the input reflection is larger than 0.55. Applying the scattering matrix technique, we actually find two matched windows for $l_{pb} = 144.9$ mm and $l_{pb} = 154.5$ mm. Fig. 5 shows the input reflection of the window for $l_{pb} = 144.9$ mm.

Both solutions have a bandwidth corresponding to a VSWR = 1.1 of approximately 30 MHz which is much too small. The bandwidth can significantly be enhanced if we make use of both solutions simultaneously. For that the two frequencies at which the window is matched have to be centered around the design frequency, see Fig. 6. This is achieved by properly choosing the length of the pillbox cavity.

The reflection coefficient at the design frequency which is related to the bandwidth of the window can then be adjusted by the thickness of the ceramic disk which is illus-

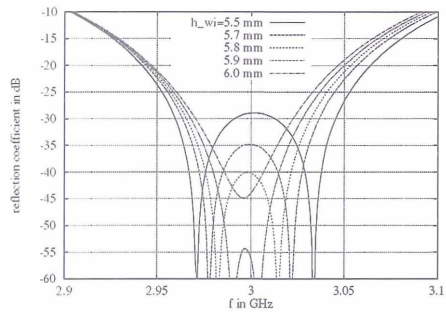

Figure 6: Reflection coefficient of the window as a function of frequency and the thickness of the ceramic disk. Parameters: $r_{pb} = 46$ mm, $l_{pb} = 148.9$ mm, $z_{iris} = 40$ mm and $a_{iris} = 57$ mm.

#	h_{wi} in mm	Δf in MHz	
		VSWR = 1.05	VSWR = 1.1
1	5.5	–	94
2	5.7	67	83
3	5.8	60	77
4	5.9	52	72
5	6.0	44	66

Table 1: Bandwidth as a function of the thickness of the ceramic disk.

trated in Fig. 6. From Fig. 3 it is clear that the solutions move closer together if the thickness of the ceramic disk is increased. This leads to a smaller reflection coefficient at the design frequency but also to a reduction of the bandwidth. Thus one has to find a trade-off between these two quantities. In Table 1, the bandwidth of the window is given for several values of h_{wi}. E.g., the VSWR is still less than 1.1 over a frequency range of 94 MHz for $h_{wi} = 5.5$ mm. However in this case one has to cope with a reflection coefficient of -28.9 dB at the design frequency.

For the final design of the window we use a waveguide transition with rounded edges according to Fig. 7. Detailed investigations using the MAFIA electrostatic module yield that a rounding radius of 10 mm leads to a field enhancement of about 30% which seems to acceptable. Furthermore it is preferred to use semicircular irises with a radius of 9 mm instead of those which sharp edges which is also illustrated in Fig. 7.

Fig. 8 presents the input reflection of the final window design as a result of the scattering matrix technique and the MAFIA time domain module. The agreement between both methods is quite well. Optimizing the bandwidth yields a useful frequency range of about 80 MHz and a reflection coefficient at the center frequency which is less than -33 dB.

3 CONCLUSIONS

The scattering matrix technique and the MAFIA computer code have been applied in order to design a modified S-band high-power pillbox-type window. It has been shown that for a ceramic disk with a thickness in the range from 4 mm to 8 mm the input reflection of the rectangular-circular waveguide transition has to be increased so that

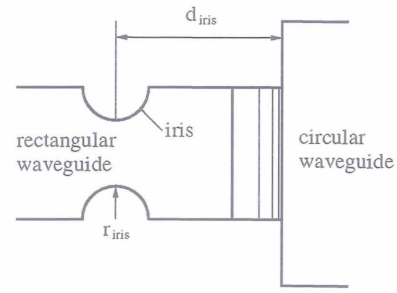

Figure 7: Schematic drawing of the waveguide transition with rounded edges.

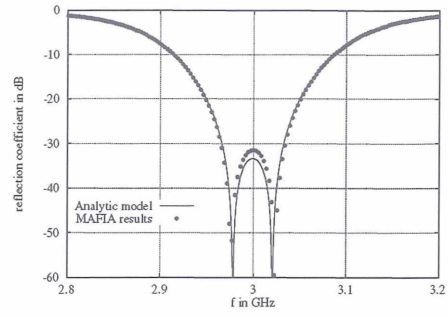

Figure 8: Reflection coefficient as a function of frequency with $r_{pb} = 46$ mm, $h_{pb} = 150.4$ mm, $h_{wi} = 6.1$ mm, $d_{iris} = 40$ mm, $r_{iris} = 9$ mm.

the overall window is matched at the design frequency. It has been demonstrated by MAFIA computations that the required input reflection of the waveguide transition can be obtained by an inductive iris one quarter wavelength in front of the rectangular-circular waveguide transition. Moreover it has been shown that the thickness of the ceramic disk has to be properly chosen for an optimum bandwidth of the window. A final design of the window with rounded off edges has been proposed; and the performance of this structure has been checked applying the time domain module of the MAFIA computer code.

4 REFERENCES

[1] D. Sprehn, "Final report on the development of a 150-MW S-band klystron", to be published in *Proceedings of Pulsed RF Sources for Linear Colliders*, 1996.

[2] A. Miura and H. Matsumoto, "Development of an S-band high-power pillbox-type rf window", *Proc. of Int. Conf. for High Energy Accelerators*, 1992.

[3] W. J. Gallagher, "The multipactor effect", *IEEE Trans. on Nucl. Sci.* , vol. NS-26, pp. 4280–4282, 1979.

[4] T. Weiland, "On the numerical solution of Maxwell's equations and applications in the field of accelerator physics", *Particle Accelerators*, vol. 15, pp. 245–292, 1984.

[5] P.B. Wilson, "SLED: A method for doubling SLAC's energy", *Technical Note SLAC-TN-73-15*, Stanford Linear Accelerator Center, Stanford University, Stanford, California, 1973.

APPLICATION OF THE MODE MATCHING TECHNIQUE TO THE ANALYSIS OF WAVEGUIDE ARRAYS

A. Jöstingmeier, M. Dohlus and N. Holtkamp, DESY, D-22607 Hamburg, Germany

Abstract

In this contribution the mode matching technique is applied to compute the absorption characteristics of a two-dimensional array of rectangular waveguides. This analysis is motivated by a proposal of a broadband absorber for TESLA. Outside the waveguide array the so-called Rayleigh expansion is used which represents the electromagnetic field in terms of space harmonics whereas the complete modal spectrum of eigenmodes is taken into account inside the waveguides. In the case of normal incidence the validity of the presented method is confirmed by MAFIA computations. The absorption characteristics for various angles of incidence are calculated for a broad frequency range. The accuracy of the results is checked by a study of convergence. It is shown that the Rayleigh expansion has to be modified if the waveguide array is excited by an ultra-relativistic beam instead of an incoming plane wave. Numerical results for the beam parameters are presented for an array of parallel-plate waveguides and compared with those obtained by other methods.

1 INTRODUCTION

A HOM (higher order modes) absorber for TESLA has been proposed in [1] which consists of an array of rectangular waveguides surrounding the beampipe (Fig. 1). This absorber is used to extract the HOM in the THz region from the superconducting accelerating structure and to attenuate the extracted fields by the ohmic wall losses of the rectangular waveguides.

For the sake of simplicity we consider instead of the circular waveguide array a two-dimensional infinite planar grating (Fig. 2). The absorption characteristics of this model are expected to be very close to those of the original absorber because the free-space wavelength is much shorter than the curvature of the structure in the relevant frequency range.

Such a grating can be analyzed by the application of the mode matching technique. Above the grating the electromagnetic field is expanded in terms of an infinite series of spatial harmonics, which is known as the Rayleigh expansion; and inside the waveguides the field is represented by the complete spectrum of TE and TM waveguide modes. Matching the waveguide aperture tangential electromagnetic field, yields an infinite algebraic system of equations the unknown of which are the field expansion coefficients [2].

The ratio describing how much of the power of the incoming wave is coupled into the waveguides is denoted as the grating efficiency. It is used to estimate the power absorption properties of the structure. This quantity is calculated for a grating with typical absorber dimensions over a broad frequency range and for various angles of incidence.

If we use a grating as HOM absorber we have to keep in mind that such a structure itself also contributes to the beam impedance. The second part of this paper is therefore dedicated to the computation of the beam parameters of infinite periodic structures.

The mode matching technique is employed to calculate the electromagnetic field which is excited by an ultra-relativistic bunch of particles in the presence of an infinite array of parallel-plate waveguides (Fig. 3). Subsequently the beam parameters are calculated by making use of the results of the field analysis. In [3] it has been demonstrated that the results of this planar model can also be used for a circular configuration if certain scaling laws are taken into account.

The Rayleigh expansion for the field representation above the grating is known to be complete which means that it can be used to represent any kind of pseudo-periodic field. Nevertheless it has to be modified for an ultra-relativistic beam since the phase advance of the exciting

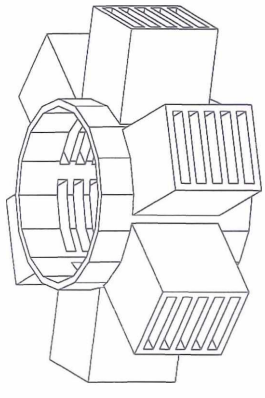

Figure 1: Sketch of the waveguide array absorber.

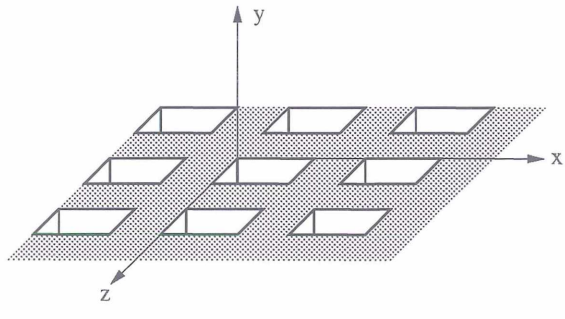

Figure 2: Two-dimensional planar grating.

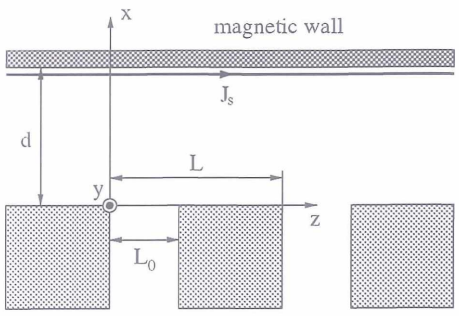

Figure 3: Infinite array of parallel-plate waveguides which is excited by an ultra-relativistic current backed by a magnetic wall.

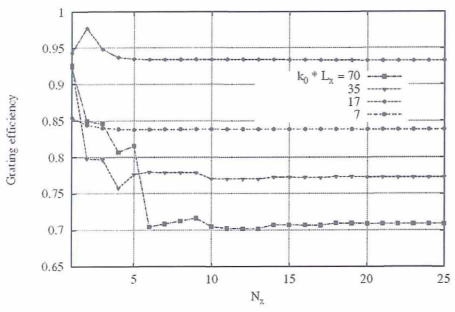

Figure 4: Grating efficiency as a function of the number of field expansion terms for various frequencies.

current is in this case equal to the vacuum wavenumber. Consequently the zeroth order spatial harmonic satisfies the Laplace equation instead of the usual wave equation. Thus we have to use a constant and a linearly increasing function in the x-direction as expansion terms for the y-component of the magnetic field instead of the zeroth order spatial harmonic of the standard Rayleigh expansion.

2 ABSORPTION CHARACTERISTICS OF A RECTANGULAR WAVEGUIDE ARRAY

The mode matching technique leads to an infinite system of equations for the unknown field expansion coefficients which has to be truncated if the method is implemented on a computer. Therefore it is essential to study the convergence of the results with respect to the number of field expansion functions.

Fig. 4 shows the grating efficiency as a function of the maximum order of the spatial harmonics in the x-direction for a grating with typical dimensions of the proposed absorber. The normalized wavenumbers $k_0 L_x = 70$, 35, 17 and 7 correspond to frequencies of approximately 2000, 1000, 500 and 200 GHz, respectively. For a frequency of 200 GHz accurate results are already obtained for $N_x = 5$ whereas $N_x = 20$ is required for a frequency of 2000 GHz. Thus $N_x = 20$ is used for all further calculations which means that approximately a (1500×1500) linear system of equations has to be solved. Assuming this parameter, a typical frequency scan with 1000 points requires about 2 d of cpu-time on a modern workstation.

If the electric field vector of the incoming wave goes along the x- or the z-direction the grating analysis reduces

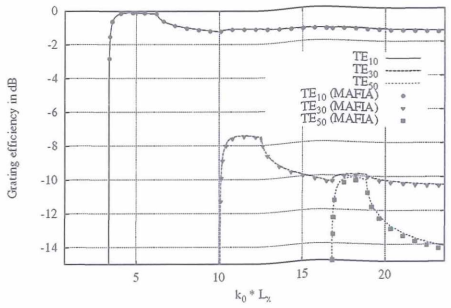

Figure 5: Comparison between the MAFIA computer code and the presented mode matching technique.

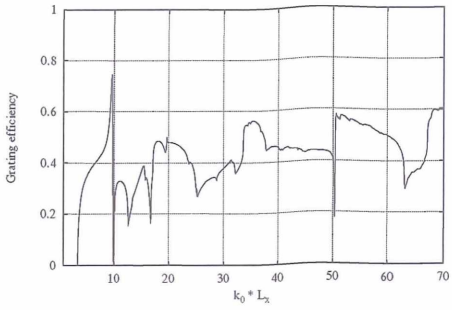

Figure 6: Absorption characteristics for a nearly grazing incident field.

to a waveguide discontinuity problem which can also be solved using the MAFIA computer code [4]. Fig. 5 shows the excitation of the TE_{10}, the TE_{30} and the TE_{50} rectangular waveguide modes as a result of both methods. It is found that in the investigated frequency range from 100 GHz to about 700 GHz the results agree very well.

In the case of normal incidence the grating efficiency is greater than 0.6 (except for frequencies which are very close to the cutoff frequency of the fundamental mode of the rectangular waveguide) which means that more than 60% of the power of the incoming wave is extracted by the grating. Nevertheless the grating efficiency decreases for obliquely incident fields. But even if the angle between the direction of propagation of the incoming wave and the grating interface is only 15° the average grating efficiency is still about 40% (Fig. 6).

3 BEAM PARAMETERS OF AN INFINITE PERIODIC STRUCTURE

Fig. 7 shows the real part of the beam impedance for a planar grating as a function of frequency. The maximum normalized wavenumber which is $k_0 L = 200$ corresponds to a frequency of about 10 THz for a period length of the grating of 1 mm. The beam impedance is calculated at 32768 frequency points and 200 spatial harmonics are taken into account.

The beam impedance is a smooth function of $k_0 L$ in the frequency range from dc to $k_0 L = \pi$. On the other hand it starts to oscillate rapidly at for higher frequencies where the first higher order spatial harmonic turns from evanescent to propagating with respect to the x-direction. This leads to resonances between the magnetic wall and

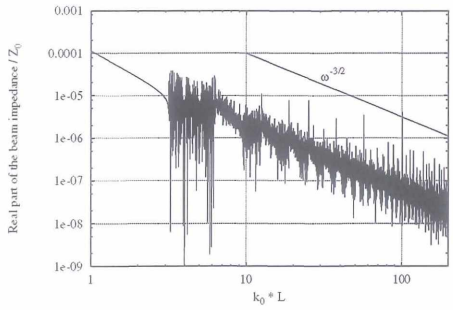

Figure 7: Real part of the beam impedance for a planar grating as a function of frequency. Parameters: $L = 4/15\,\text{mm}$, $L_0 = 0.5L$ and $d = 35\,\text{mm}$.

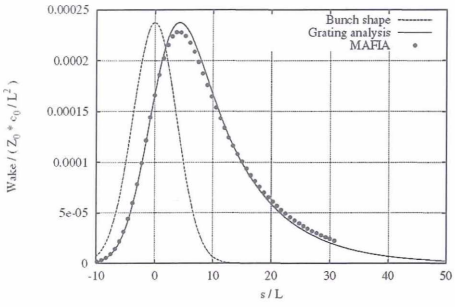

Figure 8: Comparison of the wakefields between the presented mode matching analysis and the MAFIA computer code. Parameters: $L = 4/15\,\text{mm}$, $L_0 = 0.5L$, $a = 5\,\text{mm}$ and $\sigma = 1\,\text{mm}$.

the grating interface with a high spectral density because $d = 35\,\text{mm} \gg L = 4/15\,\text{mm}$.

In Fig. 7 a logarithmic scale is used for both axis. Thus a curve which is proportional to $\omega^{-3/2}$ corresponds to a straight line with a slope of $-3/2$ which is also given in this Fig. From the two curves it can be concluded that the averaged beam impedance also drops as $\omega^{-3/2}$ which has already been shown in [5].

In Fig. 8 the wakefields corresponding to the presented mode matching analysis and the MAFIA computer code [4] are compared. For the MAFIA calculations a corrugated circular beampipe with a length of 200 periods is assumed. The wakefield corresponding to the mode matching technique is obtained by scaling the result from the equivalent planar model. The agreement of the two wakefields is quite good which confirms the validity of the presented method.

The dependence of the wakefield on the bunch length is illustrated in Fig. 9. The results which are presented in this Fig. are valid for a circular configuration with a radius a. The curves converge to an asymptotic wakefield corresponding to an infinitely small bunch length. For the given parameters the wakefield gets very close to the asymptotic curve ($\sigma/L = 0.1$) for a bunch length in the order of one grating period. Such an asymptotic wakefield has also been used in [6] where it is approximated by a special fit.

4 CONCLUSIONS

The mode matching technique has been applied for the analysis of a two-dimensional array of rectangular waveguides which serves as a model for a HOM absorber. A

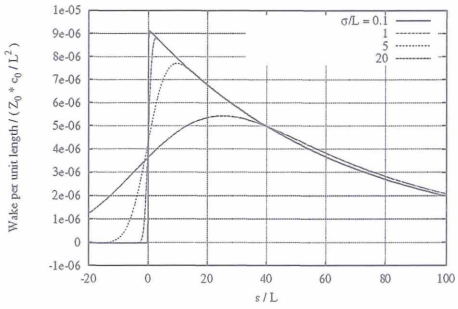

Figure 9: Dependence of the wakefield on the bunch length. Parameters: $L_0 = 0.5L$, $a = 262.5L$.

detailed study of convergence has been carried out in order to demonstrate the accuracy of the presented method. Furthermore the validity of the results has been checked by comparing the excitation of the rectangular waveguide modes with corresponding numbers from MAFIA computations for the special case of normal incidence. The analysis of a grating with typical absorber dimensions has shown that the average grating efficiency is quite high. Although this quantity decreases as we approach the case of grazing incidence the overall absorption properties of such a grating seem to be acceptable. In the second part of this contribution the mode matching technique has been applied to compute the electromagnetic field excited by a bunch of ultra-relativisitic particles traversing a planar grating. It has been shown that the standard Rayleigh expansion which is usually used to represent the field above the grating has to be modified in this case. The beam parameters have been calculated for various structures; and the validity of the presented method has been checked.

5 REFERENCES

[1] A. Jöstingmeier, M. Dohlus, N. Holtkamp and M. Shahabadi, "Computation of the absorption characteristics of a two-dimensional rectangular waveguide array using the mode matching technique", will be published as TESLA report, 1998.

[2] A. Wexler, "Solution of waveguide discontinuities by modal analysis", *IEEE Trans. Microwave Theory Tech.*, vol. MTT-15, pp. 508–517, 1967.

[3] A. Jöstingmeier, M. Dohlus, N. Holtkamp and M. Shahabadi, "Application of the mode matching technique for the computation of the beam parameters of an infinite periodic structure", will be published as TESLA report, 1998.

[4] T. Weiland, "On the numerical solution of Maxwell's equations and applications in the field of accelerator physics", *Particle Accelerators*, vol. 15, pp. 245–292, 1984.

[5] S. A. Heifets and S. A. Keifets, "High-frequency limit of the longitudinal impedance of an array of cavities," *Phys. Rev. D*, vol. 39, pp. 961–970, 1989.

[6] R. Brinkmann *et al.* (ed.), *Conceptual design of a 500 GeV e^+e^- linear collider with integrated X-ray laser facility*, DESY 1997-048, 1997.

EXPERIENCE WITH THE CONTROL OF THE VECTOR SUM AT THE TESLA TEST FACILITY

A. Gamp, S. Goloborodko, A. Kholodnyi, M. Liepe, T. Plawski, K. Rehlich,
T. Schilcher, S.N. Simrock, Y. Tchernoousko, DESY, M. Hüning, RWTH Aachen

1 ABSTRACT

In the rf system for the TESLA Test Facility each klystron will supply rf power to up to 32 cavities. The superconducting cavities are operated in pulsed mode and at high accelerating gradients. The control of significant Lorentz force detuning and precise calibration and measurement of the vector sum are the main issues to be solved. Presently installed are 8 cavities in the first cryomodule of the linac which have been in operation since June 97. Initial commissioning has been conducted in a very short time due to the extensive diagnostics available in the digital the rf control system. The paper describes commissioning of the rf system with emphasis on the calibration of the vector-sum, adaptive feedforward, and the various diagnostic tools available. RF control performance and plans for the control of 24 cavities are also presented.

2 INTRODUCTION

The rf system at the Tesla Test Facility [1] must maintain the accelerating field within given tolerances [2] during beam acceleration. The pulsed cavity field - defined as the vector sum of up to 32 cavities - consists of three segments (see fig. 1):

- cavity filling time (500 μs)
- beam-on (flat-top) time (800 μs)
- cavity field decay (τ_c = 700 μs).

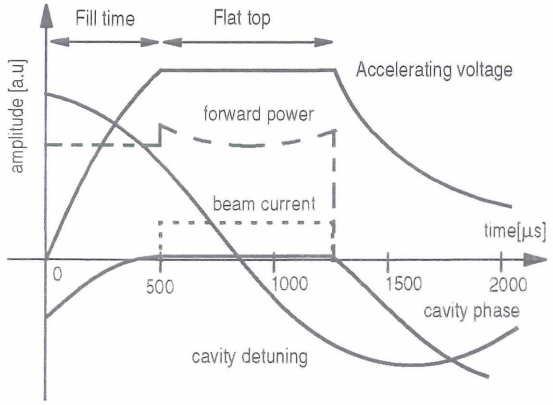

Figure 1: Various parameters related to the pulsed cavity fields in the superconducting cavities of the TESLA Test Facility.

The control of the cavity field has been considered a challenging task for the following reasons:

- the Lorentz force will detune the cavity by more than one cavity bandwidth during a 1.3 ms rf pulse. Therefore additional power is needed for rf control,
- microphonics will modulate the pre-detuning of the cavity at the begin of the pulse and increase peak power requirements necessary for control,
- the vector-sum must be calibrated to better than ±10% for the gradient and ±1° in phase for each cavity to achieve an rms energy gain stability of 2.7×10^{-4} assuming a microphonic noise level of ±10°,
- the vector-sum of 32 cavity probe signals must be regulated to an amplitude stability of the order of $\sigma_A/A \le 2\cdot10^{-3}$, and a phase stability of $\sigma_\phi \le 0.5°$,
- beam loading transients of $\Delta A/A = 1.4\cdot10^{-3}$ with TTF Injector II: the bunch charge is $5\cdot10^{10}$ e^-, and the repetition rate is 1 MHz which corresponds to an average beam current during the beam pulse of 8 mA.

The feedback system for the TTF has been designed as a fully digital system [1] to provide a time varying cavity field setpoint which is important during the cavity filling. A time varying feedforward [3] is applied to compensate repetitive perturbation such as the dynamic Lorentz force detuning and beam loading. Extensive build- in diagnostics allow for precise calibration of the vector sum [4] and inform the operator about beam phase, cavity detuning, loaded Q of the cavity, and the feedback loop phase [5].

3 OPERATOR INTERFACE

The digital rf feedback system employs tables for real and imaginary components of the cavity field setpoint, feedback gain, and feedforward signal to allow for time varying vectors for these parameters. To simplify the generation of the setpoint tables the operator only need to provide input for the following parameters:

- cavity gradient and cavity phase
- start time for cavity filling, cavity fill time and flat top duration

The feedforward tables are derived from the cavity setpoints but additional information about phase offset between setpoint phase and feedforward table, power reduction ratio after cavity filling, and beam parameters such as beam current, phase, duration, and injection time are needed. Hardware signal scaling factors require a one time adjustment during commissioning.

3 CALIBRATION OF THE VECTOR SUM

Since multiple cavities are driven by one klystron, it is not

possible to maintain field control in the individual cavities. It is therefore necessary to control the vector-sum of the individual cavity voltages. The calibration of the vector-sum is based on beam induced transients [4] and is implemented as open loop and closed loop version. The open loop implementation achieves higher resolution since it uses the 14-bit ADCs in the digital feedback while the closed loop version maintains constant acceleration but suffers from the lower resolution 12 bit ADCs used for the measurement of the incident wave.

The accuracy of the calibration depends solely on the accuracy with which the beam current is known (about 1%), the cavity shunt impedance $(r/Q)*Q_L$ and the magnitude of the transient which depends on the beam duration. With 30 μs beam pulses at an average current of 8 mA, a loaded Q of $2*10^6$, and (r/Q)=1030 Ω the induced transients are of the order of 1 MV/m which can measured with an accuracy of better than 1%.

The calibration of the vector-sum requires only 10 minutes of dedicated open loop operation. A typical calibration accuracy of 5% for gradient and 3 degrees for phase has been achieved mainly limited by the accuracy of the beam current calibration. The calibration of the vector sum has been verified with the spectrometer. Relative calibration accuracy is expected to be better than 2% and 1 deg. respectively. In the future the calibration process will be fully automated and used to track any changes in calibration.

5 RF SYSTEM OPERATION

The startup procedure has been simplified greatly by use of automated procedures. The following steps are usually necessary to run the rf system:

- Load vector-sum calibration parameters.
- Open loop operation without beam. Adjust feedforward scaling parameters to approximate operating gradient.
- Determine loop phase.
- Closed loop operation without feedforward and beam. Adjust closed loop parameters to match open behavior approximately.
- Add feedforward.
- Turn beam on.
- Determine beam phase and adjust to operation on crest
- Activate beam loading compensation and adjust necessary parameters.
- Verify loaded Q and phases of incident waves. Adjust phase of incident wave with wave guide tuner.
- Activate adaptive feedforward.

With the new operator interface described a trained operator can turn the rf system on within 10 minutes. It is planned to automate the above described procedure in the future. Presently all exception handling as a result of interlock trips such as cavity quench, coupler window arc detector and many others must be reset by the operator. During a typical run some interlock trips occur during the turn on phase while the trip rate during routine operation is very low (less than 1 trip of any type per hour).

5 RF SYSTEM DIAGNOSTICS

Several rf utilities assist the rf system user during accelerator operation.

5.1 Loop Phase

The loop can be determined easily during open loop operation. If the phase of the incident wave is held constant during the first few ten microseconds of cavity filling, the loop phase can be determined by measurement of the phase angle of the cavity field during times short compared to the time constant of the cavity. This method allows for a detuning independent measurement of the loop phase. The accuracy of the measured loop phase in a single pulse is about 1 degree but can be improved by averaging over several pulses.

5.2 Beam Phase

The beam phase is calculated by the method of system identification [5] which gives a best estimate of the parameters in the rf system model. The time varying beam phase of individual cavities or the vector-sum can be determined in open or closed loop configuration with an accuracy of a few degrees during a single macropulse. A better accuracy can be achieved by averaging if the signals are repetitive.

5.3 Loaded Q and Cavity Detuning

The loaded cavity Q and the cavity detuning at the end of the rf pulse can be determined from the slope of cavity gradient and cavity phase respectively. Using the first two hundred microseconds of the field decay one yield a single pulse accuracy of 1% for loaded Q and 0.5 Hz for the cavity detuning. Measurement of cavity detunings for several pulses allows to display the probability density of the resonance frequency which is a measure for the amplitude of the microphonic noise.

5.4 Lorentz Force Detuning

A very interesting application of system identification is the measurement of the time varying detuning during the rf pulse. The method an the result are described in detail in [5]. A typical result is shown in figure 2. It can be seen that the lorentz force detuning is about ±10Hz at 15 MV/m.

5.4 Phase of Incident Wave

Also the phase of the incident waves is determined by the system identification tool. The phase can be determined with an accuracy of 3 degrees and can be used to adjust the three stub wave guide tuner which have a typical tuning range of ±100 degrees.

6 ADAPTIVE FEEDFORWARD

In addition to the feedback control loop which suppresses stochastic errors, feedforward is applied to reduce repetitive perturbations induced by beam loading and dynamic lorentz force detuning. The error reduction with the feedforward is significant since repetitive errors are dominant. The feedforward algorithm first identifies the time varying state space model of the closed loop system by measurement of a step response. Next the pulse to pulse average of the measured perturbations is applied to the inverse state space model to obtain the correct feedforward table. The feedforward tables can be updated continuously to follow slow changes in the perturbation parameters. On-line system identification is transparent to routine beam operation due to the small step size used.

6 RF CONTROL PERFORMANCE

The requirements of $\sigma_A / A \leq 2 \cdot 10^{-3}$ for amplitude stability and of $\sigma_\phi \leq 0.5°$ phase stability can be achieved with a feedback gain of 70 while the feedforward is turned off. The residual fluctuations are dominated by a repetitive component which can be further reduced by a factor of 10 with the adaptive feedforward thereby exceeding the design goals significantly. The high degree of field stability is mainly due to the low microphonic noise levels. A typical result of measured field stability without and with the adaptive feedforward is shown in Figure 3

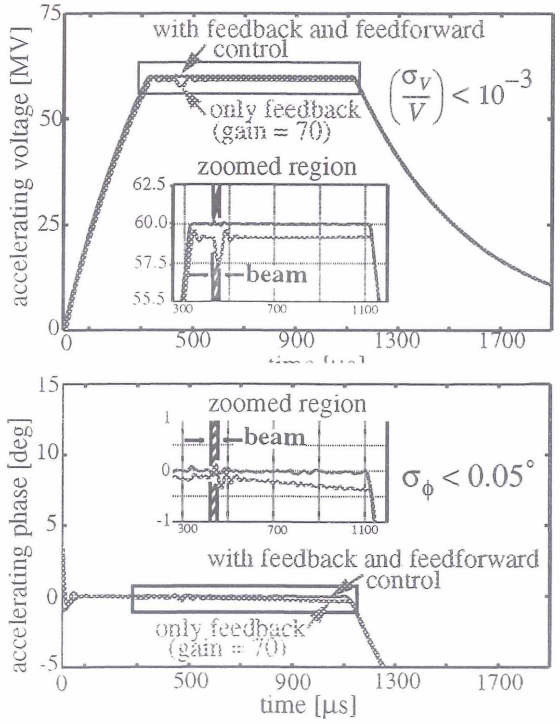

Figure 3: RF control system performance without and with adaptive feedforward.

7 CONTROL FOR 24 CAVITIES

It is planned to extend the rf feedback system for the control of the vector sum of the 24 cavities in the first three cryomodules by end of this year. The feedback algorithm will be improved and include Smith predictor and Kalman filter to allow for an increase in loop gain and simultaneous reduction of electronic noise in the loop. It is also desirable to operate individual cavities at their maximum operable gradients. This can be achieved with certain restrictions by appropriate adjustment of the loaded quality factor using the three stub wave guide tuner.

7 CONCLUSION

The digital rf control system exceeds the requirements for field stability significantly mainly due to the small microphonics levels. It will still meet the requirements up to microphonic levels of ±50 Hz.Rf operation is greatly simplified by an operator interface which calculates the tables needed for setpoint and feedforward including beam compensation from a few essential parameters. Extensive diagnostics for loop phase, beam phase, cavity detuning and other parameters allow the operator to turn the system on within 10 minutes. The critical issues such as calibration of the vector-sum, control of lorentz force detuning, microphonics and beam loading have been solved by appropriate design of the rf system.

8 ACKNOWLEDGEMENTS

We gratefully acknowledge the support from the linac operations group. Their dedicated support in all linac commissioning issues has been the basis for our success.

7 REFERENCES

[1] S.N. Simrock, I. Altmann, K. Rehlich, T. Schilcher, *Design of the Digital RF Control System for the TESLA Test Facility*, EPAC 96, Sitges (Barcelona), Spain, June 10-14, 1996, p. 349

[2] S.N. Simrock, I. Altmann, K. Rehlich, T. Schilcher, *Operational Aspects of the RF System for the Test Facility*, EPAC 96, Sitges (Barcelona), Spain, June 10-14, 1996, p. 1869

[3] M. Liepe, S.N. Simrock, *Adaptive Feed Forward for Digital RF Control System for the TESLA Test Facility*, these proceedings

[4] S.N. Simrock, T. Schilcher, *Transient Beam Loading based Calibration of the Vector-Sum for the TESLA Test Facility*, these proceedings.

[5] M. Hüning, S.N. Simrock, *System Identification for the digital RF Control for the TESLA Test Facility*, these proceedings

DESIGN OF THE RF PHASE REFERENCE SYSTEM AND TIMING CONTROL FOR THE TESLA LINEAR COLLIDER

A. Gamp, M. Liepe, T. Plawski, K. Rehlich, S.N. Simrock, DESY
Notkestr. 85, D-22603 Hamburg, Germany

ABSTRACT

The frequency distribution system for the TESLA linear collider must deliver a highly phase stable rf signal to the 616 rf stations over a length of 33 km. At the operating frequency of 1300 MHz a short term and long term stability of the order of 1 degree with respect to the accelerated beam is required. Our solution involves three coherent oscillators, a 9 MHz low loss coaxial cable distribution, 1.3 GHz fiber optics, and continuous calibrations based on beam phase measurements. This system is transparent to beam operation and will continually monitor and correct slow phase drifts.

1 INTRODUCTION

The overall layout of the TESLA linac [1] is sketched in Figure 1. The main elements are two linacs with a length of 2×12 km, the damping rings which make use of the linac tunnel, the source for electrons (laser driven rf photocathode gun), the source for the positrons which is based on the concept of high-energy photon conversion into e^+e^-, and a 3 km region for the beam delivery system in between the two linacs. The photon are generated by the spent high-energy electron beam passing a wiggler. The acceleration system in each linac consists of 9856 superconducting cavities which are powered by 308 klystrons (32 cavities per 10 MW klystron)

The various rf system that must be phase synchronized with picosecond stability over the full accelerator length are:

- the 616 rf systems operating at 1300 MHz in the two superconducting linacs.
- The 433 MHz rf systems for the damping rings
- the 1300 MHz rf system providing power to the photocathode rf gun of the electron source and the associated laser for illumination of the photocathode.

The timing system must guarantee that the bunches which are spaced by 337 ns (3 MHz repetition rate) arrive at the same time at the interaction region.

2 RF DISTRIBUTION STABILITY REQUIREMENTS

The phase stability requirements for the accelerating field in the linac cavities are dictated by the low beam energy spread requirement of $\sigma_E/E < 7\times10^{-4}$ and the timing requirements for the bunch arrival at the interaction point. Assuming that a third of the energy spread contribution originates from phase fluctuations of the accelerating field a correlated phase error of only $\sigma_\phi = 0.4°$ at 1300 MHz corresponding to a timing error of 0.8 picoseconds can be tolerated.

The phase stability of the 433 MHz rf systems of the damping rings determines that arrival time of the bunches at the interaction point. The interaction position error should not exceed one bunchlength (1 mm) resulting in the same timing stability requirements as dictated by the low energy spread.

In addition to the rf phase reference system a timing system with event coding capability is required to allow for real time synchronization of the various rf and other subsystems. The electron and positron bunches must be accelerated in selected rf buckets (every 438^{th} bucket, this number is given by the ratio of bunch spacing and the period of one rf cycle) to guarantee that the collision takes place in the center of the detector. A misplacement by 1 bucket would result in a collision position error of 23 cm (λ=c/f=23 cm). Therefore the timing system for the rf gun must guarantee a trigger signal stability of better than 770 ps. The timing system clock will also be synchronized to the master oscillator and can therefore provide phase stable timing for the digital feedback and rf system monitors.

3 DESIGN CHOICES AND ISSUES

The four basic choices for a phase stable reference system are:

- coaxial distribution system
- fiber optic distribution system
- coherent oscillators
- beam pickup

All systems with the exception of the beam pickup require a beam based calibration scheme since calibrations by measurement of the electrical length of the subsystems is not sufficiently accurate. It is desirable to use a fast coarse calibration scheme for initial start-up of the accelerator and a slow and precise calibrations scheme which is active during accelerator operation and which is transparent to the beam experiments.

The rf distribution system for the TESLA linear collider has been designed as a combination of all of the above options to utilize the advantages of each of the systems thereby maximizing performance and providing some level of redundancy.

The design employs a coaxial distribution system in the linacs. It provides a phase stable 9 MHz signal to all of the

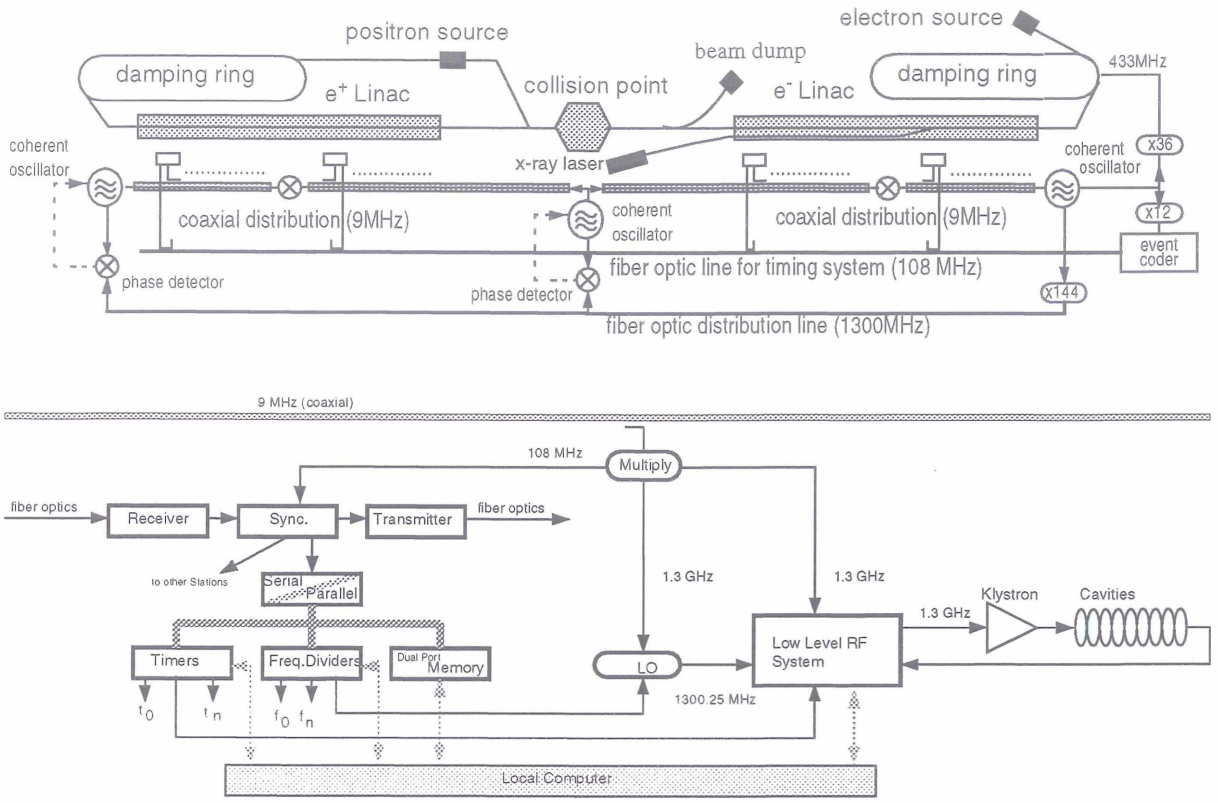

Figure.1 : Overall layout of the TESLA Linac. The phase reference system and timing control distribution are shown.

616 rf stations in the linacs and the 433 MHz systems in the damping rings. The signals are locally multiplied by 144 or 36 respectively. Coherent oscillators operating at 9 MHz are located at the beginning of each linac close to the 433 MHz rf systems (also close to rf gun for electrons and auxiliary positron source) and in the experimental hall between the linacs. The three oscillators are synchronized by a optical fiber system. Each of the oscillators provides the reference signal for half of the linac closest to it. All systems are measured against each other and calibrated with reference to the beam utilizing the beam induced transients.

3.1 Coaxial Distribution System

The distribution of rf signals by coaxial cables or waveguides appears to be the most obvious solution since the rf signal can be transported directly to its destination. For the distribution to many rf stations directional couplers are recommended for good isolation between the tap points. This scheme allows for relatively high power levels of up to a few hundred watts at the input of the distribution line and can provide several milliwatts to several watts of rf power to each station. The main parameters that need to be considered for a coaxial distribution system are:

- frequency to be distributed
- distance between signal source and destination
- numbers of destinations to which the signal must be supplied
- power level of signal required at destinations
- power level available at signal source
- attenuation of coaxial cable
- power handling capability of the cable and the directional couplers
- thermal stability (phase stability of cable)
- number of amplifier needed within the distribution system
- sensitivity to microphonics

In the case of TESLA it is advisable to distribute a lower frequency and to convert the frequency locally to the operating frequency by use of multipliers. This method reduces the rf losses in the distribution system significantly. The lower frequency limit is given by the efficiency, noise characteristics, and phase stability of the local frequency multipliers.

For the TESLA accelerator the operating frequency is 1300 MHz but the coaxial frequency distribution along the linac is operated at 9.0278 (= 1300/144) MHz. The signal sources - H^--masers controlled low noise oscillator operating at 9 MHz and boosted by 200 W amplifiers - are located at the beginning of each linac and in the experimental hall between the linacs. For the coaxial distribution system a 1 5/8" (type LDF-50A1-5/8-inch Heliax) cable has been chosen because of its low insertion loss of 0.2 dB/100 m, the excellent phase stability (10 ppm/deg. C) and power handling (42 kW) capability. With a group velocity of 0.88c this results in a phase sensitivity of 177 deg./°C/10 km. The actual sensitivity may deviate from

this number since the cable cannot expand freely due to its own mass.

The directional couplers (type HDC1460 from HD Communications) exhibit an insertion loss of 0.15 dB / coupler. The distribution scheme for the linac is shown in Figure 1. Input power for each of the 7 km long sections is 200 W. The number of couplers has been reduced to 50 with a spacing of 120 m. A three way power splitters feeds a subnet consisting of LDF 1/2" cable to the two adjacent stations. The 9 MHz signals are then locally multiplied by 144 in the linacs and 36 at the damping ring rf systems.

3.2 Fiber Optic Distribution

Over the past years, fiber optic distribution links have replaced coaxial cable distribution for phase reference systems [2]. Optical fibers are the preferred medium for distribution because of their low attenuation, immunity to EMI/RFI, and temperature stability.

The thermal coefficient of delay for a typical optical fiber is of the order of 7 ppm/°C and therefore comparable to that of phase stabilized coaxial cables. A LCD coated optical fiber from Sumitomo [3] which has been specifically designed for high thermal stability provides a stability of better than 0.4 ppm/°C at an operating temperature close to 0°C. At a more realistic operating temperature of 30°C the coefficient increases to 1 ppm/°C. The group velocity in this fiber is 0.66c resulting in a phase sensitivity of 23.6 deg./°C/10 km.

The phase noise characteristics of a fiber optic distribution system suffers from the low signal levels retrieved at the individual receivers. The minimum phase noise level at 1300 MHz is expected to be around -100 dBc (> 10 kHz) [2] corresponding to an rms phase error of 0.57 deg. or 1.2 ps timing jitter which is marginal for our application.

3.3 Coherent Oscillators

The timing stability requirements between two remote locations such as the rf stations for the damping rings which are separated by a distance of 32 km could be fullfilled with two absolutely coherent oscillators. Present technology utilizing a H^- Maser allows for a frequency stability of 2×10^{-13}/s corresponding to a phase stability of about 0.1 deg./s (or 0.2 ps/s) thereby exceeding the requirements for intrapulse and pulse-to-pulse stability. Even oven stabilized crystal oscillators can achieve a stability of the order of 2×10^{-12}/s which might be sufficient.

The coherent oscillators will be synchronized with the fiber optic distribution system with a time constant of 10 - 100 s to ensure long term stability.

3.4 Beam Based Phase Calibration

The ultimate reference for the rf systems in the linacs, the damping rings, and the timing of the bunches at the collission point will be the beam itself. It is therefore foreseen to synchronize all rf systems with respect to the beam. To achieve a measurement accuracy of better than 0.5 deg. or 1 ps, the transient beam loading based algorithm must average over several hundred measurements resulting in a measurement time of up to 100 seconds. Therefore the beam based phase correction can take place at a time scale of 100-1000 s.

4 TIMING CONTROL

The timing system provides various triggers and fixed frequency signals as well as machine parameters in a dual-port memory. A central timing signal source is synchronized with the master oscillator. This signal source generates encoded telegrams and sends them via a fiber optic distribution system to all devices along the linac and the damping rings. Repeaters every 120 meter receive the signals, resynchronize them with the 9 MHz, distribute the data to the local equipment and retransmit the signals to the next stations. The received serial telegrams have to be encoded and converted into parallel data streams. This data stream contains events and data words from the master station. Since the telegrams are synchronized with the main oscillator fixed frequencies with low phase errors can be derived from the telegrams also. The data stream is used to filter events in a timer unit and data words in the dual port memory. Programmable timers are triggered by these events to generate the start pulses for the klystrons or digital signal processors for instance. A timer unit provides several independent output channels. Some machine parameters that change from macro pulse to macro pulse need to be delivered in time to run all digital feedback loops in parallel. The data words from the telegrams are stored in a dual port memory. This information is readable from the local connected computers or signal processors.

5 CONCLUSION

The design of a rf phase reference and timing system for the TESLA linear collider is a challenging task due to the tight timing stability requirements of about 1 picosecond over a distance of more than 30 km. It should be possible to meet these requirements if a combination of coaxial distribution, optical fiber distribution, coherent oscillators and beam based calibration is used. It is planned evaluate the performance of such a scheme at the TESLA Test Facility.

REFERENCES

[1] R. Brinkmann, Linear Collider Projects at DESY, EPAC98, Stockholm, Sweden, June 22-26, 1998, in print.

[2] M. Calhoun, *Fiber Optic Reference Distribution to Remote Beam Waveguide Antennas*, JPL Report 95-0037, Reston, VA, December 5, 1994

[3] Kakuta, Tanaka, *LCD Coated Optical Fiber with Zero Thermal Coefficient of Transmission Delay Time,* Sumitomo Electric Industries Ldt., Yokohama, 244, Japan.

[4] A.N. Luiten, A.G. Mann, E.N. Ivanov, D.G. Blair, *Latest Results of the UWA Cryogenic Sapphire Oscillator*, Proc. 49th Annual Frequency Control Symposium. San Francisco, CA, 1995, pp 433-437.

SYSTEM IDENTIFICATION FOR THE DIGITAL RF CONTROL SYSTEM AT THE TESLA TEST FACILITY

M. Hüning, RWTH Aachen, Germany, S.N. Simrock, DESY, Hamburg, Germany

Abstract

The rf control system for the TESLA Test Facility employs a digital feedback system to provide flexibility in the choice of feedback algorithms and extensive diagnostics for rf system operation and exception handling. The control algorithm makes use of the state space formalism where the state describes the real and imaginary part of the cavity voltage (vector of the accelerating field) and the cavity detuning. The cavity detuning – which is time dependent due to the dynamics of lorentz-force-detuning in a pulsed cavity – can not be measured directly. Knowledge about the time-varying cavity detuning and other rf system parameters such as beam phase are derived by application of system identification to the uncalibrated measured cavity field and incident and reflected wave. In this process the calibrations for incident and reflected wave are determined which includes compensation for the finite directivity of the directional couplers.

1 INTRODUCTION

With the advent of reasonably priced high speed data conversion devices and digital signal processors which combine tremendous computing power and I/O capability, the design of rf control circuits will assume a new direction. The concept of digital control provides enormous flexibility in the control algorithms, diagnostics, and exception handling. The concept of system identification provides the possibility to extract information about rf system relevant parameters from measured data. These measurements can be performed online and are transparent to linac operation.

The model of the cavity relating input power and beam current to the time varying voltage and phase of the accelerating field is well understood. The parameters in the differential equation governing the system dynamics can be determined from the measured data. With the knowledge of the system parameters it is possible to predict the time varying cavity detuning, the phase of the accelerating field relative to the beam, and the loaded quality factor. Based on the assumption of continuity of the rf-waves at the input coupler the amplitudes and phases of the incident and reflected waves can be calibrated. A combination of both, the differential equation and the condition of continuity yield the directivity of the directional couplers.

The question remains which parameterized model to choose for a correct description of the non-linear dynamics of the lorentz force detuning . With system identification one can compare different types of models to find the best description. Surprisingly a 1st order model of the mechanical dynamics of the cavity are qualitatively as good as a model of 2nd order. Better results can be achieved if the derivative of the field amplitude is included in the differential equation, but the physics behind this equation are not understood.

2 PRINCIPLE OF SYSTEM IDENTIFICATION

System identification allows to compare different models such as transfer functions or differential equations by fitting the coefficients to match the measured data. Transfer functions are suited for time invariant linear models. An example is the ARX model where the transfer function is a fraction of two polynomials, $H(z) = B(z)/A(z)$. The difference equation of the system is

$$y_{n+k} = a_0 y_n + \ldots + a_{k-1} y_{n+k-1} + b_0 u_n + \ldots + b_l u_{n+l},$$

where $a_0, \ldots, a_k$, $b_0, \ldots, b_l$ are the coefficients of $A(z)$ and $B(z)$. When describing y_{n+k} as function of $y_n, \ldots, y_{n+k-1}, u_n, \ldots, u_{n+l}$ one can perform a regression to determine the coefficients of $A(z)$ and $B(z)$. The noise is considered to modify only the last value y_{n+k}. For linear models there there exists a selection of models characterized by the order of $A(z)$ and $B(z)$ and in which way the noise is handled. One can test different models until the data is reproduced satisfactory. Of course this way of investigation is empirical and does not necessarily lead to a model in which the physics of the system is well understood.

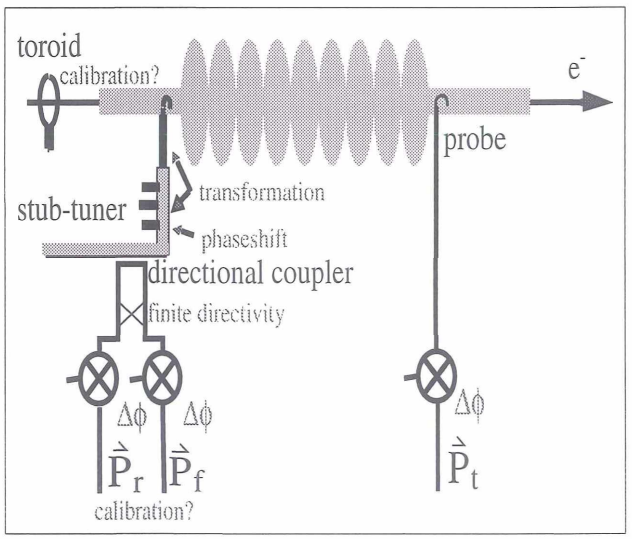

Figure 1: The signals for System Identification

The other approach is based on a parameterized model which is derived from knowledge about the physics of the

system. This can be in the same format as the standard models, but one can also choose the differential equation as a description. For time dependent problems this may be the best solution. The algorithm for numerical differentiation of the raw data is critically important for the accuracy to which the parameters in the differential equation can be determined. At the TTF we fit through every data point a 2nd order polynom to the data next to this point. It's derivative is taken as the data's derivative at the specified point. There is no need for the full regression calculation at every point since most of the calculations are repeated for each point and therefore can be taken over. Discontinuities can be detected by comparison with adjacent polynomials. With this information the differential equation can be calculated – even for time varying systems if necessary.

3 MODEL FOR THE RF-CAVITY

Resonant modes in cavities can be described using resonant LCR circuits. For superconducting cavities the differential equation for the complex field envelope can be reduced to a first order equation

$$\begin{aligned}\dot{\hat{V}}_{acc} &= -\left(\omega_{1/2} - i\triangle\omega\right)\hat{V}_{acc} \\ &\quad +\frac{1}{2}\left(\frac{r}{Q}\right)\omega_0\left(2\hat{I}_f - I_b e^{i\psi_b}\right),\end{aligned}$$

with complex amplitudes $\hat{V}_{acc}$ and $\hat{I}_f$. The beam current I_b is real but has to be multiplied with a complex phase factor. It is the Fourier component of the pulsed beam at ω_0 and therefore $I_b = 2I_{b0}$, with I_{b0} the DC current. The normalized shunt impedance is $\left(\frac{r}{Q}\right) = 520\,\Omega$ for TESLA cavities, the bandwidth is $\omega_{1/2} = \frac{\omega_0}{2Q_L}$ with Q_L in the range of $2 \cdot 10^6 \ldots 3 \cdot 10^6$ for TTF.

Due to lorentz force detuning the cavity detuning is time dependent $\triangle\omega = \triangle\omega(t)$, which means that the differential equation is time dependent. Written in polar coordinates the complex differential equation splits up into two decoupled equations whose first depends on $\omega_{1/2}$ and second depends on $\triangle\omega$. The first one is time independent and can be used for calibration purposes. From the second equation one can calculate the detuning of the cavity at every time step of one microsecond at the TTF.

4 RESULTS

4.1 Cavity Phase

One of the most important properties of the rf field in the cavities is their phase with respect to the beam. It is desireable for the linac operation that there is the possibility to measure the phase whatever operational mode is active. In the cavity-equation the beam current is introduced as a complex vector. Once $\hat{V}_{acc}$ and $\hat{I}_f$ are calibrated correctly it is possible to extract ψ_b from the data.

Figure 2 shows histograms of some measurements of the beam phase taken in the first module of the TTF-linac. The

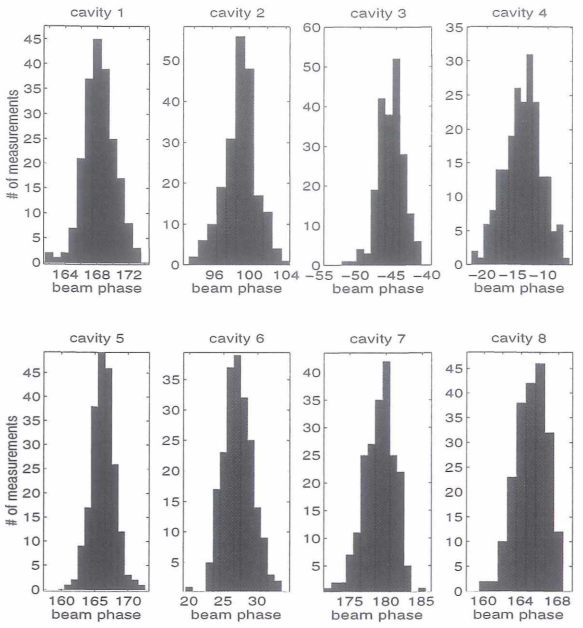

Figure 2: Measurements of the beam phase in the 8 cavities of the first TTF-module.

measurements were taken during standard linac operation with feedback and feedforward applied. It shows that determination of the beam phase is possible with a σ of about 3°. The measurements were taken when $\hat{V}_{acc}$ and $\hat{I}_f$ were consistent within each other but had some arbitrary phase offset. The right phase calibration can be achieved by correcting all measured phases in such a way that the centroid of the beam phase distributions become zero.

4.2 Time varying Cavity Detuning and Q_L

The TTF linac is operated in pulsed mode so that the cavities are dynamically detuned during every rf pulse. For optimization of the cavity tuning and as an input for sophisticated control algorithms like a smith-predictor it is necessary to know the time dependent detuning of the cavities. Starting about $50\mu s$ after beginning of the rf pulse where the gradient exceeds about 1MV/m it is possible to determine the detuning of each cavity. The main noise sources are the fluctuations of the numerical derivative and noise on the forward power.

Several models have been compared to describe the detuning curves. Reasonable results have been achieved with differential equations of 1st and 2nd order taking $|V_{acc}|^2$ as an input and $\triangle\omega$ as output. The best reproduction of the measured data could be accomplished with a model of first order when including $d|V_{acc}|^2/dt$ as input.

4.3 Calibration of Directional Couplers

The quality of the data extracted from the system identification strongly depends on the accuracy of the calibration of the forward power signal. Due to the finite directivity of the directional couplers there is always some crosstalk

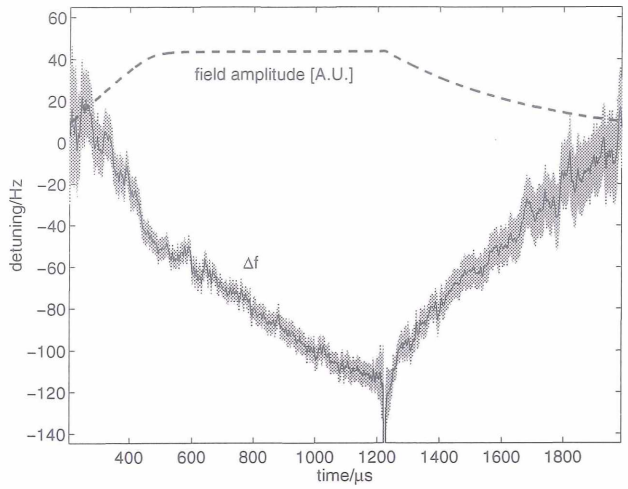

Figure 3: Time varying detuning of cavity D1 at 15 MV/m including one standard deviation of the error. For reference the field amplitude has been added to the plot.

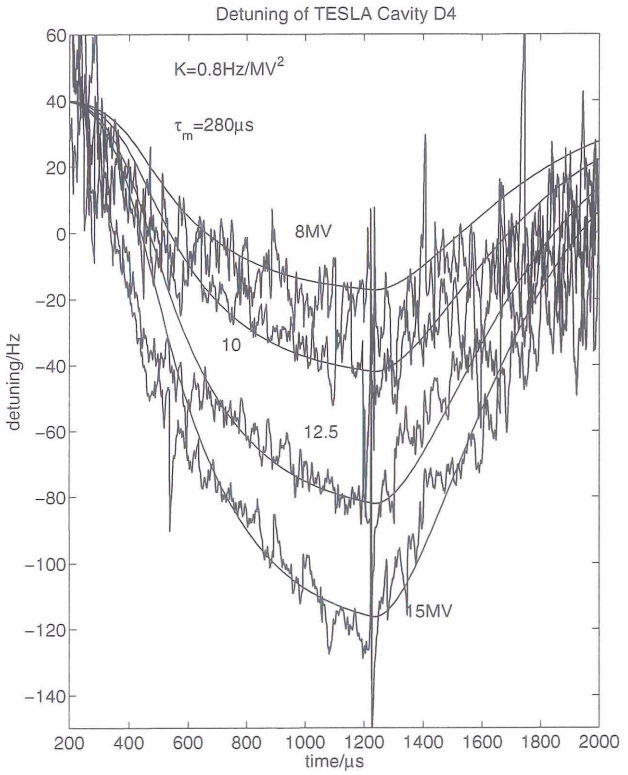

Figure 4: Detuning of cavity D4 at four different gradients. A model of first order has been adapted to the data of the strongest detuning. With this model the detuning has been simulated for all four gradients.

between the signal of the forward power and the reflected power. The reflected power signal can be eliminated from the measured forward power by subtracting $\hat{d}_r \hat{I}_r$ from $\hat{I}_f$ with $\hat{d}_f$ such that $\hat{I}_f \equiv 0$ during the field decay. From

$$\hat{V}_{acc} = R_L(f_f \hat{I}_f + f_r \hat{I}_r)$$

one finds an amplitude and phase calibration for the incident and reflected wave. As long as the reflected power is not corrected for the directivity this calibration will be wrong. From the condition $\omega_{1/2} = const$ one finds the correct calibration for $\hat{I}_f$. The comparison of both calibrations delivers the second correction factor for the directivity.

5 CONCLUSION

The methods of system identification have been applied to the digital rf feedback system at the TESLA Test Facility. Knowing the cavity model - which can be described as a time varying state space model - one can determine rf system parameters such as beam phase, time varying cavity detuning, phases of incident waves and many more by the measurement of the uncalibrated cavity probe, incident wave and refleced wave systems. The knowledge of these parameters has been critically important during the commissioning of the rf system and will be used in the future to automate most of the rf operation relevant procedures.

6 ACKNOWLEDGEMENTS

We want to express our thanks to M. Liepe who has made his expertise in system identification available to us through many invaluable discussions.

7 REFERENCES

[1] M. Hüning: "Selbstoptimierende Parametersteuerung der Hochfrequenz des supraleitenden Linearbeschleunigers TESLA Test Facility", PITHA 98/7, RWTH Aachen

REQUIREMENTS FOR THE RF CONTROL OF THE VECTOR SUM FOR SUPERCONDUCTING PROTON LINACS

M. Hüning, S.N. Simrock, DESY, Notkestr. 85, D-22603 Hamburg, Germany
T. Schilcher, PSI, CH-5232 Villigen, Switzerland

ABSTRACT

Superconducting accelerator technology has demonstrated its superior performance in large scale machines such as CEBA at TJNAF and is increasingly used for new accelerator designs. Until now this technology has found its main application in electron accelerators. However nowadays proton accelerator designs for the European Spallation Source (ESS) and the Accelerator Driven Transmutation Technology (ADTT) also study the feasibility of superconducting linacs. In contrast to the highly relativistic electron beams the proton beam exhibits an increased susceptibility to voltage fluctuations in the acceleration system induced by microphonics and dynamic Lorentz force detuning. Although low beam loss is an important criterion for linac design, studies of the longitudinal dynamics appear to be a good indicator for beam stability in presence of fluctuations of the accelerating field. Control of the vector sum of multiple cavities driven by one klystron is desirable for cost reasons but does not allow for control of individual cavity fields. In this paper we study the performance of such a system.

1 INTRODUCTION

The technology of proton accelerators has progressed considerably in the past three decades [1]. Several high intensity proton accelerators with high peak or average beam currents of the order of 100 mA are presently under study for applications such as: spallation neutron sources, kaon factory, nuclear transmutation technology, energy amplifier, and muon collider drivers. The implementation of superconducting acceleration systems [2,3] appears to be attractive since it could lead to substantial cost savings in machine operation especially if multiple cavities are driven by one common high power klystron.

An important design criterion for a high intensity proton linac is beam loss control since the beam loss should not exceed 1 nA/m to allow for hands-on maintenance after a long operation period. Particle loss is caused by a small number of particles outside the dense beam core, called the beam halo. The origin and formation and dynamics of the halo have been studied intensively and significant progress has been made in recent years. In superconducting linacs where multiple cavities are driven by a single klystron beam loss may be enhanced by microphonics which are a result of mechanical vibration modulating the resonance frequency of the high Q cavities. In this paper we develop a simple model to determine the impact of fluctuations of the accelerating field on beam energy. For simplicity only the longitudinal dynamics of the bunch centroid are analyzed. Bunches with excessive energy deviations are considered as potential candidates for beam loss. An important result of this model is an upper limit for the microphonics noise levels permitted for accelerator operation.

2 BEAM DYNAMICS MODEL

The energy gain of the bunch centroid when passing a single cavity can be described as

$$\Delta V = V_o \cdot T \cdot \cos(\phi_S),$$

where V_o is the cavity voltage, T is the transit time factor, and ϕ_S the phase angle between beam current and accelerating field. The transit time factor is a function of the bunch velocity $\beta = v/c$ and the phase angle depends also on β according to $\Delta\phi = (2\pi fL)/(c\beta)$, where f is the operating frequency of the rf cavities, and L the drift space between the center of two adjacent cavities. Thereby the dynamics inside the cavities have been approximated by a cavity with length zero and the surrounding drift space.

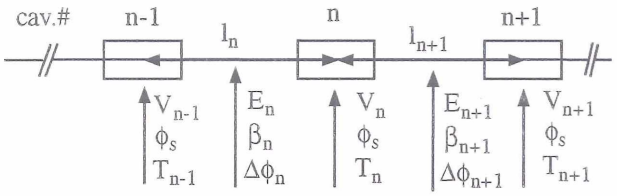

Figure 1: Definition of parameters used for the beam dynamics model.

Changes in transit time factor due to finite cavity length are however considered. For a given linac configuration one can calculate the deviations of beam energy, bunch velocity, and phase of the accelerating field with respect to a reference particle.

$$E_{n+1} = E_n + V_n \cdot \cos(\Delta\phi_n + \phi_s) \cdot T_n(\beta_n)$$

$$\beta_{n+1} = \sqrt{1 - \frac{m_p^2 c^4}{(E_{n+1})^2}}$$

$$\Delta\phi_{n+1} = \Delta\phi_n + \frac{2\pi f l_n}{c} \cdot \left(\frac{1}{\beta_n} - \frac{1}{\beta_{ref}}\right)$$

In the model the transit time factor of a m-cell cavity is derived from the transit time factor $T_1(\beta)$ of a single cell cavity as:

$$T(\beta) = T_1(\beta)2 \cdot \frac{\cos\left(\frac{m-1}{2}(x-\alpha)\right) - \cos\left(\frac{m+1}{2}(x-\alpha)\right)}{m \cdot (1-\cos(x-\alpha))}$$

with

$$T_1 = \frac{\sin(x/2)}{(x/2)} \quad \text{for} \quad E(z) = \text{const.}, \quad x = \frac{2\pi L_n}{\beta\lambda}, \quad \alpha = \frac{k}{m}\pi$$

k=1...m depending on selected passband mode. Here k/m=1 i.e. $\alpha = \pi$ for a standing wave structure. L_n is the length of the cavity.

3 LINAC PARAMETERS

To determine the impact of fluctuations of the accelerating field on the longitudinal dynamics of the bunch centroid the parameters of two recently proposed linac designs have been selected.

Table 1: Sample Linac Parameters

	LINAC 1	LINAC 2
Frequency [MHz]	700	700
Linac Energy [MeV]	1700	1300
Number of cavities	102 & 308	166
Number of cells / cavity	5 & 5	5
Injection energy [MeV]	211 & 470	70
Beta of cavity	0.64 & 0.82	0.37 .. 0.91
Cav. centroid spacing [m]	2.0 & 2.1	0.5 .. 1.36
Synchronouse phase [deg]	-35 & -30	-20

Table 1: Sample Linac Parameters

	LINAC 1	LINAC 2
Energy gain/cav. [MV]	2.5 & 4.0	3.9 .. 9.8
Cavity gradient [MV/m]	5.2 & 5.9	10

4 SIMULATION RESULTS

Based on the beam dynamics model and the sample linac parameters the quantities of interest have been determined for several cases:

1. stochastic cavity amplitude and phase errors along the linac with uniform distribution. The simulation has been performed with various sets of errors for injector and linac.
2. stochastic cavity amplitude and phase errors along linac but the vector-sum of an ensemble of 2 or 4 cavities perfectly regulated.

The deviation of the final linac energy from the reference energy can be used to determine the potential for beam loss. The simulations show that small field fluctuations result in a moderate increase in energy spread while larger errors - depending on the distribution along the linac - may result in basically zero energy gain in the linac due to phase slippage. Particles which do not experience a net energy gain in the linac are likely to be lost due to the lack of rf focusing. Some of the results of the simulations for the different case studies are shown in Table 2. The probability of beam loss is equivalent to linac energy gain less than 90%.

Table 2: Linac Energy Spread (Bunch-to-Bunch) and Particle Loss

Injector Error[1]		Linac cavity error[1]		probability of energy gain < 90% [10^{-5}] [2]						σ_E/E [10^{-4}]					
				no control[3]		vector-sum (2)[4]		vector-sum (4)[4]		no control[3]		vector-sum (2)[4]		vector-sum (4)[4]	
Δφ[°]	ΔE [%]	Δφ[°]	ΔV [%]	Linac type:											
				1	2	1	2	1	2	1	2	1	2	1	2
1	1	1	1	12	-	-	-	-	-	18	11	18	8.7	18	9.1
1	1	3	3	24	-	-	-	-	-	22	25	18	9.4	19	12
1	1	5	5	270	13	-	-	-	-	27	42	18	11	19	16
1	1	7	7	1580	30	-	-	-	-	33	57	18	12	20	21
1	1	10	10	9500	610	-	-	10	7.8	40	72	19	15	21	31
0	0	1	5	- 5	- 5	- 5	- 5	- 5	- 5	15	29	1.8	6.2	4.0	11
0	0	5	5	- 5	- 5	- 5	- 5	- 5	- 5	20	39	2.3	7.8	5.2	15
0	0	1	10	300	120	- 5	- 5	- 5	- 5	28	54	3.4	10	7.6	20
0.5	5	1	5	- 5	- 5	- 5	- 5	- 5	- 5	19	30	10	10	11	14
0.5	5	5	10	1600	1400	- 5	- 5	- 5	- 5	33	61	10	14	14	24
0	0	0.1	1	- 5	- 5	- 5	- 5	- 5	- 5	3.2	7	0.7	4	1.7	4.5
0.5	5	0.1	1	- 5	- 5	- 5	- 5	- 5	- 5	10	10	9.7	8.9	9.7	9.0
1	5	0.1	1	- 5	- 5	- 5	- 5	- 5	- 5	19	12	18	11	18	11
1	5	1	5	80	- 5	- 5	- 5	- 5	- 5	23	31	18	12	19	15
5	5	0.1	0.1	80000	60000	80000	60000	80000	60000	27	41	25	41	26	41

[1] All errors assume a uniform distribution; [2] total number of runs is 100000 [3] no rf feedack applied; [4] vector-sum of 2 repectively 4 cavities is perfectly regulated; [5] number of runs only 12000;

The number of random error sets for most simulations has been 100000 which means there is still a chance of the order of 10^{-5} that a bunch might get lost. The table shows that for a reasonable phase and amplitude injection error of 1 deg. and 1% respectively the linac can tolerate phase and amplitude perturbation levels of severals degrees and percent. A summary of the results is shown in Figure 2.

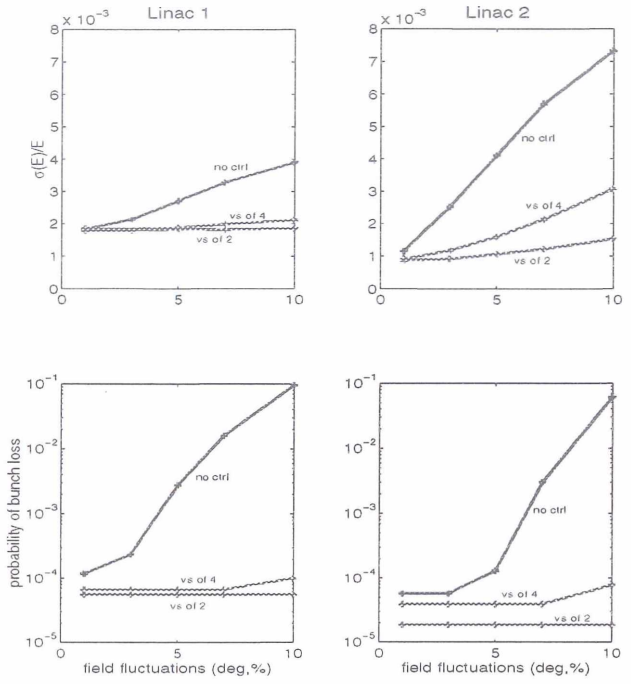

Figure 2: Energy spread and bunch loss as function of amplitude and phase errors in the linacs.

5 CONSIDERATIONS FOR THE CONTROL OF THE VECTOR SUM

The rf control for the vector sum of multiple cavities can be improved significantly if the energy gain and the beam arrival time or beam phase at the entrance of the following ensemble of multiple cavities can be controlled. This can be accomplished by control of the vector sum amplitude and phase which provide linear independent control of the beam energy gain and beam phase in the vicinity of the synchronous phase.

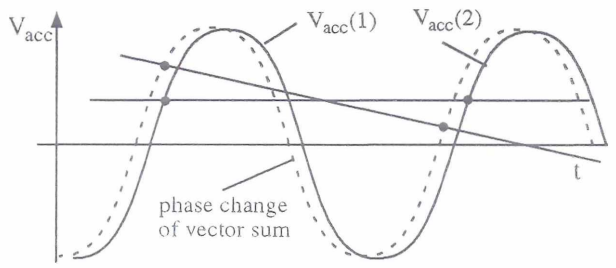

Figure 3: Principle of beam energy and beam phase

The principle of beam energy and beam phase control is shown in Figure 3. A change in cavity phase or amplitude

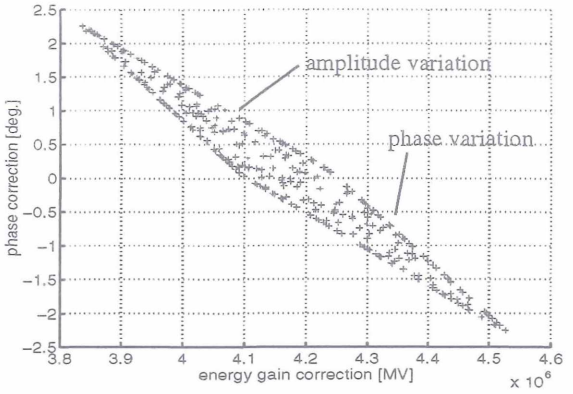

Figure 4: Energy gain and beam phase correction range at the low energy end of Linac 1. The vector sum of 2 cavities is controlled and varied by ±3 deg. in phase and ±10% in amplitude.

will result in the arrival time at the following cavity. With proper choice of vector sum amplitude and phase the energy and beam phase at the following cavity can be controlled within the boundaries shown in Figure 4. The control range is larger at the low energy end of the linac.

6 CONCLUSION

The control of microphonics and Lorentz force detuning in superconducting cavities for proton accelerators has been a major concern. This is especially true if only the vector sum of several cavities which are driven by one common klystron is controlled. The simple model presented for the analysis of the accelerating mode driven longitudinal dynamics of the bunch centroid has shown that surprisingly large levels of microphonics are acceptable even in the case of vector sum control of 4 cavities.

REFERENCES

[1] M. Pabst and K. Bongardt, *Halo simulation in a realistic proton linac design*, PAC97, Vancouver, B.C., Canada, May 12-16, 1997, in print.

[2] G.P.Lawrence and T.P. Wangler, *Integrated Normal-conducting/Superconducting High-Power Proton Linac for the APT Project*, PAC97, Vancouver, B.C., Canada, May 12-16, 1997, in print.

[3] B. Aminov, A. Gamp, E. Haebel, H. Heinrichs, H. Piel, J. Pouryamout, Th. Schilcher, D.L. Schrage, G.Schulz, S. Simrock, C.H. Rode and R. Röth, *Conceptual Design of the Superconducting High Energy Linear H⁻ Accelerator for the Future European Spallation Source (ESS)*, ESS 96-60-L, 1996.

TIME DELAY COMPENSATION FOR THE DIGITAL RF CONTROL AT THE TESLA TEST FACILITY

H. Imsieke, A. Kholodnyi, S.N. Simrock, DESY
Notkestr. 85, D-22603 Hamburg, Germany

ABSTRACT

Time delays or dead times between inputs and outputs are an inherent characteristic of digital feedback systems. The time delay limits the maximum allowable gain required for system stability. Modern control theory provides a scheme called Smith predictor which has the potential to improve control performance significantly. The method is based on model internal control which works well if the dynamics of the plant are slow compared to the time delay. In this paper we analyze the performance improvement that can be achieved in the TTF rf control system where the time delay is dominated by computational delay. In this system the time delay of 4 microseconds and sampling period of 1 microsecond are short compared to the cavity time constant of 700 microseconds. Attention is paid to both theoretical and practical aspects.

1 INTRODUCTION

The cavities in the TESLA Test Facility are operated in pulsed mode at gradients of up to 25 MV/m with each klystron driving multiple cavities. Significant Lorentz force detuning and control of the vector-sum are the main issues for the low level rf controls. A digital feedback system has been developed [1] to provide flexibility in the control algorithms, precise calibration of the vector-sum, and extensive diagnostics and exception handling. The main features are a sampling rate of 1 MHz for the individual cavity signals, digital in-phase and quadrature detection, calculation of the vector-sum which includes gradient calibration and the correction of phase offsets, and feedback algorithm.

The presently implemented version of the feedback employs a proportional controller and has demonstrated excellent performance [2] especially in combination with the adaptive feed forward [3]. Due to the large time delay of 4 microseconds in the feedback loop the loop becomes unstable at gains exceeding 40 dB. The need for a high gain to maximize error suppression results in a small range of usable gains. Therefore a compensation of the loop delay appears to be attractive since it could improve the robustness and possibly increase the performance of the feedback loops.

2 TIME DELAY

The time delay in the feedback loop is given by:

- 500 ns conversion time of the 14 bit, 2 MHz ADC
- 200 ns writing to the comm-port of the TMS320C40
- 1000 ns multiplication with rotation matrix for individual field calibration and calculation of the vector-sum
- 200 ns writing to next comm-port of C40
- 1000 ns for the feedback algorithm (subtract setpoint, multiply with gain table, and add feedforward)
- 200 ns to write to the DAC
- 200 ns delay in the klystron
- 800 ns cable delay

The sum of the delays is about 4 µs. The implementation of the Smith-Predictor and Kalman filter might add up to 2 µs to the total delay. Time delay increases the phase shift between input and output signals and thus limits the maximum allowable gain. The system becomes unstable if the loop gain exceeds unity gain while the phase exhibits 180 deg. The phase shift due to delay is proportional to the frequency and is 180 deg. at 125 kHz for a delay of 4 µs. The phase margin of the rf system with a loop gain of 40 dB, and the cavity pole (first order) at 200 Hz is approximately 60 degrees at the unity gain frequency of 20 kHz.

3 SMITH PREDICTOR STRUCTURE

In 1957 O.J. Smith presented a control scheme to predict the reaction of a plant P to the output of a controller C thereby providing the potential of improving the control loops with delay (Figure 1).

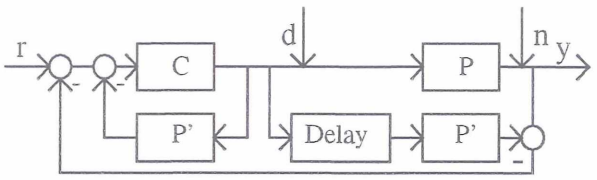

Figure 1: Smith Predictor structure

The total delay time in the feedback loop can be ascribed to the plant. P' is the model of the plant without delay time, r is the setpoint, y the output, d disturbances in and before the cavity and n measurement noise. With exact model matching and no disturbances or noise, the controller would only get signals from the model and the delay would be removed from the control loop as shown in Figure 2. The outer feedback loop in Figure 1 accounts for uncertainties of the model and disturbances.

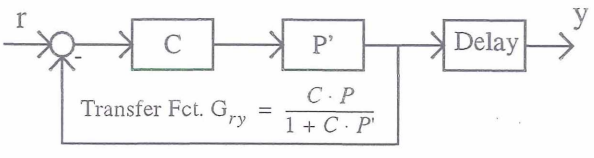

Figure 2: Desired Feedback with SP.

4 IMPLEMENTATION

The response of a single cavity to the beam current and the generator current can be described by two coupled first order differential equations for the envelope of the cavity voltage:

$$\begin{bmatrix} \dot{V}_{Re} \\ \dot{V}_{Im} \end{bmatrix} = \begin{bmatrix} -\omega_{1/2} & -\Delta\omega(t) \\ \Delta\omega(t) & -\omega_{1/2} \end{bmatrix} \begin{bmatrix} V_{Re} \\ V_{Im} \end{bmatrix} + \begin{bmatrix} R \cdot \omega_{1/2} & 0 \\ 0 & R \cdot \omega_{1/2} \end{bmatrix} \begin{bmatrix} I_{Re} \\ I_{Im} \end{bmatrix}$$

where V is the complex cavity voltage, I the complex current (generator + beam), $\omega_{1/2}$ (=π*operating frequency of 1.3 GHz/loaded quality factor ~$3*10^6$) the half width of resonance, $\Delta\omega$ the cavity detuning, and R the cavity shunt impedance.

A macropulse consists of cavity filling (500 µs), flat top with beam injection (800 µs), and field decay. The goal of the control system is to maintain a constant accelerating voltage during the flat top. The cavity is pre-detuned to minimize the power required to control the dynamic detuning which is a result of the Lorentz force. The cavity detuning should be zero in the middle of flat top. The cavity model used in the predictor should reflect the dynamics of the time varying Lorentz force detuning but has been omitted for simplicity. The field error resulting from such a simplification is comparable to the error caused by 1% quality factor or shunt impedance difference between model and plant (worst case: around 0.01%). The error caused by detuning is slowly changing and repetitive and can therefore be compensated by adaptive feedforward.

With a peak detuning of one bandwidth (realistic for 25 MV/m gradient) a step input on the real part of generator current would cause an error in the imaginary part of 7×10^{-4} after 1us. This crosstalk corresponds to a loop phase error of 0.04 deg. and can therefore be neglected.

The cavity is thus represented by a decoupled discrete State Space model with complex input and output vectors. The model parameters are calculated from the cavity bandwidth, which itself is calculated from the voltage decay time constant, and the cavity shunt impedance

$$V_{t+1} = (1 - (\omega_{1/2} \cdot T)) \cdot V_t + R \cdot \omega_{1/2} \cdot T \cdot I_t$$

where V and I stand for either real or imaginary component at time t. T is the sampling time of 1µs.

The model for multiple cavities can be obtained by superposition and can be approximated by that of a single cavity if the spread of the loaded quality factor is not too high. The spread should not exceed 25% to keep the model error below 3%. An improved model could consist of two cavities with different bandwidths. The model parameters are determined off-line.

The delay time can be adjusted in 1 µs steps by storing the control signal in memory and even in finer steps of 0.02 µs by selecting the time at which the 50 MHz DSP writes the data to the DAC. The delay is measured with a test program and then the program with correct DAC output time is written into the DSP. With model delay errors up to 0.1 µs, there's a decrease in maximum allowable gain off about 1% for every 0.01 µs mismatch.

5 PERFORMANCE

The performance of the rf system can be measured in terms of achieved field stability or disturbance rejection, the quality of setpoint tracking (important for fast varying setpoints as needed for FEL operation), and feedback loop stability which should be tolerant (or robust) with respect to parameter variations.

5.1 Stability

The maximum gain for stable operation is limited to 1400 (exactly two times the optimum gain, because overcorrection by more than 100% means instability) due to the 1 µs delay in the internal feedback loop.

While the bode plot without model uncertainties is easily interpreted due to the separation of the delay time, its meaning for the SP with parameter uncertainties is not easily understood. However since a numerical model analysis and the pole-zero map (obtained with a rational approximation of the closed loop SP transfer function) give similar results near the ideal case, stability margins were obtained with these methods. They show that realistic model mismatch of a few percent reduces the critical gain to ~1200.

If the klystron is operated close to saturation, its nonlinearity limits the maximum gain, so that it could be necessary to replace the actuator signal with the measured incident wave to the cavity. This scheme would also include time varying phase errors in the klystron and the vectormodulator. The measured klystron output would provide the correct control signal, thereby increasing stability and reducing sensitivity to klystron power fluctuations.

5.2 Setpoint tracking

Figure 3 shows the response of the SP to a change of the setpoint. Operation with optimum gain will cause the cavity field to reach the desired setpoint in 1 µs time assuming availability of sufficient power from the klystron. If a beam current induces a voltage ΔV in steady state, the cavity field will change $\Delta V/700$ in 1 µs. The optimal gain for reference tracking is therefore around 700 which is well below critical gain.

5.3 Disturbance Rejection

The ability to suppress disturbances is not improved significantly by the smith predictor, as shown in Figure 4. The slow response to a beam induced perturabtion is due to the

presence of the cavity poles in the transfer function from the disturbance to the output,

$$G_{dy} = P \cdot (1 - G_{ry}).$$

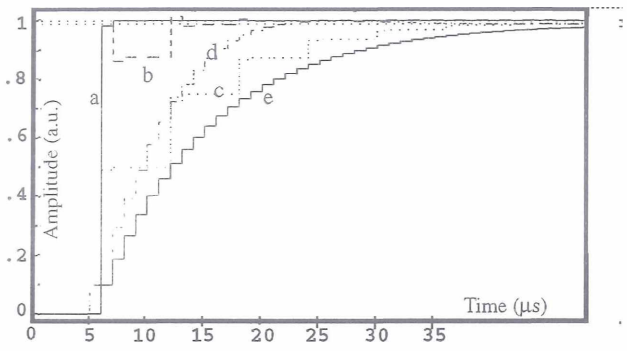

Figure 3: Step response of the transfer Function G_{ry} for a) optimal SP b) SP with 20% lower cavity quality factor c) SP with 50% gain decrease due to klystron nonlinearity d) normal feedback with gain of 70 e)SP with gain of 70

The first term in the bracket is independent of the feedback gain. This means that the time constant of the error correction is not a function of the gain. It is however possible to modify the model and the controller so that the pole cancels with a zero of the transfer function [4] or to add the difference between cavity and model to the input of the model in order to adapt it to the disturbed cavity (a scheme called observer). Pole cancellation reduces the maximum allowable gain, is sensitive to parameter uncertainties, and slower than the latter method.

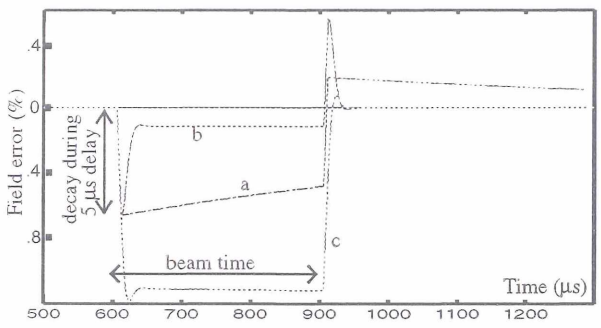

Figure 4: Reaction of the cavity field to a beam induced transient, a) optimal SP b) SP with Observer c) normal feedback.

Even with faster disturbance correction, the beam still causes a drop in the cavity field of 1/700 ~ 0.14 % per µs delay time in the feedback loop after injection. This can only be prevented by the use of feedforward. For the klystron noise, a faster disturbance rejection would have no influence. Errors caused by detuning would be reduced approximately by 50% on flat top with a gain of 700, but much better with an additional observer. The observer is useful against stochastical detuning by microphonics which cannot be suppressed by feedforward.

A controller with an integrator does not perform significantly better, and decreases stability margins due to phase advance.

6 FEEDFORWARD SCHEMES

Because the digital control system can measure the beam current in real time it can compensate it with a delay of about 1-2 µs. This scheme can reduce the beam induced transients considerably.

Another approach is the calculation of a feed forward table which is added to the control signal sent to the plant. This accounts for the absence of the beam in the model and microphonics influences. The feed forward table is repeatedly calculated from the difference between model and plant, with the error decreasing each step. In this way it also adapts itself to slowly changing system parameters. In contrast to this adaptive feed forward, a feed forward table needed to trace the setpoint optimally in the ideal case is calculated with model parameters and proportional gain and is added to both model and plant. This has to be updated only when these parameters are changed. Without Smith Predictor, there would be only one (adaptive) feed forward for all repetitive errors.

7 CONCLUSION

The main advantage of the Smith Predictor is faster setpoint tracking. With the existing feed forward, this workload is removed from the feedback with the exception of stochastic errors. These errors act almost exclusively in or before the plant, so the SP offers only little improvement. A major drawback is the amplification of measurement noise with higher gains, which has to be suppressed significantly. For this purpose a Kalman filter, which estimates the state of the plant in presence of klystron and measurement noise, is currently under development. The measurement is also disturbed by an offset in the rf mixer output which varies over the macropulse. This has to be cancelled out too to allow better performance than present feedback.

The klystron nonlinearity restricts the SP performance. The power margin could be too little for the desired high gains, and with equal gain, a standard feedback controller would outperform the SP. To assure stability the nonlinearity has to be known for the model calculations.

REFERENCES

[1] S.N. Simrock, I. Altmann, K. Rehlich, T. Schilcher, *Design of the Digital RF Control System for the TESLA Test Facility*, EPAC 96, Sitges (Barcelona), Spain, June 10-14, 1996, p. 349

[2] A. Gamp et al., *Experience with the Control of the Vector Sum in the TESLA Test Facility*, EPAC98, Stockholm, Sweden, June 22-26, in print

[3] M. Liepe, S.N. Simrock, *Adaptive Feed Forward for Digital RF Control System for the TESLA Test Facility*, Stockholm, Sweden, June 22-26, in print

[4] William S.Levine editor, *The Control Handbook*, CRC Press 1996, p. 231

Operation of the Upgraded H^--Injection System of the Linac III at DESY

C.-M. Kleffner, N. Holtkamp, M. Nagl, H. Poggensee, J. Peters
Deutsches Elektronensynchrotron DESY, D-22603 Hamburg, Germany
A. Schempp, IAP, University of Frankfurt, Germany

Abstract

During the winter shutdown 1997/98, the injection system of the H^--Linac III was upgraded. At present two different kinds of H^--sources are operated at DESY. The new cesium-free rf ion source is planned to operate parallel to the magnetron ion source.

In addition a new MEBT (Medium Energy Beam Transport line) between two distinct RFQ accelerators and the Alvarez accelerator of Linac III was installed to match the beam of each ion source to the Alvarez acceptance. This scheme makes it possible to operate either H^--source with the Alvarez linac with a miniumum of effort to switch from one to the other. The design of the transport line also facilitates the development and tests of newly proposed ion sources, for example deuterium and polarized proton sources.

After assembly of the RFQs and ion sources as well as the new components for the MEBT, a relatively easy commissioning could be demonstrated, although the ions have to be transported on a long distance from the RFQ to the Alvarez linac. First results of measurements will be presented.

1 INTRODUCTION

Linac III at DESY started operating as an H^--injector for the DESY III synchrotron in 1989 [1] and is part of the injector chain for the HERA collider. The negative charged ions are produced by a surface-plasma magnetron source at 18 keV and are accelerated with an RFQ to an energy of 750 keV. A conventional Alvarez linac is used to obtain the injection energy of 50 MeV into DESY III.

Further developments at the DESY cesium-free rf-volume source led to an operable and reliable design [2]. To integrate this volume source into the proton linac for standard operation it was desirable to find a technical solution to switch back to the magnetron source at any time. This improves the reliability of the proton injector chain to HERA. It was therefore decided to reconstruct the preaccelerator of the linac to allow both ion sources to operate for the linac simultaneously.

The upgraded injection system in front of the Alvarez linac consists of the existing devices as well as of a new beamline with an additional RFQ and a rebuncher cavity. The assembly of the new MEBT beamline and the two ion sources also necessitated an extension of the accelerator tunnel. The shutdown period of the DESY accelerators

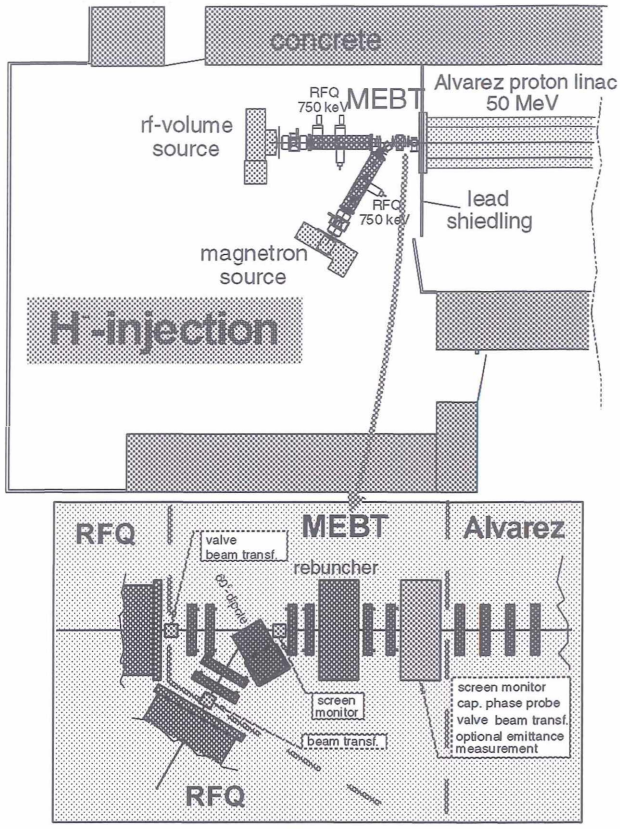

Figure 1: Floor plan of the injection system and a detailed view on the MEBT.

in winter 1997/98 was used for dismantlement of the preaccelerator, the reconstruction of parts of the tunnel and related facilities and the assembly of the new components.

The low beam energy of 750 keV, small beam losses and a new arrangement of lead- and concrete-shielding permits access to the injection system during linac operating time.

2 CHARACTERISTICS OF THE MEBT

Beam transport of ions under space charge conditions at low energies reduces the variety of possible transport line designs. The goal was to control the longitudinal bunch shape with only one rebuncher cavity between the RFQs and the Alvarez linac. Therefore it was essential to keep the overall length of the transport line below 1 m. The mechanical components had to be composed in a very compact manner. Details of the MEBT have been given previously

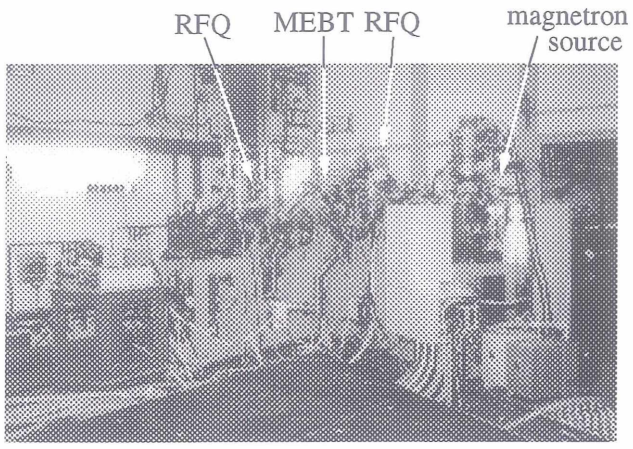

Figure 2: View of the rebuilt injection system in the Linac III tunnel.

[3], briefly the design is as follows:

The new rf-volume source is installed on the axis of the Alvarez linac, whereas the beam coming out from the magnetron source is bent by a 60°-dipole to this axis. Fig. 1 shows a survey of the injection system.

The main components including ion sources, RFQs and the MEBT are mounted independently on frames made of aluminium. These frames are put onto a rail system and are thus retracktable along the beam axis. It is therefore easy to install additional beam diagnostic elements for further investigation of beam properties at any place in one of the paths. Fig. 2 and Fig. 3 show the arrangement of the injection system and details of the MEBT transport line.

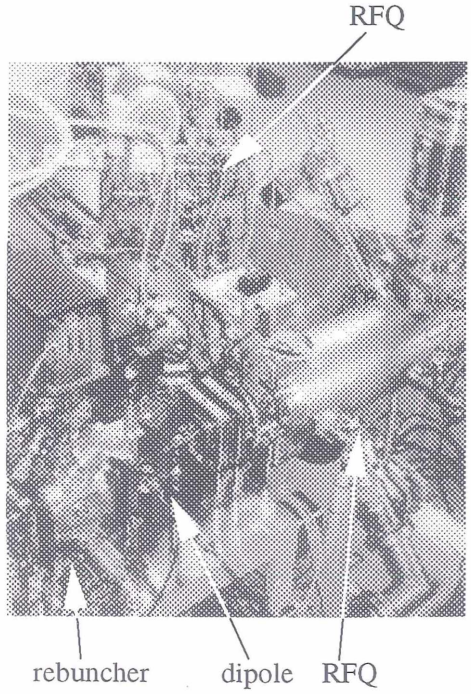

Figure 3: Side view of the MEBT beam transport line.

Table 1: Basic parameters of the new cavities for the injection system.

	RFQ	rebuncher
f_0	202 MHz	202 MHz
U_{rod} / U_{eff}	80 kV	58 kV
P	80 kW	4 kW
L	120 cm	12 cm

The 4-rod RFQ and the rebuncher cavity were delivered by the University of Frankfurt [3]. A parameter list is given in Table 1. The rf-amplifier for the rebuncher was designed and constructed at DESY. The design is based on the rf-preamplifier of the existing rf-amplifiers for Linac III.

3 FIRST OPERATION WITH THE MEBT

After the assembly and adjustment of the new injection system first acceleration tests with the magnetron source were performed. The rf-volume source is already assembled in position but not in operation yet. It is expected, that first beam tests with the new source can be performed in autumn.

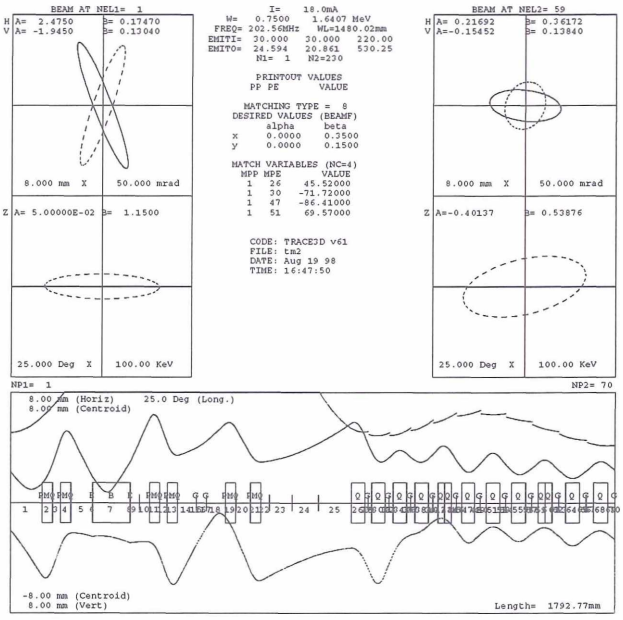

Figure 4: Matched beam envelopes (5σ) calculated by TRACE3D.

Once the beam delivered by the magnetron coasted through the MEBT line, only little empirical tuning of the MEBT quadrupole focusing strength was necessary. The numerical simulations (s. Fig. 4) led to a solution with good transmission through MEBT and the Alvarez linac. Only one quadrupole was displaced by 0.7 mm for beam steering reasons. Whereas the transmission of the solenoid focusing channel in front of the RFQ is found to be limited under space-charge conditions to 50 % [4], the transmission from the RFQ up to the end of the high energy trans-

port line after the Alvarez linac under typical conditions reaches 75 %. At the injection point to DESY III currents of 10 to 15 mA are obtained, depending on the current of the magnetron source of typically 30 to 65 mA.

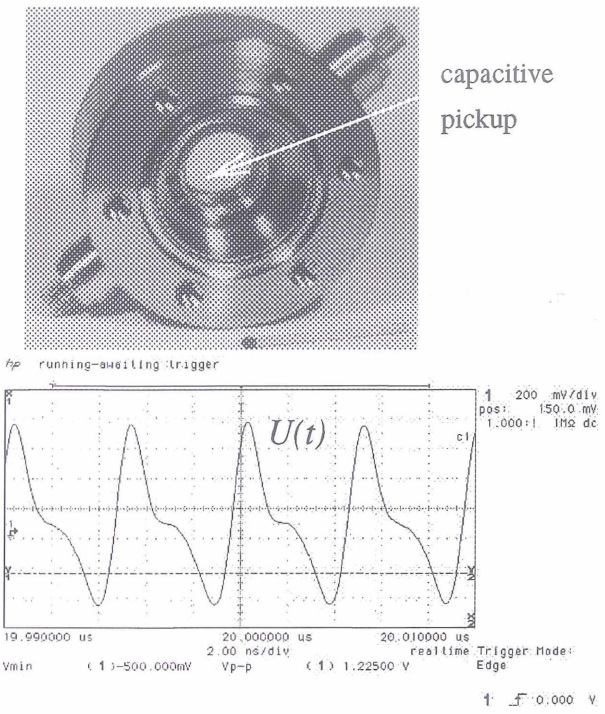

Figure 5: Signal of a bunched beam with $\Delta\varphi\,(2\sigma) = \pm 30°$ measured with the capacitive probe above.

The cavity phase and amplitude settings of the RFQ and rebuncher with respect to the Alvarez tanks was to be found more laborious. The phase settings of the cavities is based mainly on the measurements of energy and momentum spread after the Alvarez linac. A capacitive phase probe built at DESY (see Fig. 5) between rebuncher and the Alvarez was used to estimate the longitudinal bunchlength at the end of the MEBT.

The bunch shape monitor [5] in the Alvarez Tank 1 was used for fine tuning of the relative phase setting between the rebuncher cavity and the Tank 1 as well for the amplitude settings of these cavities. Fig. 6 shows a offline estimated 3D-view of the bunch train.

The phase tuning was to be found slightly depending on the beam current delivered by the ion source. Fig. 7 shows a typical devolution of momentum spread and energy during tuning of the cavity settings.

4 ACKNOWLEGMENT

The authors wishes to thank all contributing colleagues and the collaborating institutes for their technical support and helpful discussions.

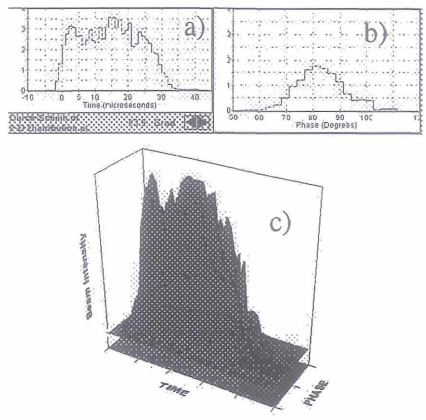

Figure 6: Current density along the bunch train **(a)**, phase spread **(b)** and a 3D-view **(c)** of the buch train measured with the bunch shape monitor at the Alvarez Tank 1.

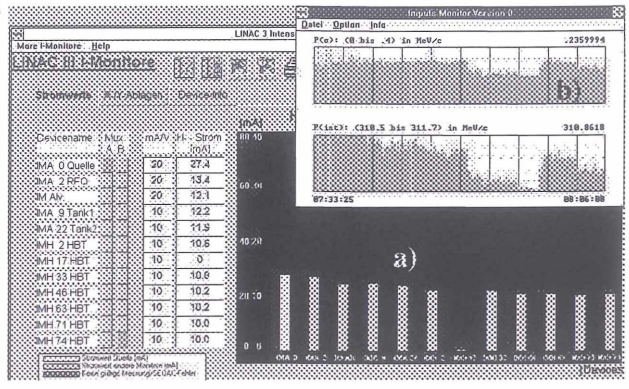

Figure 7: Transmission along the linac **(a)** and a history of evaluated beam properties **(b)** shown on a PC console station.

5 REFERENCES

[1] LINAC III collaboration, Rev. Sci. Instruments **62** (4), April 1991.

[2] J. Peters, Review of Negative Hydrogen Ion Sources High Brightness/High Current, this conference

[3] C.-M. Kleffner, G. Jacobs, N. Holtkamp, M. Nagl, I. Peperkorn, J. Peters, Deutsches Elektronen Synchrotron DESY, Germany, A. Schempp, IAP, Universität Frankfurt, Germany, and V. Paramonov, INR Moscow, Russia, Upgrade of the H^--Injection System at the DESY Proton Linac III, Proc. of the 1997 PAC, Vancouver, Canada, 12-16 May 1997

[4] A. Sauer, diploma thesis, IAP Frankfurt, 1998.

[5] A.V. Feschenko, A.V. Liiou, A.N. Mirzojan, A.A. Menshov, P.N. Ostroumov, N. Holtkamp, C.-M. Kleffner, M. Nagl, I. Peperkorn, Bunch Shape Monitors for the DESY H^--Linac, Proc. of the 1997 PAC, Vancouver, Canada, 12-16 May 1997

ADAPTIVE FEED FORWARD FOR THE DIGITAL RF CONTROL SYSTEM AT THE TESLA TEST FACILITY

M. Liepe, S.N. Simrock, DESY, Hamburg, Germany

1 ABSTRACT

The rf control system of the TESLA Test Facility regulates the vector sum of multiple superconducting cavities which are operated in pulsed mode at accelerating gradients exceeding 15 MV/m. In addition to the feed back control loop which suppresses stochastic errors, feedforward [1] is applied to reduce repetitive perturbations induced by beam loading and dynamic lorentz force detuning. In the case of TESLA repetitive errors are dominating. The feedforward algorithm first identifies the time varying state space model of the closed loop system by measurement of a step response. Next the pulse to pulse average of the measured perturbations is applied to the inverse state space model to obtain the correct feedforward table. The feed forward tables can be updated continuously to follow slow changes in the perturbation parameters. On-line system identification is transparent to routine beam operation due to the small step size used.

2 INTRODUCTION

The requirements for amplitude and phase stability of the vector-sum of 16 cavities are driven by the maximum tolerable energy spread for the TESLA Test Facility. The goal is an rms energy spread of $\sigma_E/E = 2 \cdot 10^{-3}$. The requirements for gradient and phase stability are therefore of the order of $2 \cdot 10^{-3}$ and $0.5°$ respectively [1].

The amplitude and phase errors to be controlled are of the order of 5% for the amplitude and 20 degrees for the phase a result of Lorentz force detuning and microphonics. These errors must be suppressed by a factor of at least 40 which implies that the loop gain must be adequate to meet this goal. Fortunately, the dominant source of errors is repetitive (Lorentz force and beam loading) and can be reduced by use of feedforward significantly.

3 DESIGN OF THE TTF RF CONTROL SYSTEM

The digital rf control system at the TTF [2] has been designed for maximum flexibility of the control algorithm. The main features are:

- digital IQ detection of the cavity field of each individual cavity. The fields are sampled at a rate of 1 MHz.
- calibration of the individual measured cavity field vectors by multiplication with an appropriate rotation matrix
- calculation of the vector-sum and subtraction from a (time varying) setpoint to form the error signal.
- application of the feedback control algorithm which is presently implemented as proportional controller in form of a time varying gain matrix
- a time varying feedforward is added to eliminate repetitive disturbances

All time varying signals are implemented as tables consisting of 2048 pairs of real (r) and imaginary (i) values covering a pulse length of 2048 µs. The goal of the adaptive feedforward is to determine the optimum feedforward table which minimizes the residual amplitude and phase error and to continually update the feedforward tables to track slowly varying repetitive perturbations.

4 SOURCES OF PERTURBATIONS

The major perturbations of the pulsed accelerating fields in the superconducting cavities are induced by microphonics, dynamic Lorentz force detuning, beamloading, and power fluctuations of the klystron. While microphonics and power fluctuations of the klystron are of random nature and cannot be predicted in advance of the rf pulse, the effects of lorentz force detuning and beam loading can be measured before they influence the cavity field. While typical microphonic noise amplitudes are of the order of ±5 Hz, the lorentz force detuning reaches ±200 Hz at a gradient of

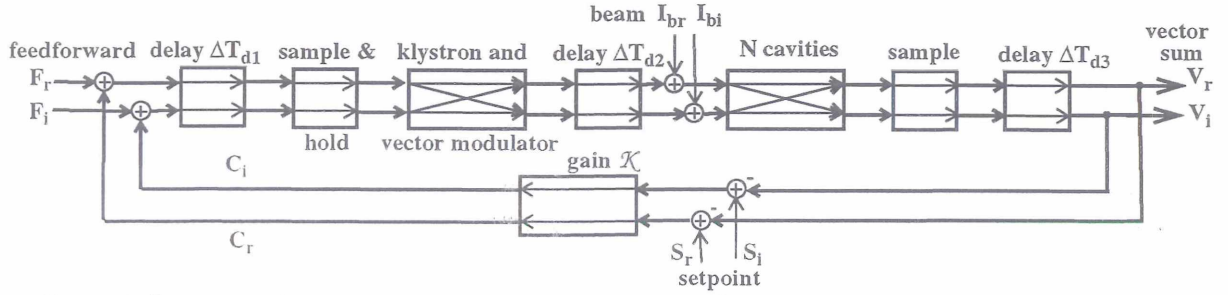

Figure 1: Schematic block diagram of the closed loop system of the TTF RF control

25 MV/m. Both errors have to be compared to the cavity bandwidth of 200 Hz (HWHM). The steady state beam loading at 8 mA beam current is equal to the accelerating gradient. The klystron power and phase fluctuates as a function of (slow) line voltage variations with a typical magnitude of 1% for power and 4 degrees in phase.

5 SYSTEM IDENTIFICATION

5.1 RF SYSTEM MODEL

The closed loop system consists of the vector-modulator, the klystron, the cavities, the feedback controller, and various delays which are dominated by computational delay as shown in figure 1.

The dynamics of the closed loop system are dominated by the low frequency poles of the rf cavity which can be described by the state space equation:

$$\begin{bmatrix} v_r(t) \\ v_i(t) \end{bmatrix} = \begin{bmatrix} -\omega_{1/2} & -\Delta\omega(t) \\ \Delta\omega(t) & -\omega_{1/2} \end{bmatrix} \cdot \begin{bmatrix} v_r(t) \\ v_i(t) \end{bmatrix} + \frac{R\omega_{rf}}{2Q} \cdot \begin{bmatrix} \frac{1}{m} I_{gr}(t) + I_{br}(t) \\ \frac{1}{m} I_{gi}(t) + I_{bi}(t) \end{bmatrix} \quad (1)$$

where v_r, v_i, I_{br}, I_{bi}, I_{gr}, I_{gi} are the real and imaginary parts of the cavity voltage, beam current, and generator current respectively. The remaining parameters are the cavity detuning $\Delta\omega$, the cavity bandwidth $\omega_{1/2}$, the cavity shunt impedance $R=(r/Q)*Q_L$, and the rf frequency ω_{rf}. The Lorentz force will detune the cavity dynamically resulting in a time varying detuning $\Delta\omega(t)$.

The closed loop model of the time discrete system with delay can be obtained using standard techniques as described in various textbooks on control theory [3]. It is given by equation 2, where V describes the cavity vector-sum voltage, F is the feedforward signal, S the cavity voltage setpoint, N the number of cavities, ΔT_s the sampling period, $\mathcal{K}$ the feedback gain, $g_a,...,g_d$ the gain of klystron and vector modulator, $k_{dm}=\Delta T_{d3}/\Delta T_s$, and $k_{dg}=(\Delta T_{d1}+\Delta T_{d2})/\Delta T_s$. The indices r and i denote real and imaginary part of the relevant quantity.

The parameters of the closed loop state space model described by equation 2 can be determined from a step response at the desired operating point. For this purpose a step function is applied as feedforward signal. The system response to the single step is measured and the model parameters are calculated. Based on the model it is now possible to calculate the change of feedforward table ΔF which is required to achieve a given state response ΔV, see equation 3.

5.2 SYSTEM REPONSE MATRIX

Another approach to describe the closed loop system with respect to feedforward input is the system response matrix [3]. This approach employs a set of step functions instead of the single step that can be used for system identification. The result is a feedforward system-response matrix which allows to identify a time varying system even if a parameterized model is not available. The inversion of the response matrix allows calculation of the feedforward δf which is necessary to achieve a given state response ΔV:

$$\begin{bmatrix} \delta f_{r1} \\ \dots \\ \delta f_{rn} \\ \delta f_{i1} \\ \dots \\ \delta f_{in} \end{bmatrix} = \mathcal{R}^{-1} \cdot \begin{bmatrix} \Delta V_{r1} \\ \dots \\ \Delta V_{rn} \\ \Delta V_{i1} \\ \dots \\ \Delta V_{in} \end{bmatrix} \quad (4)$$

where:

$$\Delta F_{*k} = \sum_{j=1}^{k} \delta f_{*j} . \quad (5)$$

The method is computationally more intensive than the system identification with a single step described before.

6 PRINCIPLE OF ADAPTIVE FEEDFORWARD

As mentioned before the feedforward system will eliminate only repetitive errors. In practise however stochastic errors will be superimposed and require averaging methods for sufficiently precise measurement of the predictable perturbations. Repetitive perturbations as well as the plant model may however vary slowly as function of time and may require a continuous update of feedforward table and model. It is therefore desirable to measure the step responses continually to maintain a current system model. The step size should be small to prevent excessive perturbations of

Equation 2:

$$\begin{bmatrix} V_r \\ V_i \end{bmatrix}_{k+k_{dm}+1} = \begin{bmatrix} 1-\omega_{1/2}\Delta T_S & -\Delta\omega\Delta T_S \\ \Delta\omega\Delta T_S & 1-\omega_{1/2}\Delta T_S \end{bmatrix}_{k+k_{dm}} \cdot \begin{bmatrix} V_r \\ V_i \end{bmatrix}_{k+k_{dm}} + \frac{R\omega_{rf}\Delta T_S}{2Q} N \cdot \begin{bmatrix} I_{br} \\ I_{bi} \end{bmatrix}_k + \frac{R\omega_{rf}\Delta T_S}{2Q} \begin{bmatrix} \frac{\sqrt{N}}{m} g_a(t) & \frac{\sqrt{N}}{m} g_b(t) \\ \frac{\sqrt{N}}{m} g_c(t) & \frac{\sqrt{N}}{m} g_d(t) \end{bmatrix}_{k-k_{dg}} \cdot \left(\begin{bmatrix} F_r \\ F_i \end{bmatrix} + \mathcal{K} \begin{bmatrix} S_r - V_r \\ S_i - V_i \end{bmatrix} \right)_{k-k_{dg}}$$

Equation 3:

$$\begin{bmatrix} \Delta F_r \\ \Delta F_i \end{bmatrix}_{k-k_{dg}} = \left(\mathcal{K} \begin{bmatrix} \Delta V_r \\ \Delta V_i \end{bmatrix} \right)_{k-k_{dg}} + \frac{2Q}{R\omega_{rf}\Delta T_S} \cdot \begin{bmatrix} \frac{\sqrt{N}}{m} g_a(t) & \frac{\sqrt{N}}{m} g_b(t) \\ \frac{\sqrt{N}}{m} g_c(t) & \frac{\sqrt{N}}{m} g_d(t) \end{bmatrix}^{-1}_{k-k_{dg}} \left(\begin{bmatrix} \Delta V_r \\ \Delta V_i \end{bmatrix}_{k+k_{dm}+1} - \begin{bmatrix} 1-\omega_{1/2}\Delta T_S & -\Delta\omega\Delta T_S \\ \Delta\omega\Delta T_S & 1-\omega_{1/2}\Delta T_S \end{bmatrix}_{k+k_{dm}} \begin{bmatrix} \Delta V_r \\ \Delta V_i \end{bmatrix}_{k+k_{dm}} \right)$$

the state but sufficiently large to allow for an acceptable signal to noise ratio. A flow diagram of the adaptive feedforward algorithm as implemented at the TTF is shown in figure 2.

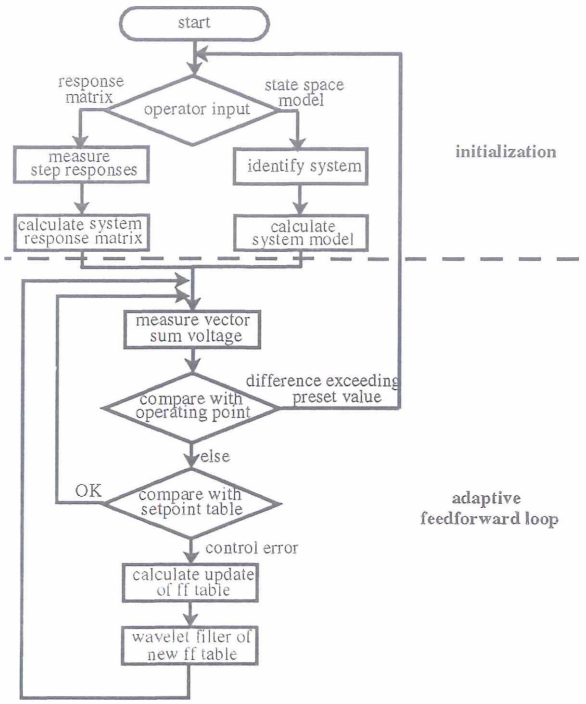

Figure 2: Flow diagram of the adaptive feedforward

7 PERFORMANCE OF THE ADAPTIVE FEEDFORWARD

The adaptive feedforward scheme for the digital rf control system at the TESLA Test Facility has been implemented in a very early stage of the project. A comparison of the residual amplitude and phase errors without and with adaptive feedforward show a significant improvement (approximately a factor of 10) in system performance which is reflected in the low energy spread of the beam. The rf field stability is considerably better than required as can be seen in figure 3.

8 CONCLUSION

Initial tests have demonstrated that by application of the adaptive feedforward control in addition to the feed back control the required field stability is exceeded by a substantial factor. The adaptive feedforward control proved to be an effective way of compensating the repetitive part of the perturbations. The delay in the system and its nonlinearity can be handled by the adaptive feedforward via linearization at a chosen operating point.

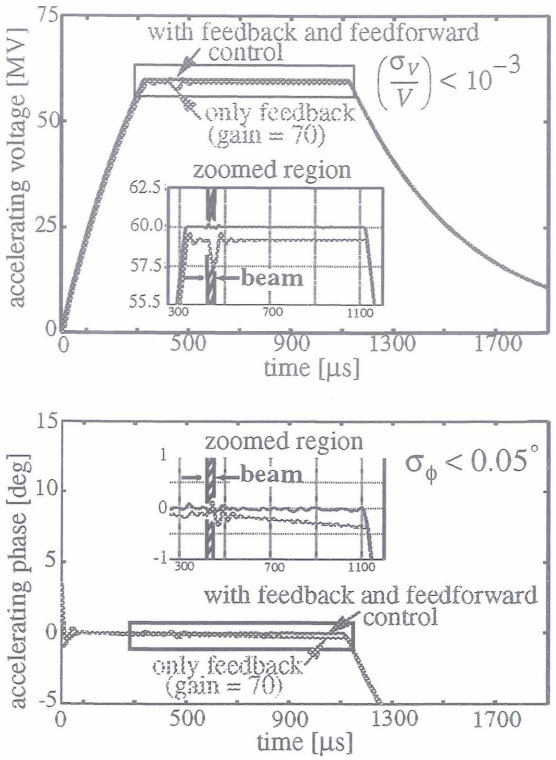

Figure 3: RF control system performance without and with adaptive feedforward.

9 ACKNOWLEDGEMENTS

We gratefully acknowledge the contributions from TTF Linac operations group. Their dedicated support in has been the basis for our success.

10 REFERENCES

[1] M.Liepe, *Adaptive feedforward for the digital RF control system at the TESLA TEST FACILITY,* DESY Print TESLA, to be published

[2] S.N. Simrock, I. Altmann, K. Rehlich,T. Schilcher, *Design of the Digital RF Control System for the TESLA Test Facility,* EPAC96, Sitges (Barcelona), Spain, June 10-14, 196, p. 346

[3] W.S. Levine (Editor), *The Control Handbook*, CRC Press 1996

[4] Renshan Zhang,Ilan Ben-Zvi, Jialin Xie, *A self-adaptive feedforward control system for linacs,* Nuclear Instruments and Methods in Physics Research A324, 1993, p. 421-428

The Performance of the 1.3 GHz Superconducting RF Cavities in the First Module of the Tesla Test Facility Linac

Wolf-Dietrich Möller for the Tesla collaboration
Deutsches Elektronen Synchrotron DESY, 22603 Hamburg, Germany

Abstract

The design goal of the 1.3 GHz 9-cell superconducting RF cavities for the Tesla Test Facility (TTF) is a gradient Eacc ≥ 15 MV/m at a quality factor of Qo ≥ $3 \cdot 10^9$. The cavities are operated in pulsed mode: 0.8 ms constant gradient with 10 Hz repetition rate.

After the vertical acceptance test and prior to the assembly in the linac the cavities are tested in a horizontal cryostat fully equipped with helium vessel, high power input coupler, higher order modes coupler and tuning system. After installing module 1 the first 120 MeV beam has been delivered successfully.

We report about the measured results in vertical and horizontal tests, the processing of the superconducting cavity system in the first module and the performance of the cavity system before, during and after operating the linac.

1 INTRODUCTION

In order to prove the technical basis of TESLA[1] the TTF (Tesla Test Facility)[2] was established at DESY within the frame of an international collaboration. In May 1994 the infrastructure was ready to prepare and test superconducting cavities. Twenty-seven 9-cell cavities, manufactured by four different European companies have been processed and measured so far.

9 cavities from the first production are operating in the TTF linac and 8 more cavities are now being installed. In end of 1997 26 more cavities were ordered which are now under fabrication or final processing. Two of them have been measured already.

2 CAVITY TREATMENT

The standard cavity preparation before the vertical test consists of the following steps: 80 µm removal from the inner surface by buffered chemical polishing (BCP), a 2 h heat treatment (HT) at 800 °C, a 4 h HT at 1400 °C with titanium getter and additional 100 µm removal by BCP. The cavity is then rinsed with high pressure (100 bar) deionized ultra pure water. After welding the He-tank and prior to the horizontal test a 20 µm BCP and a high pressure water rinse takes place.

3 VERTICAL TEST RESULTS

The average gradient of the 27 cavities tested so far is 19.5 MV/m. The average gradient of the last 13 cavities measured is even 24.6 MV/m, 3 of them showed gradients Eacc > 28 MV/m (see Fig. 1). The main limitation now is field emission. It is remarkable, that all 4 manufacturers delivered cavities with gradients higher or close to 25MV/m.

However at the time of selecting the capture cavity and the 8 cavities for module 1, only 4 cavities were available with gradients > 15 MV/m. 5 cavities were limited by quench below 15 MV/m in the vertical test (see table 1). The reasons for this limitation were found as foreign inclusions in the material and improper cleaning of weld area before welding[3,4]. In the future this type of defects will be excluded by eddy current scan of all niobium sheets and by the current fabrication method.

Table 1: Cavity performance during vertical and horizontal tests and after installation into the linac. The numbers are the gradients in MV/m. The 1. linac test was done before and the 2. test after 3 month of linac operation. At the vertical test the dissipated power is set to 100W in order to compare the cw measurement in the vertical test with the pulsed measurement (duty cycle 1%).

cavity	vertical test Pdiss <100W	horiz. test Pcryo <1W	linac 1. test Pcryo <1W	linac 2. test Pcryo <1W	linac 2. test Pcryo <3W
D3	25.3	21.0	15.5	19.1	19.5
S8	12.5	16.0	11.9	11.9	12.5
S10	14.2	13.4	13.2	14.7	15.9
D1	21.3	19.0	21.0	23.1	23.5
D2	17.7	23.5	23.6	24.5	25.6
S11	13.5	17.3	12.9	11.8	13.4
D4	13.3	13.5	11.5	12.4	13.5
S7	12.6	-	11.3	12.2	13.2
C19	19.6	19.0	12.7	-	-
sum	150	155*	134	142†	151†
average	16.7	17.2*	14.8	15.8†	16.8†

*: S7 test result taken from the vertical test
†: C19 test result taken from the 1. test of linac

4 HORIZONTAL TESTS

13 cavities for module 1, injectors and first for the module 2, equipped with all auxiliary components (helium-vessel, high-power-coupler, HOM-couplers, tuning mechanism and magnetic shielding) were tested in a horizontal cryostat. Because of the low Q_{ext} of the high power input coupler only measurements in the pulsed mode were

possible (500 μs rise time and 800 μs constant gradient at a repetition rate of 10 Hz)

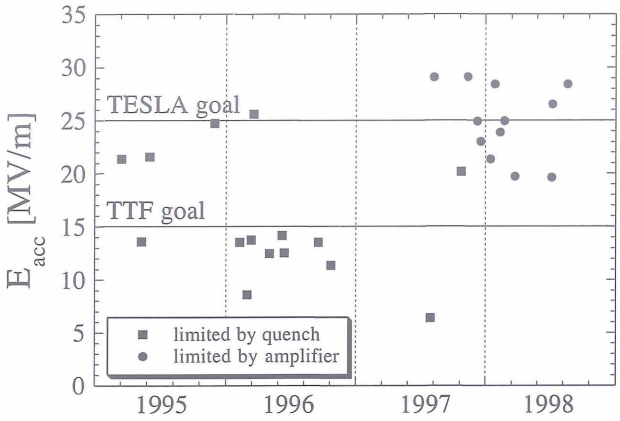

Fig. 1: Result of vertical cavity tests. The gradients below 15 MV/m before mid '97 are due to fabrication errors.

These 13 cavities reached an average gradient of 19.7 MV/m in the horizontal test compared to an average gradient of 20.3 MV/m in cw mode in the vertical test stand. In the horizontal tests, field emission has been observed higher intensities. The reason is probably particle contamination due to the more complicated assembly and the processing of the main power coupler. The higher field emission loading is responsible for the slight degradation in performance.

The performance of the cavities selected for module 1 are listed in table 1. Three cavities (D2, S8, S11) showed a higher field in the horizontal test under pulsed conditions than in the vertical cw test. This is most likely caused by the slow thermal development of the quench as compared to the rf pulse length. The other cavities suffered from higher field emission or stayed constant.

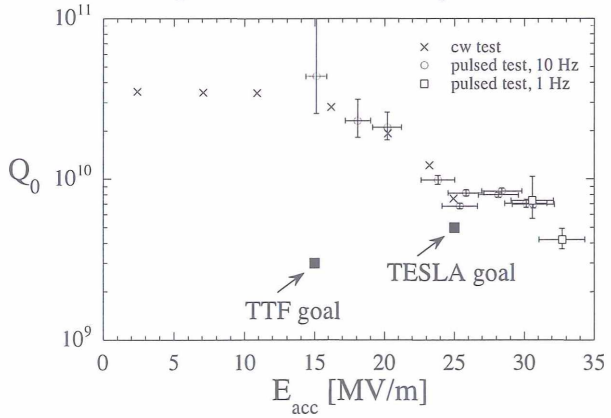

Fig. 2: The best horizontal test so far. The Q values during the pulse tests are calculated from the cryogenic losses. The cw measurement from the vertical test is given for comparison.

The best cavity tested so far in the horizontal test cryostat reached 33 MV/m with a quality factor $Q = 4 \cdot 10^9$ (Fig. 2). At 34 MV/m a quench occurred. In the vertical test, this cavity reached 25 MV/m, limited by available power.

Cavities showing strong field emission can be further improved by applying HPP[5]. For this purpose, short pulses of high instantaneous power (≤500 μs, up to 1 MW) are applied to destroy field emitters. The power coupler has to be carefully processed up to 1 MW, which may take several days. Due to a tight time-schedule HPP was not always applied during the horizontal test.

5PROCESSING OF THE MODULE 1

5.1High power input coupler

The two types (Fermilab and DESY design) of high power couplers[6] consist each of two RF vacuum windows. The coaxial window near the cavity at 70 K and the room temperature window in front of the wave-guide (Fermilab) or as a part of the wave-guide to coax transition (DESY) outside the cryostat. The coupler vacuum of all eight couplers on the module is connected and pumped by a common ion getter pump.

All 8 cavities in module 1 are driven by one 5 MW klystron. A linear RF distribution system is branching off identical amount of power for each cavity by directional couplers.

5.2Processing couplers and cavities

The TESLA design parameters call for a transfer of 206 kW peak RF power per cavity to the beam with a pulse length of 1.3 ms and a repetition rate of 5 Hz. In addition it is also foreseen to apply HPP to the cavities in situ which requires 1 MW at a maximum pulse length of 500 μs and at a repetition rate ≤ 1 Hz. Therefor the couplers have to be conditioned to this limits.

The coupler processing procedure at TTF starts with the cavity and coupler at room temperature. Therefor gases released by RF stimulated desorption can be pumped away. In the beginning of the conditioning the cavity is off resonance. The first power rise (dependent from the vacuum pressure and e^- and light in the vacuum) is done with a pulse length of 20 μs, then the pulse length is doubled for the next power rise and so forth. At the full pulse length the power is sweeped for some hours. After this the cavity and coupler are cooled down and the same processing procedure is carried out again. The last part of processing is done with the cavities on resonance.

5.1.Processing results on module 1

Due to limited time the processing of couplers in module 1 was restricted to 200 kW and 600 μs. The processing of the coupler on the module at room temperature was done at two couplers at a time in order to distinguish the vacuum reactions in the common coupler vacuum. It was always observed, that initially it is possible to rise the power very quickly without being limited by outgassing, electron signals or light. After a

sudden burst of outgassing on the coupler side of the cold window at a typical power level of 50 - 100 kW many hours are needed to once again reach the earlier achieved power level. Once the maximum power of 200 kW is reached for the shortest pulse length the power rises for longer pulses are straight forward. After about 48 to 72 h only one multipacting level at 125 kW is visible at the charged particle detectors. But the signals are smaller by a factor of 10 compared to the first processing hours. A second multipacting level at 65 kW is processed away.

When the module was cooled down to the operating temperature of 1.8 K the same processing procedure took place. All multipacting levels were processed after 30 h. The temperatures of the Fermilab cold window increased due to dynamic losses by about 5 K. Due to a fabrication failure during brazing metallization of the cold DESY windows occurred. This causes a much stronger temperature rise of about 100 K which does not effect the coupler behavior but creates higher losses at the 70 K shield circuit of the module.

When the cavities are on resonance the field distribution in the coupler differs from the off resonance full reflection condition. An additional processing is necessary. After only a few (1-5) more hours the couplers were fully operational without limiting the cavities. No interlock events were observed up to the TTF operating power of 125 kW during the first 30 days of operation time. After a few days power off time no new processing was needed to operate the module again.

6OPERATION OF THE CAVITIES IN THE LINAC

After installation in the linac the cavities were measured again individually under pulsed conditions. Here the capture cavity C19 showed a reduced performance due to field emission loading (Tab. 1). The 8 cavities mounted in the module 1 reached almost the same results as in the vertical tests. One cavity D2 showed a slightly higher, one cavity D3 a slightly lower gradient, caused by field emission.

Operating all cavities with one klystron and a uniform power distribution the module performance is limited by the worst cavity. Therefor the quench of cavity S7 limits the maximum gradient of the module 1 to 12 MV/m at the full pulse length of 800 µs flat top and 10 Hz repetition rate. For shorter RF pulses of 300 µs rise time and 100 µs flat top at 2 Hz repetition rate acceleration gradients of 16.7 MV/m were obtained.

7CAVITIES FOR MODULE 2

In Fig. 3 the vertical test results of the 8 cavities forseen for the module 2 are shown. The module 2 will be installed in the linac by end of September '98. The expected average gradient for this module is ≥20 MV/m.

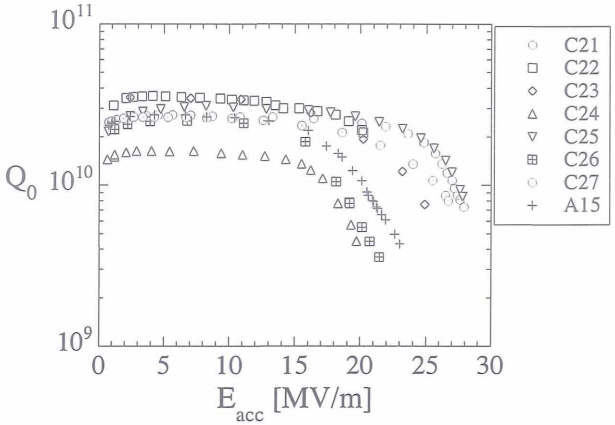

Fig. 3: Vertical test results of the 8 cavities selected for module 2.

8 CONCLUSIONS

Gradients well above 20 MV/m have been demonstrated with 9-cell TTF cavities. Excluding only the cavities with a well identified fabrication error, the average gradient of 13 cavities is 24.6 MV/m.

The highest gradient in the horizontal cryostat with a fully equipped cavity was 33 MV/m.

The main limitation is field emission, indicating the high standard of niobium quality and fabrication methods. Further progress in gradient can be expected by improving cleanliness during final treatment and assembly.

The first beam of 8 mA has been successfully accelerated. The average gradient of the first 8 cavity module is limited by one of the above mentioned cavity. Further improvement of the gradient is possible by optimizing the RF distribution.

A slight reduction in gradient from horizontal test to module operation was observed and is caused by high field emission loading. It shows that improvements in clean assembly and coupler handling is still necessary.

REFERENCES

[1] Conceptual Design of a 500 GeV e^+e^- Linear Collider with integrated x-ray Laser Facility, Ed. R. Brinkmann, G. Materlik, J. Rossbach, A. Wagner, DESY 1997-048, ECFA 1997-182.

[2] D.A. Edwards: `TESLA TEST FACILITY LINAC - Design Report', TESLA 95-01, 1995.

[3] W. Singer et. al.: Diagnoses of defects in high purity niobium, Eighth Workshop on RF Superconductivity, Albano Terme (Padova), Italy, 1997.

[4] A. Brinkmann et. al.: Performance degradation in several TESLA 9-cell cavities due to weld imperfections, Eighth Workshop on RF Superconductivity, Albano Terme (Padova), Italy, 1997.

[5] J. Graber, Ph.D. thesis, Cornell University, 1993

[6] M. Champion, Seventh Workshop on RF Superconductivity, Gif Sur Yuette, France 1995.